JOURNAL OF CAVE AND KARST STUDIES

April 2015
Volume 77, Number 1
ISSN 1090-6924
A Publication of the National Speleological Society

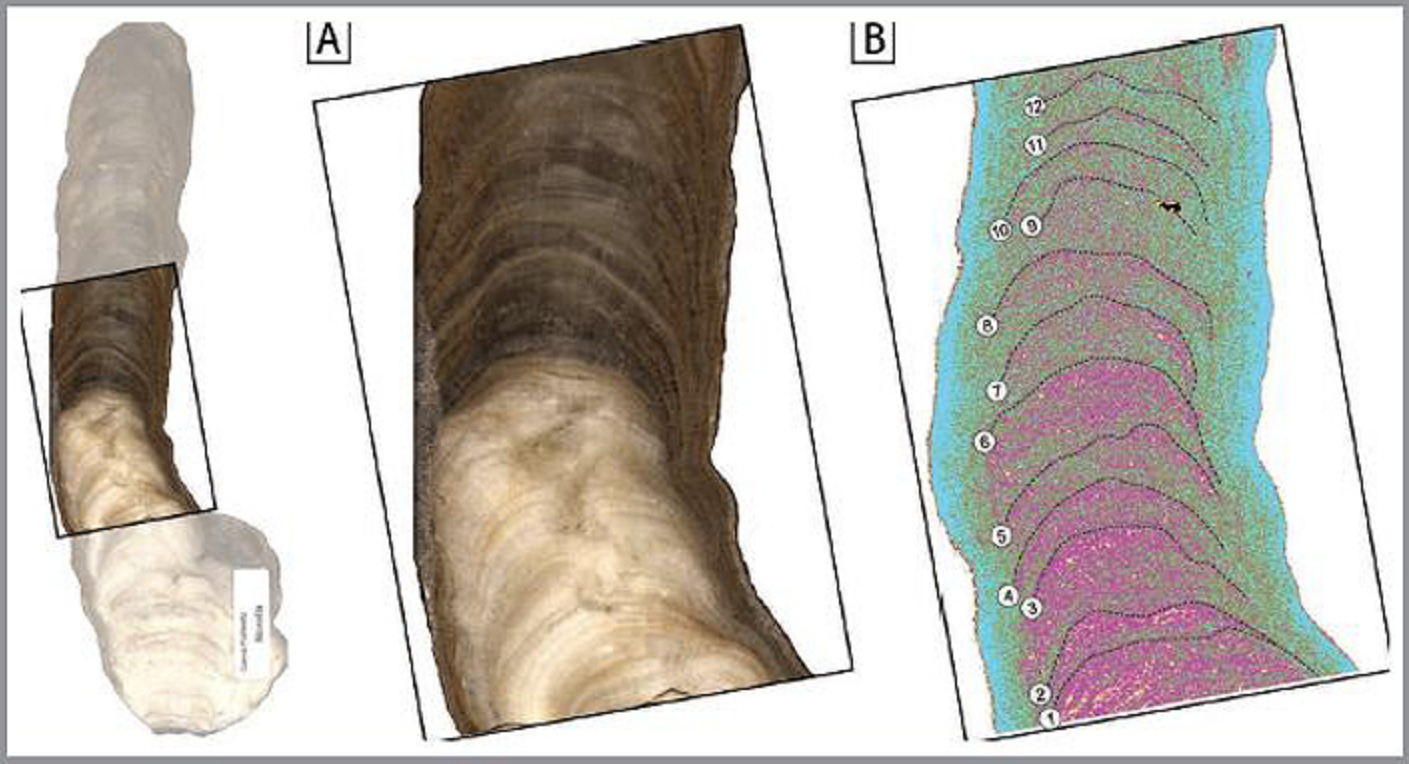

DEDICATED TO THE ADVANCEMENT OF SCIENCE, EDUCATION, AND EXPLORATION

Published By
The National Speleological Society

The *Journal of Cave and Karst Studies* (ISSN 1090-6924, CPM Number #40065056) is a multi-disciplinary, refereed journal published three times a year by the National Speleological Society, 6001 Pulaski Pike NW, Huntsville, AL 35810-4431 USA; Phone (256) 852-1300; Fax (256) 851-9241, email: nss@caves.org; World Wide Web: http://www.caves.org/pub/journal/.
Check the *Journal* website for subscripion rates. Back issues are available from the NSS office.

POSTMASTER: send address changes to the *Journal of Cave and Karst Studies*, 6001 Pulaski Pike NW, Huntsville, AL 35810-4431 USA.

The *Journal of Cave and Karst Studies* is covered by the following ISI Thomson Services Science Citation Index Expanded, ISI Alerting Services, and Current Contents/Physical, Chemical, and Earth Sciences.

Front cover: Phase transition area in stalagmite from Northern Spain. See Vanghi et al. in this issue.

W.J. Stemp, G.D. Wrobel, J. Haley, and J.J. Awe – Ancient Maya stone tools and ritual use of Deep Valley Rockshelter, Belize. *Journal of Cave and Karst Studies,* v. 77, no. 1, p. 1–11. DOI: 10.4311/2012AN0271

ANCIENT MAYA STONE TOOLS AND RITUAL USE OF DEEP VALLEY ROCKSHELTER, BELIZE

W. James Stemp[1], Gabriel D. Wrobel[2], Jessica Haley[3], and Jaime J. Awe[4]

Abstract: This paper discusses the technological and microscopic use-wear analyses of the chert debitage excavated from Deep Valley Rockshelter. This rockshelter, located in the Caves Branch River Valley of central Belize, was primarily used by the ancient Maya from the Late Preclassic to Terminal Classic periods (AD 80–950) and may demonstrate a pattern of rockshelter usage by the Classic period Maya. To test whether such a pattern exists, lithic data from Caves Branch Rockshelter and other rockshelters in Belize, specifically those in the Sibun Valley and the Ek Xux Valley, are compared. Interpretations are complicated, however, by the severe mixing of deposits, which makes segregating the lithic artifacts into different reduction or use events nearly impossible. Moreover, this mixing severely hampers reconstructions of diachronic change in stone-tool use in the rockshelter. While acknowledging these limitations, our analysis suggests that the lithics in the rockshelter are primarily the result of reduction and use-related activities that originally occurred at other nearby surface sites rather than in the rockshelter itself. Consequently, the chipped-stone artifacts recovered from this rockshelter most likely result from secondary deposition of debitage for ritual purposes and represent accumulation over many years. We suspect this type of secondary deposition of debitage was also occurring at other rockshelters in Belize, based on comparisons to the chipped stone assemblages from these locations. We cannot discount the possibility that some stone tool production and use may have originally occurred in Deep Valley Rockshelter, but support for this is minimal.

Introduction

The use of caves has long fascinated archaeologists working in Belize (see McNatt, 1996). That they are connected to ritual activity is considered a certainty (e.g., Brady and Prufer, 2005; Prufer and Brady, 2005). However, the ritual activities that occurred within caves and rockshelters are believed to have varied and likely involved different types of ritual specialists (Prufer, 2002, p. 43–51, 2005; Vogt and Stuart, 2005). As a further contribution to the unfolding story of how the ancient Maya used these spaces, this paper presents the results of the technological and microscopic use-wear analyses of the chipped-stone artifacts from Deep Valley Rockshelter (DVR1). To provide a larger framework for understanding chipped-stone tools in caves and rockshelters, the DVR1 lithic data are compared to those from other rockshelters and caves used by the ancient Maya. The possible uses of chipped–stone tools in DVR1 are also considered in relation to ethnographic and ethnohistoric evidence.

Maya Cave Rituals and Ritual Objects

Our understanding of the ideological significance of caves to the ancient Maya is based on archaeological, ethnohistoric, and ethnographic information. Caves and the natural water-filled sinkholes called cenotes were places where human sacrifices, often children, were made, where the Maya buried their dead, and where the living went to make offerings of various types to gain the favor of their ancestors and supernatural beings, such as earth and rain gods (Brady, 1989; Gibbs, 1998; Ishihara, 2008; Moyes et al., 2009; Prufer, 2002, 2005; Tozzer, 1941; Vogt and Stuart, 2005). Many objects have been used as offerings by past and present-day Maya, including animals, blood, ceramics, wood, candles, incense, maize, cacao, shells, crystals, pebbles, obsidian blades, and chipped-chert flakes and implements (e.g., Awe et al., 2005; Bassie-Sweet, 1991; Brady and Prufer, 1999; Halperin et al., 2003; Morehart, 2005; Moyes et al., 2009; Prufer, 2002, 2005; Prufer and Hurst, 2007; Prufer et al., 2003). Like their modern descendants, the ancient Maya associated chert with lightning (Freidel et al., 1993, p. 200), and given that many underworld rituals focused on rain, fertility, and sustenance, the deposition of chert debitage in caves and rockshelters may very likely have been related to this ideology. With regard to chert flakes, some contemporary Maya will collect debitage for use as ritual objects during divination (Brown 2000, p. 330). Brady (1989, p. 319) mentions that the Chorti Maya kept unshaped chert pieces

[1] Dept. of Sociology, Anthropology and Criminology, Keene State College, 229 Main St., Keene, NH, 03435-3400, USA jstemp@keene.edu
[2] Dept. of Anthropology, Michigan State University, 655 Auditorium Drive, East Lansing, MI, 48824, USA
[3] Loyola Intensive English Program, 6363 St. Charles Avenue, Campus Box 205, New Orleans, LA 70118, USA
[4] Dept. of Anthropology, Northern Arizona University, 575 E. Pine Kooll Dr. Flaystaff, AZ, 86011, USA

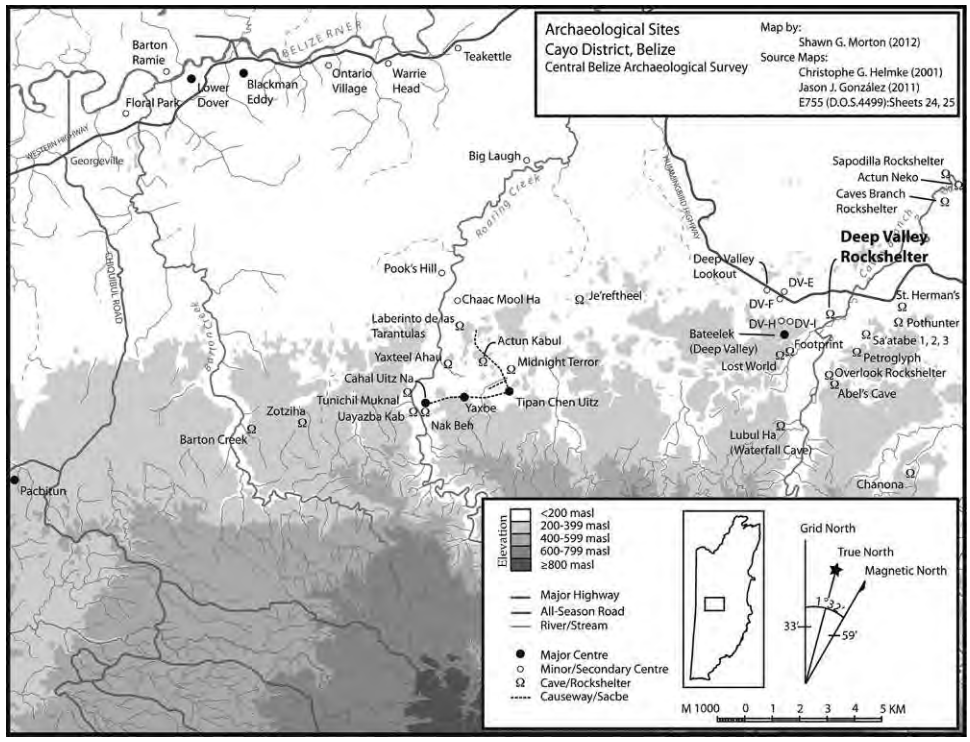

Figure 1. Locations of Deep Valley Rockshelter and Caves Branch Rockshelter in the Cayo District of Western Belize.

on altars and that chert is associated with the rain gods who are believed to dwell in caves (see Wisdom, 1940, p. 382). Ethnographic evidence also indicates that jute, the freshwater gastropod *Pachychilus* sp., was included in rituals (Healy et al., 1990, p. 171). The Q'eqchi' Maya transported the shells of consumed jute to caves, where they would be deposited to thank the Earth goddess (Halperin et al., 2003). The Lacandon Maya of Naha are also reported to have consumed jute daily during periods of ritual seclusion (Brady 1989, p. 381).

DEEP VALLEY ROCKSHELTER

Deep Valley Rockshelter is an open rockshelter with a western exposure that is approximately 58 m long by 15 m deep. The site was encountered during reconnaissance in the Cayo District, Belize (Fig. 1), in the area near the Caves Branch Rockshelter in 2006 and excavated over two four-week periods in 2006 and 2007. It is located 2 km southwest of CBR, in a limestone cliff face overlooking the Caves Branch River. The rockshelter has an 18 m high ceiling and relatively shallow overhang (Fig. 2). At the southeastern end of the rockshelter, there are two short, narrow passages leading into a cave approximately 15 m deep.

Investigations at DVR1 included base-line mapping, topographic mapping, and test-pitting. Throughout the site, artifacts littered the surface, and they were also found in large quantities in a wall crevice near its center. Four operations were established at DVR1, each placed strategically to take advantage of visible surface artifacts or notable morphological features (Fig. 3). The artifacts discussed in this study came from two of these, Operations 1A and 1B, located in the center of the rockshelter. The other two operations, 1C and 1D, contained no lithic artifacts and very little cultural material in general. Operation 1A measured 2 by 2 meters and was terminated at 80 cm below surface, prior to reaching sterile soil, because of time issues. Operation 1B measured 1 by 2 meters and was terminated at 170 cm upon reaching sterile soil. All soil was screened through 1/8 inch (3.12 mm) mesh. Within the units, artifacts were surprisingly dense throughout; thousands of ceramic sherds and jute shells were collected. Several carved-shell beads, polished jade pieces, and fishing weights were also found (Hardy, 2009).

During excavations, we were generally unable to recognize any natural or cultural stratigraphy in the form of distinct variations in the soil or other features. All soil in the excavation units appeared to be relatively consistent in its grayish-brown color and silty texture. In Operation 1B, this relatively uniform cultural layer ended directly over the natural cave floor, which was composed of stone and a red, sterile matrix of decomposing limestone. As a result, we were unable to accurately group artifacts within temporally distinct lots for comparison. A lack of evident stratigraphy has been noted at other rockshelter sites in Mexico (Rissolo, 2003) and Belize (Hardy, 2009; Michael and Burbank, 2013; Prufer, 2002; Wrobel, 2008; Wrobel and Shelton, 2011; Wrobel and Tyler, 2006; Wrobel et al., 2010; Wrobel et al.,

Figure 2. The western exposure of the Deep Valley Rockshelter in a view looking south.

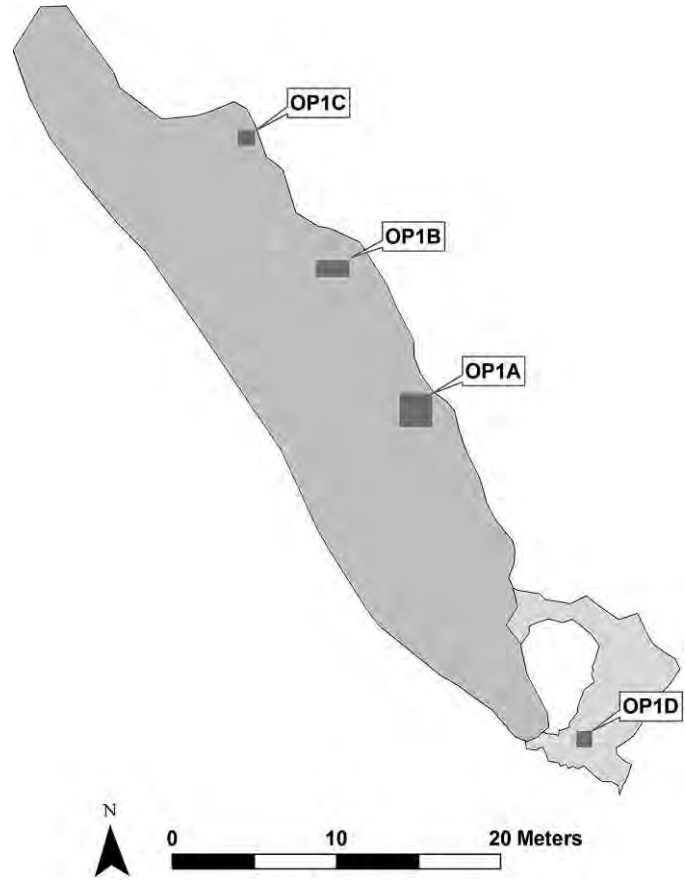

Figure 3. Map of Deep Valley Rockshelter showing excavation units. OP1A and OP1B are the sources of the lithic artifacts discussed in the paper.

2013), but some excavations at rockshelters in surrounding regions, such as El Gigante in Honduras (Scheffler, 2008) and Guila Naquitz in Oaxaca (Flannery, 1986), have shown a clear stratigraphy corresponding to specific events. In an effort to get some sense of change over time in the activities at our site, we collected artifacts from arbitrary 20 cm levels, which was the usual strategy in the excavation of the sites mentioned above that lacked visible stratigraphy.

In the absence of any radiocarbon dates for DVR1, diagnostic ceramics categorized using Gifford's (1976) type-variety system provide the best evidence for determining the period of utilization. The sherds comprised a wide variety of finishes, including plain, painted, appliquéd, and polychrome, but unfortunately analysis identified relatively few diagnostic pieces. Among typed specimens, dates spanned the Late Preclassic through the Terminal Classic (AD 80–950), which is consistent with an informal evaluation of the rockshelter's surface deposits. Within the excavations, the most commonly represented periods were the Protoclassic and Early Classic. Late and Terminal Classic pottery appears to be limited to the surface and the topmost 20 cm level, with no examples identified deeper in the excavations. However, ceramics dating to between the Late Preclassic and Early Classic were found at all depths. This mixing of ceramics throughout the matrix makes evaluation of the site's history difficult. However, other clues do provide some insight. For instance, all recovered ceramics appear to have been deposited as individual sherds, with few refits and no whole vessels evident. This kind of variation in ceramic sherds is fairly typical at rockshelters in the area (Hardy, 2009; Shelton, 2013).

There are a couple of possible explanations for the type of soil and artifact commingling described above. At other sites, such as the Caves Branch Rockshelter, this was easily attributable to extensive mixing of grave fill during the burials of hundreds of individuals throughout the nearly thousand-year span of site use (Wrobel et al., 2007). Although one of the DVR1 units was placed specifically around human bone fragments found on the surface, excavations revealed very few human remains, prohibiting interpretations of funerary use. The paucity of human bone in DVR1 clearly was not due to taphonomic issues, because human and faunal remains were generally well preserved. Therefore, mixing in the DVR1 rockshelter occurred by some other bioturbation mechanism, possibly water or burrowing animals.

Table 1. Non-obsidian artifacts from Deep Valley Rockshelter.

Tool Type	Chert	River Cobble Chert	Chalcedony	River Cobble Chalcedony	Limestone	Quartzite
			Formal Tools			
Blades	1	…	…	…	…	…
Large bifaces	2	…	…	…	…	…
Miscellaneous thin bifaces	1	…	…	…	…	…
			Informal Tools/Debitage			
Flakes (cortical)	76	6	…	1	4	…
Flakes (non-cortical)	102	…	…	…	1	3
Bifacial thinning flakes (non-cortical)	1	…	1	…	…	…
Retouched macroflakes (cortical)	1	…	…	…	…	…
Retouched flakes (cortical)	…	1	…	…	…	…
Flake-blades (cortical)	1	…	…	…	…	…
Flake-blades (non-cortical)	4	…	…	…	…	…
Small bifacial edge retouch flakes - percussion (cortical)	2	…	…	…	…	…
Small unifacial retouch flakes (non-cortical)	1	…	…	…	…	…
Simple flake cores	2	…	…	…	…	…
Simple flake core fragments	11	…	…	…	…	…
Blocky fragments/shatter	31	…	…	…	2	…
Heavily burnt fragments (including potlids)	14	…	…	…	…	…
Total	250	7	1	1	7	3

The Chipped-Stone Assemblage from Deep Valley Rockshelter

The chipped-stone assemblage consists of 274 artifacts. Most of the artifacts were made from chert (257 or 93.8%) that was obtained locally in the form of cobbles from nearby creeks or rivers or from nodules and lenses that formed in natural limestone in the area surrounding the rockshelter. Small quantities of other locally available stone include chalcedony (2 or 0.7%), limestone (7 or 2.6%), and quartzite (3 or 1.1%). The only imported stone is obsidian from the Guatemalan highlands (5 or 1.8%), which was identified based on visual sourcing (see Braswell et al., 2000). This pattern of heavy dependence on local chert sources is also seen in other caves and rockshelters in western and southern Belize (Peterson, 2006; Prufer, 2002; Stemp, 2009; Stemp et al., 2013).

Nearly all of the chipped-stone artifacts are debitage (268 or 97.1%), defined as "the waste produced by manufacturing processes using reductive technologies" (Moholy-Nagy, 1990, p. 269), including stone flakes and flake fragments of various types, shatter, and exhausted cores (Table 1). Only eight formal tool fragments were recovered. Four are obsidian prismatic blade segments that were punched from prepared cores and were most likely brought into the rockshelter in finished form. This is a pattern observed at other rockshelters and caves in the Maya world, in which there is little evidence for obsidian blade manufacture in the form of obsidian cores, early-stage thick blades, and flake debitage (e.g., Aoyama, 2001; Brady, 1989; Helmke, 2009; Peterson, 2006; Prufer, 2002; Stemp and Awe, 2014; Stemp et al., 2013). Whether the four obsidian blades were used for ritual activities, such as blood-letting or sacrifice (Aoyama, 2001; Stemp, 2009; Stemp and Awe, 2014; Stemp et al., 2013), inside the rockshelter cannot be ascertained.

The other formal tool fragments are made of chert and include part of an oval biface, an oval biface edge flake, the distal end of a thin biface, and a blade segment. No whole formal tools were recovered from the Deep Valley Rockshelter. In southern Belize, Prufer (2002, p. 237, Table 7.1) notes similar patterns at some rockshelters, in which there are either few or no formal chert tools and substantial quantities of debitage. The absence in rockshelters of whole or nearly complete chert tools, specifically large, thin bifaces, which are common in the ritual deposits of other caves (e.g., Brady, 1989; Graham et al., 1980; Helmke, 2009; Pendergast, 1971; Peterson, 2006), suggests the possibility that formal tool deposition in caves differs from that in rockshelters.

The debitage from DVR1 overwhelmingly consists of a variety of both cortical flakes, with some of the original rough, weathered surface of a nodule retained on the dorsal surface of the flake, and non-cortical chert flakes (Fig. 4). Evidence suggests that most reduction was the result of simple flake production using hard-hammer percussion. Both the flake dimensions and the high frequency of cortical and flat striking platforms (89.1%) support this

Figure 4. Examples of chert debitage from Deep Valley Rockshelter. The scale is in centimeters.

conclusion. There are only two examples of bifacial thinning flakes resulting from biface manufacture, and two other flakes have lipped platforms that suggest removal from bifaces. The lack of manufacturing failures or biface preforms further suggests that the majority of debitage from DVR1 is not the result of biface production. When the chert debitage from DVR1 is compared to the assemblages from other rockshelters, both similarities and differences are noted. Although Caves Branch Rockshelter and Pine Torch Rockshelter both yielded large quantities of debitage, non-cortical flakes are much more frequent at these locations (Table 2), which would suggest different reduction patterns than those seen at DVR1, if flaking originally occurred in the rockshelters themselves.

Only two pieces (0.7%) of microdebitage (flakes measuring less than 3 mm in maximum dimension, see Hayden and Cannon, 1983) were found in DVR1, which suggests that primary tool production was unlikely in the rockshelter itself (see Behm, 1983; Clark, 1991; Morrow, 1996). Because all excavated soil was screened, we do not believe the very small amount of microdebitage is the result of recovery methods. Unfortunately, the contextual issues noted above render determinations of how much primary tool production versus secondary disposal of debitage occurred in DVR1 extremely difficult (Wilson, 1994; see Moholy-Nagy, 1990). Nevertheless, the lack of manufacturing tools like hammerstones seems to support the interpretation that most, if not all, core reduction originally occurred outside DVR1 (Moholy-Nagy, 1990). Prufer (2002, p. 225) and Stemp et al. (2013) noted the absence of flaking implements and a paucity of cores in the assemblages from Caves Branch Rockshelter and the rockshelters in the Ek Xux Valley.

Another possible indicator of secondary deposition of chert artifacts is the near absence of refits in the assemblage

Table 2. Percentage of the original rough, weathered surface of a nodule retained on the dorsal surface of local chert and chalcedony flakes from area rockshelters.

Dorsal Cortex	CBR[a]	Pine Torch Rockshelter[b]	DVR
0%	1420 (76.6%)	82 (75%)	102 (54.8%)
1–50%	339 (18.3%)	…	64 (34.4%)
51–99%	83 (4.5%)	…	14 (7.5%)
100%	12 (0.6%)	…	6 (3.2%)
Total	1854	110	186

[a] (Stemp et al., 2013).
[b] (Peterson, 2006, p. 165).

(Andrefsky, 2009; Morrow, 1996). We tried to rearticulate flakes to bifaces and cores, as well as to other flakes that may have been involved in the same reduction process. The attempted refitting of tools and debitage included all chert artifacts from the rockshelter. The artifacts were subdivided into groups based on similarity of color and stone texture. Fifteen such groups, ranging in size from a half dozen to over forty pieces, were created, with an additional catch-all group that consisted of any single flakes or fragments that could not be assigned to another group. Each group was examined individually for refits and then compared to the pieces in the catch-all group. No flakes could be refit to formal tool fragments or flake cores. From only one of the groups, two flakes could be rearticulated, and they each came from different levels in different excavation units. Nevertheless, both the relatively small sample size and the mixing of deposits (Morrow, 1996) cannot be discounted as factors in reducing the number of refits.

Microscopic Use-wear Analysis: Methods and Results

Tool use for the lithic artifacts from Deep Valley Rockshelter was determined following a program of microscopic use-wear analysis similar to that used by Stemp (2001; Stemp et al., 2010, 2013) for assemblages from other Maya sites. It involves both the low-power (40×) and high-power (100 to 400×) microscopic examination of tool surfaces for edge-chipping, striations, and polishes related to human use. Used areas identified on the artifacts were tabulated and categorized following an independent-use-zone [IUZ] system (see Aoyama, 2009). Recognition of motion types and contact material types is primarily based on comparisons with experimentally used tools (Stemp, 2001).

Of the 265 chert, chalcedony, limestone, and quartzite informal tools and debitage recovered, 31(11.7%) were so badly burnt or heavily patinated that use-wear analysis was not possible. Only 40 (17.1%) of the remaining artifacts possessed some evidence for having been used in the past. The number of IUZs identified on these artifacts is 47 (20.1%). Use-wear analysis indicates that debitage was used for a fairly wide variety of tasks (Table 3). This observation has been made by use-wear analysts who have examined debitage from other Maya sites (e.g., Aoyama, 2009; Lewenstein, 1987; Stemp, 2001; Stemp et al., 2010).

Most of the flakes from DVR1 were used for cutting, slicing, and sawing, which may be due to the generally low edge-angles of these flakes. This is followed in frequency by scraping and planing motions. These are similar to data from Caves Branch Rockshelter, but, unlike CBR, there is no use-wear evidence at DVR1 for adzing/chopping, drilling, incising, or graving (Stemp et al., 2013). In terms of contact materials, most flakes from DVR1 were used to work bone, meat, hide (Figs. 5, 6), and wood, which is similar to results from CBR, but the data from DVR1 demonstrate more contact with bone and hard materials (Fig. 7) and less with wood. There is no evidence for contact with ceramic, shell, or soil on the debitage from DVR1.

Overall, the use of debitage for the completion of many tasks and the kinds of motions and contact materials are consistent with subsistence and other utilitarian, domestic tasks that would be undertaken by the Maya in their daily lives (Lewenstein, 1987; Stemp, 2001; Stemp et al., 2010). Although the high percentage of tools with meat, bone, and hide polish might support some interpretations that ceremonial or ritual butchery or sacrifice of animals occurred in DVR1 (see Sievert, 1992, p. 40–41, Table 4.4), few faunal remains, with the exception of jute shells, were recovered within the rockshelter. This suggests tool use associated with animals may have taken place at locations outside this space, but the meat, hide, and bone polishes on the chert debitage from DVR1 could also be the result of hunting and butchering activities, including some carcass processing, as well as domestic crafting (Lewenstein, 1987; Sievert, 1992, p. 37–38, Table 4.3). The greasy appearance of polish on some of the bone-working tools may indicate contact with cooked bone (Keeley, 1980, p. 44), which would be more closely associated with subsistence activities. Nevertheless, some bones may have been associated with ritual activity (see Kavountzis, 2009; Pohl, 1983), and it is possible small animals, such as rodents, were sacrificed (Aoyama, 2001; Sievert, 1992, p. 89).

Like many caves and rockshelters in the Maya world (e.g., Brady, 1989; Graham et al., 1980; Halperin et al., 2003; Helmke, 2009; MacLeod and Puleston, 1978), dense deposits of jute shells were also recovered from DVR1 (Hardy, 2009). This has been noted at CBR (Bonor and Martínez Klemm, 1995; Wrobel and Tyler, 2006; Hardy, 2009) and in mortuary rockshelters in the Ek Xux Valley (Prufer, 2002) as well. Large quantities of jute shells have been associated with human burials in caves and rockshelters (Ferguson and Gibbs, 1999; Prufer, 2002), possibly to demonstrate a link between death and a watery place like the Underworld or a connection to rain and fertility (Girard, 1962).

Table 3. Independent use zones showing evidence of various uses on non-obsidian artifacts from Deep Valley Rockshelter.

	Formal Tools[a]		Informal Tools/Debitage			
IUZs	Thin Bifaces	Blades	Flakes	Bifacial Thinning Flakes and Biface Edges	Blocky Fragments	Cores and Core Fragments
Bone						
cut/slice	…	…	5	…	…	…
pierce	1	…	…	…	…	…
saw	…	…	1	…	…	…
scrape/plane	…	…	2	…	1	1
Dry Hide						
cut/slice	…	…	1	…	…	…
scrape/plane	…	…	2	…	…	…
Meat/Fresh Hide						
cut/slice	…	…	3	…	…	…
scrape/plane	…	…	…	1	…	…
Meat/Bone						
cut/slice	…	…	5	…	…	…
scrape	…	…	1	1	…	…
Plant						
cut/slice	…	…	1	…	…	…
Stone						
saw	…	…	1	…	…	…
rub/grind	…	…	1	…	…	…
Wood						
cut/slice	…	…	3	…	…	…
saw	…	…	2	…	1	…
scrape/plane	…	…	…	…	1	…
whittle	…	…	1	…	…	…
Soft						
cut/slice	…	…	2	…	…	…
scrape/plane	…	…	…	…	1	…
Hard						
cut/slice	…	…	3	…	…	…
saw	…	1	2	…	…	…
Indeterminate						
cut/slice	…	…	3	…	…	…
indeterminate	…	…	1	…	…	…
Total	1	1	40	2	4	1

[a] The oval biface fragment was unavailable for use-wear analysis.

Both modern and ancient Maya used jute as a source of protein, and some modes of consumption involved the removal of the apex or spire of the shell (Healy et al., 1990). Based on the presence of chert flakes and jute shells at many rockshelters, one suggestion is that chert flakes were used to open the jute shells for consumption. It may be that chert flakes were initially used in jute consumption for subsistence purposes at surface sites and the jute shells were then later ritually deposited in the rockshelters (Halperin et al., 2003; Peterson 2006, p. 210). However, even though most of the jute shells from DVR1 are spire-lopped (Hardy, 2009, p. 127), use-wear analysis does not indicate a connection between stone flakes and jute consumption based on the absence of flakes with evidence for contact with shell.

The reliance on unmodified chert flakes and their use-wear patterns suggest similarities to assemblages used in domestic activities at some surface sites in which there is an emphasis on wood (Lewenstein 1987; Stemp 2001; Stemp et al. 2010). It is also possible that use-wear indicating contact

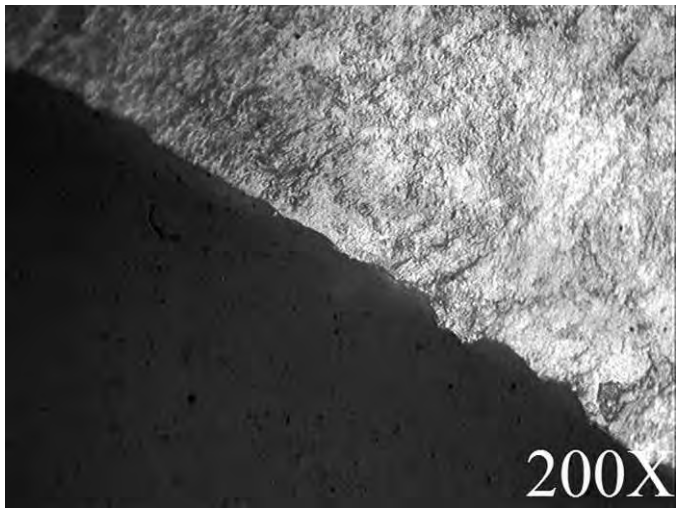

Figure 5. Photomicrograph of a thin-edged chert flake used to cut meat/fresh hide and showing some contact with bone, as indicated by invasive, greasy polish on both lower and higher microtopography with some patches of brighter, micropitted polish; few fine, shallow striations parallel and mildly diagonal to the flake edge; and minimal microchipping on the thinnest portions of the edge (snap fractures).

with wood or plants might be the result of ritual activity or the production of ceremonial items (e.g., Morehart, 2005; Pendergast, 1974; Prufer et al., 2003; Sharon, 2003). Although some of the debitage may have been associated with specialized craft-production involving wood (Aldenderfer, 1991), segregating this evidence from the stone tools

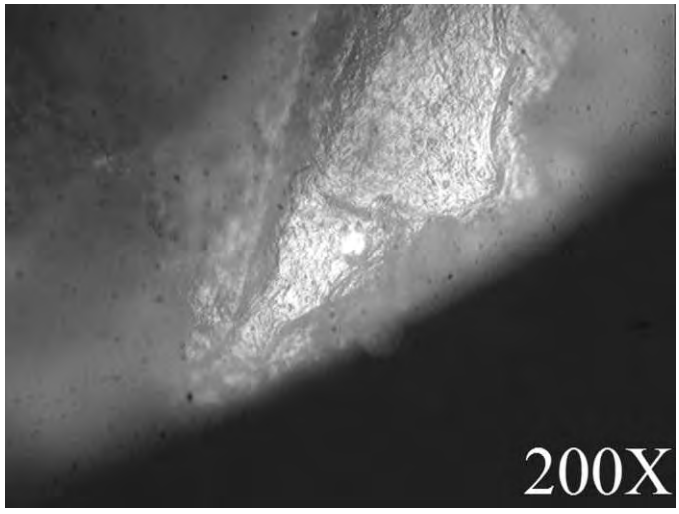

Figure 6. Photomicrograph of a ventral surface of a thick-edged chert flake used to scrape bone and meat or fresh hide (defleshing/butchery?), as indicated by greasy, bright, micropitted polish near tool edge, mild edge rounding, and primarily unifacial microflaking of tool edge.

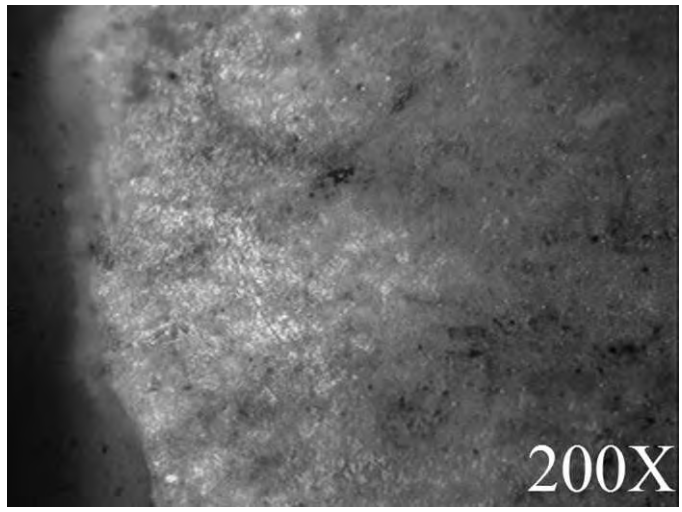

Figure 7. Photomicrograph of a ventral surface of a re-touched chert flake used to saw a hard material, as indicated by striations parallel to the edge and a flat, semi-bright polish. Note: Burning and patination of the tool surface complicates use-wear analysis.

that may have been used for domestic activities or ritual is not possible.

DISCUSSION AND CONCLUSION

The stone tool assemblage from DVR1 is similar in many ways to those from other rockshelters in Belize for which secondary deposition of lithic artifacts for ritual purposes has been proposed (Peterson, 2006; Prufer, 2002; Stemp et al., 2013) and suggests that chert debitage was brought into the rockshelter at different points in time as special deposits (Moholy-Nagy, 1990; see Brown, 2000). Prufer (2002, p. 225) suggests that chert debitage recovered from the rockshelters in the Maya Mountains "may be parts of ceremonial trash (Walker, 1995) carried into the sites. They may also be objects that were collected by ritual specialists and placed into the rockshelters (Brown, 2000)".

Large accumulations of chert and obsidian debitage are also sometimes associated with burials, particularly the tombs of elites or high-status individuals (Moholy-Nagy 1990, p. 271–272, 1997), as demonstrated at surface sites in the Cayo District of Belize (e.g., Chase and Chase 1996; Chiarulli and Barrick, 1997; McAnany and Peterson, 2004) and in a least one cave (Griffith, 1998, p. 59). Dense layers of debitage are believed to represent connections to the Underworld (Hall 1989, p. 308). The layers of stone may also be associated with the rain gods (Wisdom, 1940, p. 383) or lightning (see above). However, the flakes from DVR1 were not recovered as a dense lens in association with any burials. The flakes were scattered throughout the rockshelter and were recovered from multiple depths. Moreover, there were very few human skeletal remains excavated from the rockshelter, indicating that it was not

primarily used as a location for the interment of the dead (see Bonor and Martínez Klemm, 1995; Prufer, 2002; Wrobel and Tyler, 2006; Wrobel et al., 2007 for mortuary rockshelters).

Although evidence indicates most, if not all, tool production and use originally occurred outside DVR1, we believe these activities occurred relatively close to the rockshelter. Hayden and Cannon (1983, Fig. 16) observed that the modern Maya spend minimal time and effort in disposing of trash, and that 82% of waste material is discarded within their compound or within a minute's walk from their houses. Similarly, Deal and Hayden (1987) noted that disposal of sharp glass fragments or implements by modern highland Maya typically occurred close to areas of habitation. Clark (1991) made similar observations concerning the disposal of flaking debris by the Lacandon Maya, who dumped their flaking waste into trash piles not very distant from their homes. However, given the ritual or votive nature of artifact deposition in the rockshelter, pilgrimage to this location from distances farther away cannot be completely discounted (Adams and Brady, 2005; Patel, 2005).

The use-wear on the debitage is similar to that associated with subsistence and domestic activities at surface sites (Lewenstein, 1987; Sievert, 1992, p. 30, Table 4.1; Stemp, 2001; Stemp et al., 2010). We therefore believe that most tool use first occurred outside the rockshelter, in association with basic subsistence and domestic tasks. However, we cannot completely rule out the possibility that some of this use-wear may be the product of ritual activity that occurred within the rockshelter itself.

A comparison among available lithic data from the Deep Valley Rockshelter, the Caves Branch Rockshelter, the Sibun rockshelters, and those from the Maya Mountains indicate minimal variation in their respective chipped stone assemblages, while some important similarities, such as debitage, broken tools, and few imports, have been noted. Any significant variations in assemblage composition do not appear to be due to primary tool-using activities occurring within the rockshelters. Instead, variation of assemblage composition and use-wear patterns is most likely a result of where the debitage was originally produced and used at surface sites prior to secondary deposition in the rockshelters.

It may be that rockshelters in the same valley or region represent a ritual circuit with locations visited at different times and possibly for different reasons. Although this is hard to substantiate archaeologically, one indicator might be the successful refitting of debitage and tools recovered from *different* rockshelters, which would link these spatially distinct places through a shared sequence of lithic reduction (see Close, 1996). Similarly, a recent study of the much smaller Overlook Rockshelter near DVR1 interpreted the thorough mixing of the ceramic assemblage and lack of sherd refits as likely resulting from the ritual deposition of individual fragments from complete vessels as part of a ritual circuit (Wrobel et al., 2013). Clearly, further research involving stone tools from caves and rockshelters is required to better understand the relationships between lithic artifacts and these locations; this is especially true when contextual difficulties are encountered.

Acknowledgments

We would like to thank many individuals and organizations for their support and assistance. Much gratitude is owed to John Morris, Rafael Guerra, and the Belize Institute of Archaeology, as well as Bryan Haley, David Hayles, Ian Anderson, and all the staff at the Caves Branch Adventure Lodge. We would like to acknowledge support from the Belize Archaeological Research and Education Foundation, the University of Mississippi's Office of Research and Sponsored Programs, the Department of Sociology and Anthropology at Ole Miss, and Keene State College's Office of Sponsored Projects and Research. We thank the three anonymous reviewers whose comments and suggestions assisted in improving the clarity and overall quality of the manuscript. Finally, we would like to acknowledge the dedication and hard work of the many students who participated in the 2006 and 2007 CBAS (Caves Branch Archaeological Survey summer field-schools.

References

Adams, A.E., and Brady, J.E., 2005, Ethnographic notes on Maya Q'eqchi' cave rites: Implications for archaeological interpretation, *in* Brady, J.E., and Prufer, K.M., eds., In the Maw of the Earth Monster: Mesoamerican Ritual Cave Use: Austin, University of Texas Press, p. 301–327.

Aldenderfer, M.S., 1991, Functional evidence for lapidary and carpentry craft specialties in the Late Classic of the Central Peten lakes region: Ancient Mesoamerica, v. 2, no. 2, p. 205–214. doi:10.1017/S0956536100000523.

Andrefsky, Jr., W., 2009, The analysis of stone tool procurement, production and maintenance: Journal of Archaeological Research, v. 17, no. 1, p. 65–103. doi:10.1007/s10814-008-9026-2.

Aoyama, K., 2001, Ritos de plebeyos mayas en la Cueva Gordon no. 3 de Copán (Honduras) durante el periodo Clásico: Análisis de las microhuellas de uso sobre la litica menor de obsidiana: Mayab, v. 14, p. 5–16.

Aoyama, K., 2009, Elite Craft Producers, Artists, and Warriors at Aguateca: Lithic Analysis: Salt Lake City, University of Utah Press, Monographs of the Aguateca Archaeological Project First Phase, v. 2, 210 p.

Awe, J.J., Griffith, C., and Gibbs, S., 2005, Cave stelae and megalithic monuments in western Belize, *in* Brady, J.E., and Prufer, K.M., eds., In the Maw of the Earth Monster: Mesoamerican Ritual Cave Use: Austin, University of Texas Press, p. 223–248.

Bassie-Sweet, K., 1991, From the Mouth of the Dark Cave: Commemorative Sculpture of the Late Classic Maya: Norman, University of Oklahoma Press, 287 p.

Behm, J.A., 1983, Flake concentrations: Distinguishing between flint-working activity areas and secondary deposits: Lithic Technology, v. 12, no. 1, p. 9–16.

Bonor, J.L., and Martínez Klemm, C., 1995, Trabajos recientes en la región de Caves Branch, Distrito de el Cayo, Belice: V Encuentro Internacional Investigadores de la Cultura Maya, v. 4, p. 250–267.

Brady, J.E., 1989, An investigation of Maya ritual cave use with special reference to Naj Tunich, Petén, Guatemala [Ph.D. thesis]: Los Angeles, University of California, 478 p.

Brady, J.E., and Prufer, K.M., 1999, Caves and crystalmancy: Evidence for the use of crystals in ancient Maya religion: Journal of Anthropological Research, v. 55, no. 1, p. 129–144.

Brady, J.E., and Prufer, K.M., eds., 2005, In the Maw of the Earth Monster: Mesoamerican Ritual Cave Use: Austin, University of Texas Press, 438 p.

Braswell, G.E., Clark, J.E., Aoyama, K., McKillop, H.I., and Glascock, M.D., 2000, Determining the geological provenance of obsidian artifacts from the Maya region: A test of the efficacy of visual sourcing: Latin American Antiquity, v. 11, no. 3, p. 269–282.

Brown, L.A., 2000, From discard to divination: Demarcating the sacred through the collection and curation of discarded objects: Latin American Antiquity, v. 11, no. 4, p. 319–334.

Chase, D.Z., and Chase, A.F., 1996, Maya multiples: Individuals, entries, and tombs in structure A34 of Caracol, Belize: Latin American Antiquity, v. 7, no. 1, p. 61–79.

Chiarulli, B., and Barrick, S., 1997, Analysis of lithic material associated with Tomb 1 from Chau Hiix: Society for American Archaeology Conference, 62nd Annual Meeting, Nashville, Tennessee, Abstracts, 38 p.

Clark, J.E., 1991, Modern Lacandon lithic technology and blade workshops, *in* Hester, T.R., and Shafer, H.J., eds., Maya Stone Tools: Selected Papers from the Second Maya Lithic Conference: Madison, Prehistory Press, Monographs in World Archaeology No.1, p. 251–265.

Close, A.E., 1996, Carry that weight: The use and transportation of stone tools: Current Anthropology, v. 37, no. 3, p. 545–553.

Deal, M., and Hayden, B., 1987, The persistence of pre-Columbian lithic technology in the form of glassworking, *in* Hayden, B., ed., Lithic Studies among the Contemporary Highland Maya: Tucson, University of Arizona Press, p. 235–331.

Ferguson, J., and Gibbs, S.A., 1999, Report on the 1998 excavations at Actun Uayazba Kab, Roaring Creek Valley, Belize, *in* Awe, J.J., and Lee, D.F., eds., The Western Belize Regional Cave Project: A Report of the 1998 Field Season: Durham, Occasional Paper No. 2, Department of Anthropology, University of New Hampshire, p. 112–145.

Flannery, K.V., 1986, Guilá Naquitz: Archaic Foraging and Early Agriculture in Oaxaca, Mexico: Orlando, Academic Press, Studies is Archaeology, 538 p.

Freidel, D., Schele, L., and Parker, J., 1993, Maya Cosmos: Three Thousand Years on the Shaman's Path: New York, William Morrow, 543 p.

Gibbs, S.A., 1998, Human skeletal remains from Actun Tunichil Muknal and Actun Uayazba Kab, *in* Awe, J.J., ed., The Western Belize Regional Cave Project: A Report of the 1997 Field Season: Durham, Occasional Paper No. 1, Department of Anthropology, University of New Hampshire, p. 71–95.

Gifford, J.C., 1976, Prehistoric Pottery Analysis and the Ceramics of Barton Ramie in the Belize Valley: Cambridge, Harvard University Press, Memoirs of the Peabody Museum of Archaeology and Ethnology, v. 18, 359 p.

Girard, R., 1962, Los Mayas Eternos: Mexico City, Antigua Librería Robredo, 493 p.

Graham, E., McNatt, L., and Gutchen, M.A., 1980, Excavations at Footprint Cave, Caves Branch, Belize: Journal of Field Archaeology, v. 7, no. 2, p. 153–172.

Griffith, C.S., 1998, Excavations and salvage operations in Actun Tunichil Muknal and Actun Uayazba Kab, Roaring Creek Valley, Belize, *in* Awe, J.J., ed., The Western Belize Regional Cave Project: A Report of the 1997 Field Season: Durham, Occasional Paper No. 1, Department of Anthropology, University of New Hampshire, p. 39–69.

Hall, G.D., 1989, Realm of death: Royal mortuary customs and polity interaction in the Classic Maya lowlands [Ph.D. thesis]: Cambridge, Harvard University, 385 p.

Halperin, C.T., Garza, S., Prufer, K.M., and Brady, J.E., 2003, Caves and ancient Maya ritual use of *jute*: Latin American Antiquity, v. 14, no. 2, p. 207–219.

Hardy, J., 2009, Understanding functional and symbolic variation in rockshelters of the Caves Branch River Valley of Western Belize, Central America [M.A. thesis]: Oxford, University of Mississippi, 172 p.

Hayden, B., and Cannon, A., 1983, Where the garbage goes: Refuse disposal in the Maya Highlands: Journal of Anthropological Archaeology, v. 2, no. 2, p. 117–163. doi:10.1016/0278-4165(83)90010-7.

Healy, P.F., Emery, K., and Wright, L.E., 1990, Ancient and modern Maya exploitation of the *jute* snail (*Pachychilus*): Latin American Antiquity, v. 1, no. 2, p. 170–183.

Helmke, C.G.B., 2009, Ancient Maya cave usage as attested in the glyphic corpus of the Maya lowlands and the caves of the Roaring Creek Valley, Belize [Ph.D. thesis]: London, Institute of Archaeology, University College, 697 p.

Ishihara, R., 2008, Rising clouds, blowing winds: Late Classic Maya rain rituals in the Main Chasm, Aguateca, Guatemala: World Archaeology, v. 40, no. 2, p. 169–189. doi:10.1080/00438240802030001.

Kavountzis, E.G., 2009, Evaluating cave use through spatial analysis of animal remains from Maya caves in Guatemala and Belize [M.A. thesis]: Gainesville, University of Florida, 219 p.

Keeley, L.H., 1980, Experimental Determination of Stone Tool Uses: A Microwear Analysis: Chicago, University of Chicago Press, Prehistoric Archeology and Ecology series, 212 p.

Lewenstein, S.M., 1987, Stone Tool Use at Cerros: The Ethnoarchaeological Use-Wear Analysis: Austin, University of Texas Press, 228 p.

McAnany, P.A., and Peterson, P.A., 2004, Tools of the trade: Acquisition, use, and recycling of chipped stone, *in* McAnany, P.A., ed., K'axob: Ritual, Work, and Family in an Ancient Maya Village, Monograph 22: Los Angeles, Cotsen Institute of Archaeology, University of California, p. 279–305.

MacLeod, B., and Puleston, D.E., 1978, Pathways into darkness: The search for the road to Xibalba, *in* Robertson, M.G., and Jeffers, D.C., eds., Tercera Mesa Redonda de Palenque, v. 4: Monterey, Herald Peters, p. 71–77.

McNatt, L., 1996, Cave archaeology of Belize: Journal of Cave and Karst Studies, v. 58, no. 2, p. 81–99.

Michael, A.R., and Burbank, J.A., 2013, Excavations at Sapodilla Rockshelter, Caves Branch River Valley, *in* Wrobel, G.D., Morton, S.G., and Andres, C.R., eds., The Central Belize Archaeological Survey Project: A Report of the 2011 Field Season: East Lansing, Michigan, Belize Archaeological Research and Education Foundation, Occasional Report, no. 3, p. 20–37.

Moholy-Nagy, H., 1990, Misidentification of Mesoamerican lithic workshops: Latin American Antiquity, v. 1, no. 3, p. 268–279.

Moholy-Nagy, H., 1997, Middens, construction fill, and offerings: Evidence for the organization of Classic period craft production at Tikal, Guatemala: Journal of Field Archaeology, v. 24, no. 3, p. 293–313.

Morehart, C.T., 2005, Plants and caves in ancient Maya society, *in* Prufer, K.M., and Brady, J.E., eds., Stone Houses and Earth Lords: Maya Religion in the Cave Context: Boulder, University Press of Colorado, p. 167–185.

Morrow, T.M., 1996, Lithic refitting and archaeological site formation processes: A case study from the Twin Ditch site, Greene County, Illinois, *in* Odell, G.H., ed., Stone Tools: Theoretical Insights into Human Prehistory: New York, Plenum Press, Interdisciplinary Contributions to Archaeology series, p. 345–376.

Moyes, H., Awe, J.J., Brook, G.A., and Webster, J.W., 2009, The ancient Maya drought cult: Late Classic cave use in Belize: Latin American Antiquity, v. 20, no. 1, p. 175–206.

Patel, S., 2005, Pilgrimage and caves on Cozumel, *in* Prufer, K.M., and Brady, J.E., eds., Stone Houses and Earth Lords: Maya Religion in the Cave Context: Boulder, University of Colorado Press, p. 91–112.

Pendergast, D.M., 1971, Excavations at Eduardo Quiroz Cave, British Honduras (Belize): Toronto, Royal Ontario Museum, Art and Archaeology Occasional Paper No. 21, 123 p.

Pendergast, D.M., 1974, Excavations at Actun Polbilche, Belize: Toronto, Royal Ontario Museum, Archaeology Monograph No. 1, 103 p.

Peterson, P.A., 2006, Ancient Maya ritual cave use in the Sibun Valley, Belize [Ph.D. thesis]: Boston, Boston University, 339 p. Reprinted 2006 as Austin, Association for Mexican Cave Studies, Bulletin 16, 148 p.

Pohl, M., 1983, Maya ritual faunas: Vertebrate remains from burials, caches, caves, and cenotes in the Maya lowlands, *in* Leventhal, R.M., and Kolata, A.L., eds., Civilization in the Ancient Americas: Essays in Honor of Gordon R. Willey: Albuquerque, University of New Mexico Press, p. 55–103.

Prufer, K.M., 2002, Communities, caves, and ritual specialists: A study of sacred spaces in the Maya Mountains of Southern Belize [Ph.D. thesis]: Carbondale, Southern Illinois University, 755 p.

Prufer, K.M., 2005, Shamans, caves, and the roles of ritual specialists in Maya society, *in* Brady, J.E., and Prufer, K.M., eds., In the Maw of the Earth Monster: Mesoamerican Ritual Cave Use: Austin, University of Texas Press, p. 186–222.

Prufer, K.M., and Brady, J.E., eds., 2005, Stone Houses and Earth Lords: Maya Religion in the Cave Context: Boulder, University of Colorado Press, 392 p.

Prufer, K.M., and Hurst, W.J., 2007, Chocolate and the underworld space of death: Cacao seeds from an Early Classic mortuary cave: Ethnohistory, v. 54, no. 2, p. 273–301. doi:10.1215/00141801-2006-063.

Prufer, K.M., Wanyerka, P., and Shah, M., 2003, Wooden figurines, scepters, and religious specialists in pre-Columbian Maya society: Ancient Mesoamerica, v. 14, no. 2, p. 219–236. doi:10.1017/S095653 6103142022.

Rissolo, D., 2003, Ancient Maya Cave Use in the Yalahau Region, Northern Quintana Roo, Mexico: Austin, Association for Mexican Cave Studies, Bulletin 12, 151 p.

Scheffler, T.E., 2008, The El Gigante Rock Shelter, Honduras [Ph.D. thesis]: University Park, The Pennsylvania State University, 434 p.

Sharon, D., ed., 2003, Mesas and Cosmologies in Mesoamerica: San Diego, San Diego Museum of Man, Museum Papers 42, 148 p.

Shelton, R., 2013, A contextual analysis of ceramics from the 2011 excavations of Sapodilla Rockshelter, Caves Branch River Valley, *in* Wrobel, G.D., Morton, S.G., and Andres, C.R., eds., The Central Belize Archaeological Survey Project: A Report of the 2011 Field Season: East Lansing, Belize Archaeological Research and Education Foundation, Occasional Report, no. 3, p. 38–51.

Sievert, A.K., 1992, Maya Ceremonial Specialization: Lithic Tools from the Sacred Cenote at Chichén Itzá, Yucatán: Madison, Prehistory Press, Monographs in World Archaeology 12, 162 p.

Stemp, W.J., 2001, Chipped Stone Tool Use in the Maya Coastal Economies of Marco Gonzalez and San Pedro, Ambergris Caye, Belize: Oxford, British Archaeological Reports International Series 935, 307 p.

Stemp, W.J., 2009, From a land down under: Stone tools from Maya caves in Belize: Maya at the Playa Conference, 3rd Annual Meeting, Palm Coast, Florida, Abstracts, 15 p.

Stemp, W.J., and Awe, J.J., 2014, Ritual use of obsidian from Maya caves in Belize: A functional and symbolic analysis, *in* Levine, M.N., and Carballo, D.M., eds., Obsidian Reflections: Symbolic Dimensions of Obsidian in Mesoamerica: Boulder, University Press of Colorado, p. 223–254.

Stemp, W.J., Helmke, C.G.B., and Awe, J.J., 2010, Evidence for Maya household subsistence and domestic activities: Use-wear analysis of the chipped chert assemblage from Pook's Hill, Belize: Journal of Field Archaeology, v. 35, no. 2, p. 217–234. doi:10.1179/009346910X 12707321520558.

Stemp, W.J., Wrobel, G.D., Awe, J.J., and Payeur, K., 2013, Stir it up, little darlin': The chipped stone assemblage from mixed deposits from Caves Branch Rockshelter, Belize: Canadian Journal of Archaeology, v. 37, no. 1, p. 123–167.

Tozzer, A.M., 1941, Landa's Relación de las Cosas de Yucatán: A translation: Cambridge, Papers of the Peabody Museum of American Archaeology and Ethnology, v. 18, 394 p.

Vogt, E.Z., and Stuart, D., 2005, Some notes on ritual caves among ancient and modern Maya, *in* Brady, J.E., and Prufer, K.M., eds., In the Maw of the Earth Monster: Studies of Mesoamerican Ritual Cave Use: Austin, University of Texas Press, p. 155–185.

Walker, W.H., 1995, Ceremonial trash?, *in* Skibo, J.M., Walker, W.H., and Nielsen, A.E., eds., Expanding Archaeology: Salt Lake City, University of Utah Press, Foundations of Archaeological Inquiry series, p. 67–79.

Wilson, D.C., 1994, Identification and assessment of secondary refuse aggregates: Journal of Archaeological Method and Theory, v. 1, no. 1, p. 41–68. doi:10.1007/BF02229423.

Wisdom, C., 1940, Chorti Indians of Guatemala: Chicago, University of Chicago Press, Publications in Anthropology, Ethnological Series, 490 p.

Wrobel, G.D., 2008, Report on the Caves Branch Rockshelter excavations: 2006 and 2007 field seasons, *in* Helmke, C.G.B., and Awe, J.J., eds., The Belize Valley Archaeological Reconnaissance Project: A Report of the 2007 Field Season: Belmopan, Institute of Archaeology, National Institute of Culture and History, p. 1–19.

Wrobel, G.D., Morton, S., and Andres, C.R., 2010, An introduction to the first season of the Caves Branch Archaeological Survey, *in* Morris, J., Jones, S., Awe, J., Thompson, G., and Badillo, M., eds., Archaeological Investigations in the Eastern Maya Lowlands: Papers of the 2009 Belize Archaeology Symposium: Belmopan, Institute of Arhaeology, Research Reports in Belizean Archaeology, v. 7, p. 73–84.

Wrobel, G.D., and Shelton, R., 2011, Preliminary salvage operations at Sapodilla Rockshelter, *in* Andres, C.R., and Wrobel, G.D., eds., Report on the Caves Branch Archaeological Survey Project, Summer 2010 Field Season: Oxford, Mississippi, Belize Archaeological Research and Education Foundation, Occasional Report, no. 2, p. 18–40.

Wrobel, G.D., Shelton, R., Morton, S.G., Lynch, J., and Andres, C., 2013, The view of Maya cave ritual from Overlook Rockshelter, Caves Branch River Valley, Central Belize: Journal of Cave and Karst Studies, v. 75, no. 2, p. 126–135. doi:10.4311/2011AN0233.

Wrobel, G.D., and Tyler, J.C., 2006, Revisiting Caves Branch Rockshelter: Results of the 2005 excavations, *in* Helmke, C.G.B., and Awe, J.J., eds., The Belize Valley Archaeological Reconnaissance Project: A Report of the 2005 Field Season: Belmopan, Institute of Archaeology, National Institute of Culture and History, p. 1–10.

Wrobel, G.D., Tyler, J., Hardy, J., 2007, Rockshelter excavations in the Caves Branch River Valley, *in* Morris, J., Jones, S., Awe, J., and Helmke, C., 2007, Archaeological Investigations in the Eastern Maya Lowlands: Papers of the 2007 Belize Archaeology Symposium: Belmopan, Institute of Archaeology, Research Reports in Belizean Archaeology, v. 4, p. 187–196.

K.J. Knierim, E.D. Pollock, P.D. Hays, J. Khojasteh – Using stable isotopes of carbon to investigate the seasonal variation of carbon transfer in a northwestern Arkansas cave. *Journal of Cave and Karst Studies,* v. 77, no. 1, p. 12–27. DOI: 10.4311/2011ES0264

USING STABLE ISOTOPES OF CARBON TO INVESTIGATE THE SEASONAL VARIATION OF CARBON TRANSFER IN A NORTHWESTERN ARKANSAS CAVE

Katherine J. Knierim[1], Erik D. Pollock[2], Phillip D. Hays[1,3], and Jam Khojasteh[4]

Abstract: Stable-isotope analyses are valuable in karst settings, where characterizing biogeochemical cycling of carbon along groundwater flow paths is critical for understanding and protecting sensitive cave and karst water resources. This study quantified the seasonal changes in concentration and isotopic composition ($\delta^{13}C$) of aqueous and gaseous carbon species—dissolved inorganic carbon (DIC) and gaseous carbon dioxide (CO_2)—to characterize sources and transfer of these species along a karst flow path, with emphasis on a cave environment. Gas and water samples were collected from the soil and a cave in northwestern Arkansas approximately once a month for one year to characterize carbon cycling along a conceptual groundwater flow path. In the soil, as the DIC concentration increased, the isotopic composition of the DIC became relatively lighter, indicating an organic carbon source for a component of the DIC and corroborating soil DIC as a proxy for soil respiration. In the cave, a positive correlation between DIC and surface temperature was due to increased soil respiration as the organic carbon signal from the soil was transferred to the cave environment via the aqueous phase. CO_2 concentration was lowest in the cave during colder months and increased exponentially with increasing surface temperature, presumably due to higher rates of soil respiration during warmer periods and changing ventilation patterns between the surface and cave atmosphere. Isotopic disequilibrium between CO_2 and DIC in the cave was greatest when CO_2 concentration was changing during November/December and March/April, presumably due to the rapid addition or removal of gaseous CO_2. The isotopic disequilibrium between DIC and CO_2 provided evidence that cave CO_2 was a mixture of carbon from several sources, which was mostly constrained by mixture between atmospheric CO_2 and soil CO_2. The concentration and isotopic composition of gaseous and aqueous carbon species were controlled by month-to-month variations in temperature and precipitation and provided insight into the sources of carbon in the cave. Stable carbon isotope ratios provided an effective tool to explore carbon transfer from the soil zone and into the cave, identify carbon sources in the cave, and investigate how seasonality affected the transfer of carbon in a shallow karst system.

Introduction

The carbon cycle is one of the most energetic biogeochemical cycles on the planet. Understanding processes such as photosynthesis, respiration, dissolution, and precipitation that exchange carbon between reservoirs, including surface water, groundwater, bedrock, soil, biomass, and the atmosphere, is important for quantifying carbon cycling and has applications for carbon sequestration (Trautz et al., 2013), paleoclimate reconstruction (Spötl et al., 2005; Wong et al., 2011), and nutrient management (Lohse et al., 2009). Stable-isotope analysis is a useful tool for understanding the exchange of carbon between reservoirs, because biogeochemical reactions change isotopic compositions in predictable ways (Kendall, 1998). Carbon isotopes ($\delta^{13}C$) are particularly useful in karst settings, where characterizing biogeochemical cycling along groundwater flow paths is critical for understanding and protecting sensitive cave and karst water resources (Doctor et al., 2006; Graening and Brown, 2000; Katz et al., 1997; Lee and Krothe, 2001).

The amount of inorganically derived carbon in karst depends on groundwater pH, temperature, and the relative openness of the system for continuing input of carbon dioxide (CO_2) (Fairchild et al., 2006; Palmer, 2007). In an open system, as CO_2 in the soil zone reacts with and dissolves carbonate bedrock ($CaCO_3$), soil CO_2 is continuously replenished, but in a closed system, the CO_2 is ultimately consumed by reaction with $CaCO_3$ (Clark and Fritz, 1997; Palmer, 2007). Epigenetic dissolution by these

[1] Department of Geosciences, 216 Ozark Hall, University of Arkansas, Fayetteville, AR 72701, USA
[2] University of Arkansas Stable Isotope Lab, 850 W. Dickson Street, University of Arkansas, Fayetteville, AR 72701, USA
[3] U.S. Geological Survey, Arkansas Water Science Center, 700 W. Research Center Blvd., Fayetteville, AR 72701, USA
[4] Educational Statistics and Research Methods Program, 324 Graduate Education Building, University of Arkansas, Fayetteville, AR 72701, USA

processes occurs in the absence of deep sources of acidity that are found in hypogene systems (Palmer, 2007). The concentration and isotopic composition of dissolved inorganic carbon (DIC) is controlled by combined soil CO_2 and bedrock $CaCO_3$ inputs. DIC concentration for closed systems will be lower and δ^{13}C-DIC will be enriched in ^{13}C (i.e., heavier) because of a greater proportion of bedrock-derived carbon compared to open systems (Clark and Fritz, 1997; Fairchild et al., 2006). Carbon-isotope fractionation results from exchange of gaseous CO_2 and aqueous DIC, which is dominated by bicarbonate (HCO_3^-) between pH of 6.4 and 10.3, and isotopic enrichment $\left(\varepsilon^{13}C_{HCO_3\text{-}CO_2(g)}\right)$ is approximately 7.9‰ at 25 °C (Clark and Fritz, 1997).

Inorganic carbon from the atmosphere and soil zones can be transferred into the cave environment via gaseous or aqueous phases; atmospheric CO_2 can be drawn into caves by temperature and pressure contrasts (Kowalczk and Froelich, 2010; Palmer, 2007), soil CO_2 can sink into caves via fractures in bedrock (Palmer, 2007), and CO_2 can degas from infiltrating drip water when the water is supersaturated with aqueous CO_2 compared to gaseous CO_2 in the cave atmosphere (Spötl et al., 2005). How these carbon sources are transferred in to and out of the cave controls the geochemistry of the cave atmosphere and water (Tooth and Fairchild, 2003). For example, prior calcite precipitation is a mechanism distinct from rock-water interaction that can control calcium (Ca) and magnesium (Mg) concentrations due to CO_2 degassing in voids, causing calcite precipitation along the groundwater flow path prior to entry into the cave (Spötl et al., 2005; Tooth and Fairchild, 2003; Wong et al., 2011). In karst, characterizing inorganic carbon sources and transformations helps define heterogeneous groundwater flow paths for meteoric water as it flows through the soil zone, epikarst, and into groundwater aquifers (Lee and Krothe, 2001).

Karst hydrogeology dominates northwestern Arkansas, and intense agricultural activities and rapid population growth in the region have led to degraded water quality (Davis et al., 2000; Graening and Brown, 2000). Nationally, Arkansas is ranked second in broiler-chicken production and fourth in turkey production, and three of the top five counties in Arkansas for agricultural sales are in the northwestern region of the state (U.S. Department of Agriculture, 2002; U.S. Department of Agriculture, 2007). Organic matter, nutrients, and bacteria from animal waste can contribute to non-point-source pollution of surface water and groundwater (Boyer and Pasquarell, 1999; Pronk et al., 2006), especially in karst, where direct connections between the surface and subsurface cause rapid transfer of contaminants into springs, caves, and groundwater aquifers (Davis et al., 2000; Graening and Brown, 2000; Johnson, 2008). To better protect these sensitive karst systems, the carbon transfer, which is ubiquitous in karst, needs to be better quantified because of the close linkages between inorganic and organic carbon reservoirs (Lohse et al., 2009; Winston, 2006).

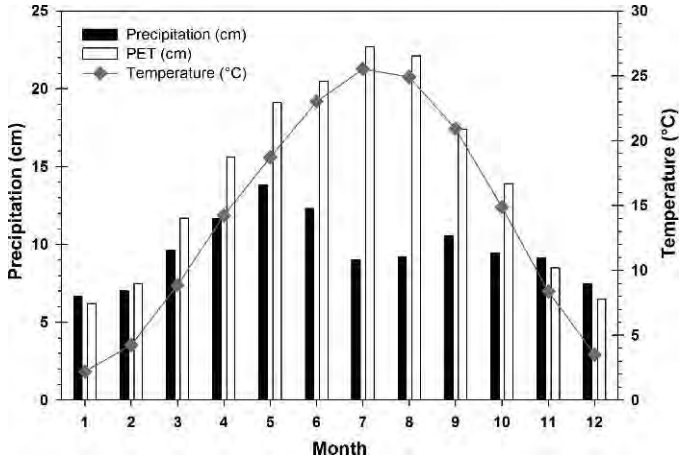

Figure 1. Monthly temperature and precipitation averages based on records from 1895 to 2009 for the Northwest Arkansas Division (National Oceanic and Atmospheric Administration, 2009). Potential evapotranspiration (PET) was calculated by Brye et al. (2004) using a modified form of the Penman-Montieth equation.

Compared to the body of work from, for example, Ireland (Baldini et al., 2006; Baldini et al., 2008; Tooth and Fairchild, 2003) and Texas (Breecker et al., 2012; Wong and Banner, 2010; Wong et al., 2011), little work has been completed in northwestern Arkansas on inorganic carbon transfer. This study provides quantification of approximately monthly changes in concentration and isotopic composition of aqueous DIC and gaseous CO_2 carbon species in a shallow karst hydrologic system and characterization of source inputs and transformations of these carbon species along a conceptual groundwater flow path, with emphasis on behaviors in a cave environment in northwestern Arkansas. Year-long data sets are particularly useful in areas like Arkansas where water quality changes throughout the year due to seasonal variation in temperature and precipitation (Davis et al., 2000; Winston, 2006).

Study Site

The study site is located in the southern portion of the Ozark Plateau physiographic province, which receives an average 112 cm of precipitation annually (Adamski et al., 1995). Annual precipitation shows a bimodal distribution (Fig. 1); precipitation peaks in May with a monthly average of 13.8 cm, and a second, lower maximum typically occurs in September with a monthly average of 10.5 cm (National Oceanic and Atmospheric Administration, 2009). Average summer air temperature (June, July, August) is 24.5 °C and winter (December, January, February) is 3.3 °C (National Oceanic and Atmospheric

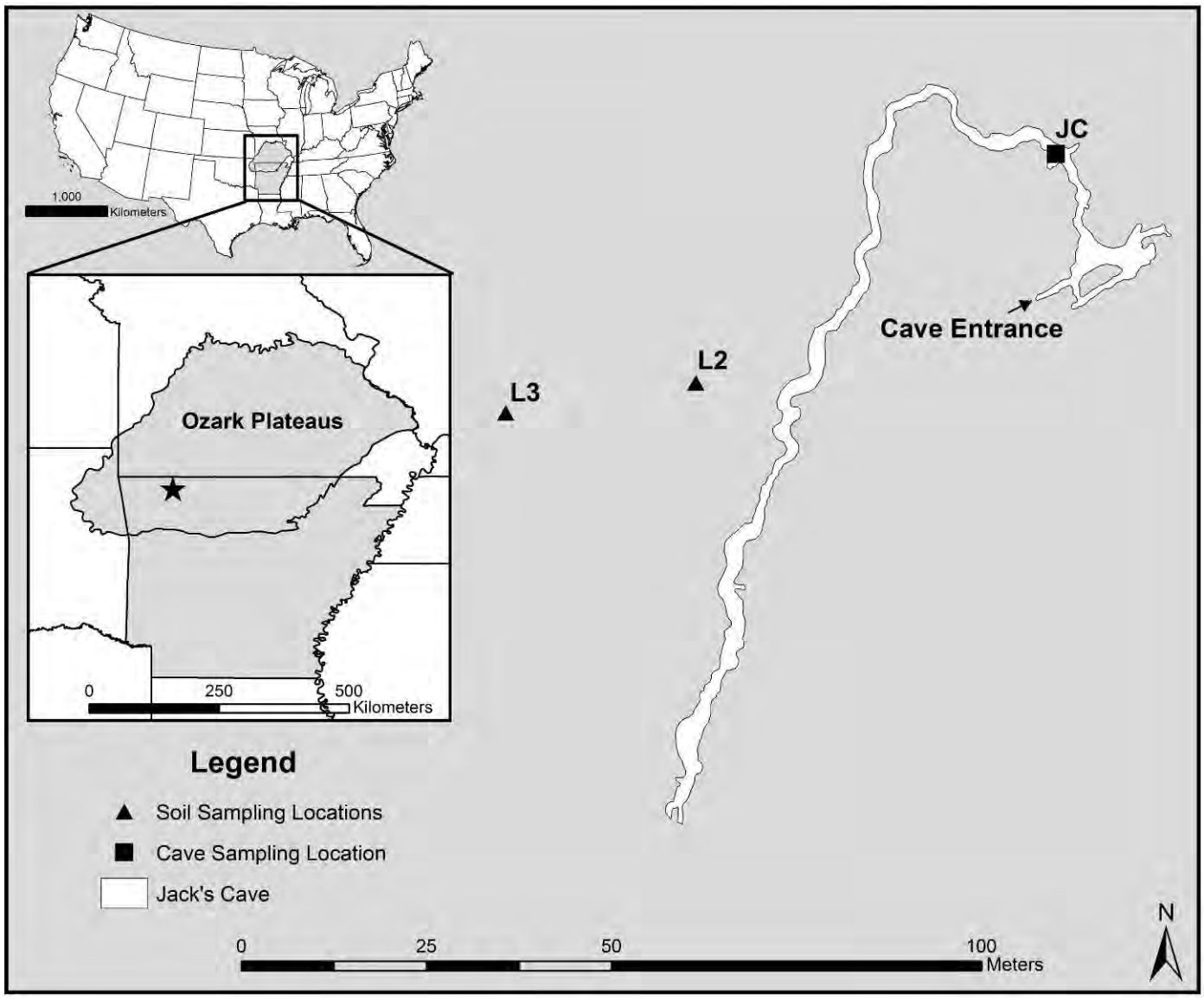

Figure 2. The study area is located in the southern part of the Ozark Plateaus in northwestern Arkansas (star). Lysimeters were installed in the soil above the cave (L2 and L3). Infiltrating water collects in a drip-water pool (JC) in the main room of Jacks's Cave and flows along the cave passage towards the southwest.

Administration, 2009). Potential evapotranspiration (PET) follows seasonal temperature patterns, being highest during the summer and lowest during the winter (Brye and West, 2004; Fig. 1).

The Ozarks in the study area consist of Paleozoic carbonate and clastic lithologies incised by streams to create valleys (Adamski et al., 1995). The lithostratigraphy at the study site, located in northwestern Arkansas (Fig. 2), includes Mississippian and Ordovician age bedrock; Devonian and Upper Ordovician units are missing due to local thinning on the flanks of an anticline to the south (Johnson, 2008). Higher hills are capped by Mississippian limestone of the Boone Formation, which includes the St. Joe Member. The entrance to Jack's Cave is a fracture in the Ordovician Kings River Sandstone Member (less than 10 m thick) of the Everton Formation and the cave is developed in an underlying Everton Formation dolomite unit. Jack's Cave is representative of the physical and chemical hydrogeology of caves and karst in northwestern Arkansas. The morphology of most caves in the Ozarks is that of single passages controlled by joints that terminate in narrowing, sediment-filled rooms (Taylor et al., 2009).

The study site is a mix of forest and pasture. Cattle were grazed on the property until the 1990s, when efforts to restore the native ecosystem were initiated and agricultural activities ceased. Open areas are mowed yearly to stimulate growth of native grasses and disrupt encroachment by herbaceous and woody plants. Soils are very gravely, silty

loam, and thickness varies depending on slope, but is generally less than 1 to 2 m (Natural Cooperative Soil Survey, 2008).

Meteoric water recharges the shallow groundwater system at the site via diffuse flow through the soil and bedrock matrix and rapid flow via fractures in the limestone and sandstone (Knierim et al., 2011). Numerous springs discharge from the base of the St. Joe Member where the Kings River Sandstone Member perches infiltrating water. Soil water above Jack's Cave infiltrates through the Kings River Sandstone Member caprock along fractures, collects in a small drip-water pool approximately 1 m wide by 0.1-m deep, and flows along the cave passage from the in-cave sampling site JC initially towards the northwest, then towards the southwest (Fig. 2). This inflow to the cave typically ceases during the period of high evapotranspiration in the summer months (Fig. 1). Direct hydrologic connections between the soil and cave were observed at the study site during a separate experiment using isotopic tracers; travel times for water released at the surface and observed in the drip-water pool ranged from approximately 0.5 hr to 22 hr during a dry period in early September, depending on the rate of discharge (Knierim et al., 2011).

The discharge points of the cave waters have not been identified (Knierim, 2009). Springs discharging below the cave level from the dolomite units of the Everton Formation are typically smaller than those discharging above the St. Joe/Kings River contact. The lower and upper springs combine into surface drainages that flow south approximately 0.8 km to Rockhouse Creek or east approximately 1 km to the Kings River. The Kings River regionally controls base level at approximately 335 m above sea level.

Materials and Methods

Sample Collection and Laboratory Analysis

Gas and water samples were collected from downslope (L2) and upslope (L3) soil lysimeters installed less than 1-m deep and in the cave (JC) approximately once a month from August 2008 until July 2009 to characterize carbon cycling along a conceptual groundwater flow path (Fig. 2). Meteoric water flows through the soil, along fractures in the Kings River Sandstone Member, and into Jack's Cave (Knierim et al., 2011). Therefore, samples collected from L2 and L3 are representative of soil gas and water above the cave. Samples were not collected from all locations on the same date because of time constraints.

For the analysis of the isotopic composition of gaseous CO_2 ($\delta^{13}C$-CO_2), gas samples were collected from L2, L3, and JC into pre-combusted 100 mL serum vials purged with helium. Soil-gas samples were pumped from the lysimeters, and cave gas samples were collected adjacent to the drip-water pool at site JC (Fig. 2). During sample collection, a Vaisala CARBOCAP handheld carbon dioxide meter was used to measure the concentration of CO_2. Gas samples were analyzed for $\delta^{13}C$-CO_2 at the University of Arkansas Stable Isotope Laboratory in Fayetteville, Arkansas, on a gas-chromatography combustion isotope-ratio mass spectrometer (IRMS).

Water samples were pumped from lysimeters at sites L2 and L3 and collected from the drip-water pool at site JC. Physical parameters, including water temperature, conductivity, and pH, were measured in the cave pool during sample collection. Water samples for isotopic analyses of DIC ($\delta^{13}C$-DIC) were filtered through 0.7-μm filters into pre-combusted total organic carbon vials and chilled to 4 °C until samples were analyzed at the Colorado Plateau Stable Isotope Laboratory in Flagstaff, Arizona, on a total organic carbon analyzer interfaced to an IRMS following a procedure modified from St-Jean (2003). Water samples for cations and anions were collected in high-density polyethylene bottles provided by the Arkansas Department of Environmental Quality and analyzed at their laboratory in Little Rock, Arkansas. Cations were analyzed on an inductively coupled plasma mass spectrometer; only the Ca and Mg data will be discussed.

Bedrock samples from the Mississippian Boone Formation and the Ordovician Everton Formation were collected from above and within the cave, respectively, for carbon isotopic analysis ($\delta^{13}C$-$CaCO_3$). Samples were analyzed at the University of Arkansas on a Delta Plus XP isotope-ratio mass spectrometer interfaced with a Gas Bench II universal headspace sampler (Révész et al., 2002). All carbon-isotope ratios are reported relative to the Vienna Peedee Belemnite (Coplen, 1996). See Knierim (2009) for further details on sampling and analysis procedures.

Data Analysis

One-way Analysis of Variance (ANOVA) and Tukey's post-hoc tests were completed to assess differences in concentration and isotopic composition of carbon species among sites (SAS 9.3). Correlation coefficients were calculated between the concentration and isotopic composition of each carbon species (CO_2 versus $\delta^{13}C$-CO_2 and DIC versus $\delta^{13}C$-DIC) for the soil and cave sites (SAS 9.3). All correlation analyses were completed using an alpha of 0.05, and *p*-values are provided where correlations were significant. Average values are reported with plus or minus one standard deviation.

The concentrations and stable isotope ratios of CO_2 and DIC were compared with meteorological data to characterize approximately monthly changes in carbon cycling. Daily minimum surface temperature and daily precipitation data from a NOAA weather station at Huntsville, Arkansas, located approximately 23 km southwest of the study site, were averaged for the 14-day period prior to and including the date of sample collection (Fig. 3). The 14-day averages eliminated short-term fluctuations in temperature and precipitation. Linear and exponential regressions were

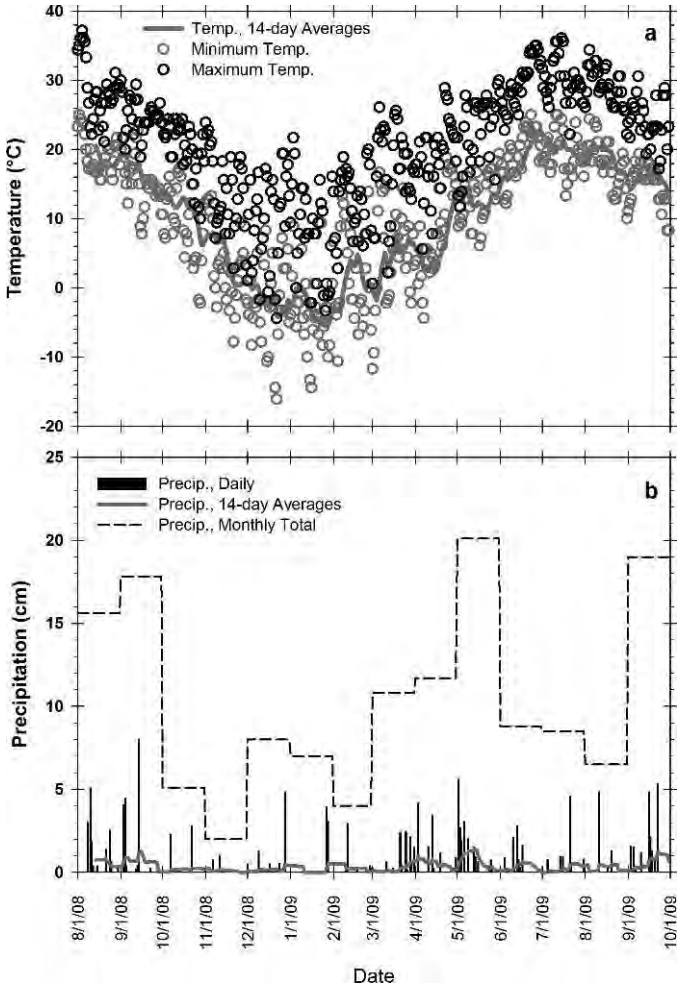

Figure 3. During the period of the study from 2008 to 2009, temperature and precipitation followed patterns similar to historical averages (Fig. 1). 14-day moving averages of daily precipitation and minimum daily temperature are shown because these are the data, taken for the sample dates, which are used in calculations, Figures 5 and 8, and the tables.

completed on the geochemical and isotopic data and compared to the 14-day temperature and precipitation averages to determine any relationships. Regressions were focused on monthly blocks of time because northwestern Arkansas experiences seasonal changes in temperature and precipitation (Fig. 1). Important regressions between carbon and temperature /precipitation data are discussed, but were not explicitly tested for statistical significance.

Equilibrium calculations of carbon species were completed for the cave water and atmosphere. Calcite saturation was calculated using the log ratio of the ion activity product to the solubility product (Palmer 2007), where the activities for Ca and CO_3^{2-} were calculated using the Debye-Hückel equation for solutions with ionic strengths less than 0.1 (Fetter, 2001). The differences in isotopic composition between DIC in the cave pool and CO_2 in the cave atmosphere $\left(\Delta^{13}C_{DIC\text{-}CO_2(g)}\right)$ were compared to temperature and pH dependent equilibrium fractionation values, where $\Delta^{13}C_{DIC-CO_2(g)}$ is an approximation for isotopic enrichment $\left(\varepsilon^{13}C_{HCO_3\text{-}CO_2(g)}\right)$ and DIC is assumed to be dominated by HCO_3^- (Clark and Fritz, 1997). Using the proportion of individual carbon species as controlled by pH and temperature, the gross isotopic enrichment between DIC and CO_2 $\left(\varepsilon^{13}C_{DIC\text{-}CO_2(g)}\right)$ was also calculated (Clark and Fritz, 1997; Peyraube et al., 2013) for comparison to the empirically derived $\varepsilon^{13}C_{HCO_3\text{-}CO_2(g)}$ values.

Possible sources of cave CO_2 were assessed using a concentration-dependent, two-component mixing model (Faure, 1986) that constrains the isotopic composition of end-member CO_2 sources (i.e., $\delta^{13}C\text{-}CO_2$) using the following equations:

$$\delta_{cave} = \frac{a}{X_{cave}} + b, \tag{1}$$

where

$$X_{cave} = f\,X_{atm} + (1-f)\,X_{end}, \tag{2}$$

$$a = \frac{X_{atm}\,X_{end}(\delta_{end} - \delta_{atm})}{X_{atm} - X_{end}}, \tag{3}$$

and

$$b = \frac{X_{atm}\,\delta_{atm} - X_{end}\,\delta_{end}}{X_{atm} - X_{end}}. \tag{4}$$

where X is the concentration of CO_2, δ is $\delta^{13}C\text{-}CO_2$, and f is the proportion of an end-member from 0 to 1, or no contribution to 100% contribution. See Faure (1986) for a full derivation of the equations.

One source of CO_2 to the cave was assumed to be atmospheric CO_2, with a CO_2 concentration (X_{atm}) of 380 ppm (Palmer, 2007) and an isotopic composition (δ_{atm}) of −7.7‰ (Faure and Mensing, 2005), so that the isotopic composition of the second end-member source (δ_{end}) was calculated at f equal to 0. Equation 1 was calculated iteratively to graphically find the two mixing lines that would bracket the observed CO_2 data. Concentration-dependent mixing models are important to use when the concentration of an element such as carbon varies between the two end-member sources, which can induce error in calculations of isotopic composition if a linear mixing model is used (Phillips and Koch, 2002).

RESULTS

CARBON DIOXIDE

Gaseous CO_2 concentrations ranged between 1,400 and 19,450 ppm in the soil, and L2 exhibited lower CO_2 than L3 (Table 1). Soil CO_2 was lowest from January through March, excluding one high value of 8,000 ppm for L2 in March (Fig. 4a). CO_2 increased at L3 between March and April. At L2, CO_2 decreased after a March increase and

Table 1. Geochemical and isotopic data for carbon species in the soil including carbon dioxide (CO_2) and dissolved inorganic carbon (DIC).

Sample Name	Date	$\delta^{13}C-CO_2$(‰)	CO_2 (ppm)	$\delta^{13}C-DIC$(‰)	DIC (mg L^{-1})	Calcium (mg L^{-1})	Magnesium (mg L^{-1})	Surface Temperature[a](°C)	Precipitation[b] (cm)
L2	08/21/08	…	…	−22.7	27.5	…	…	17.4	0.86
	09/11/08	…	…	−22.5	33.6	…	…	17.9	0.66
	09/25/08	…	…	−22.7	31.8	…	…	14.6	0.64
	11/05/08	…	11,560	…	…	…	…	7.5	0.01
	11/13/08	…	9,785	−18.3	19.2	…	…	7.2	0.14
	11/18/08	−16.3	9,670	…	…	…	…	3.0	0.13
	01/03/09	…	1,530	−21.7	11.5	8.6	0.97	−1.8	0.38
	02/08/09	−24.5	1,690	−22.1	11.6	5.6	0.65	−0.4	0.50
	03/15/09	−19.7	8,000	−22.9	15.0	5.8	0.65	4.8	0.05
	04/07/09	−24.1	1,400	−22.5	12.6	5.7	0.62	2.6	0.79
	06/02/09	−16.4	3,560	−20.5	10.6	6.1	0.68	15.4	0.11
	07/06/09	−21.8	11,750	−16.3	7.2	…	…	20.9	0.05
L3	09/11/08	…	…	−21.1	13.6	…	…	17.9	0.66
	09/25/08	…	17,330	…	…	…	…	14.6	0.64
	11/05/08	…	11,500	…	…	…	…	7.5	0.01
	11/13/08	…	11,765	…	…	…	…	7.2	0.14
	01/03/09	−26.4	8,320	−21.1	4.5	…	…	−1.8	0.38
	02/08/09	−19.4	7,400	−20.1	3.5	…	…	−0.4	0.50
	03/15/09	−21.0	8,000	−22.0	5.9	12.5	2.58	4.8	0.05
	04/07/09	−24.3	15,060	…	…	…	…	2.6	0.79
	07/06/09	−20.4	19,450	−20.2	9.6	…	…	20.9	0.05

[a] Minimum daily temperature data at the surface were averaged over the 14–day period prior to and including the date of sample collection.
[b] Daily precipitation data were averaged over the 14–day period prior to and including the date of sample collection.
Note: CO_2 data are from soil gas and all other data are aqueous species in the soil water.

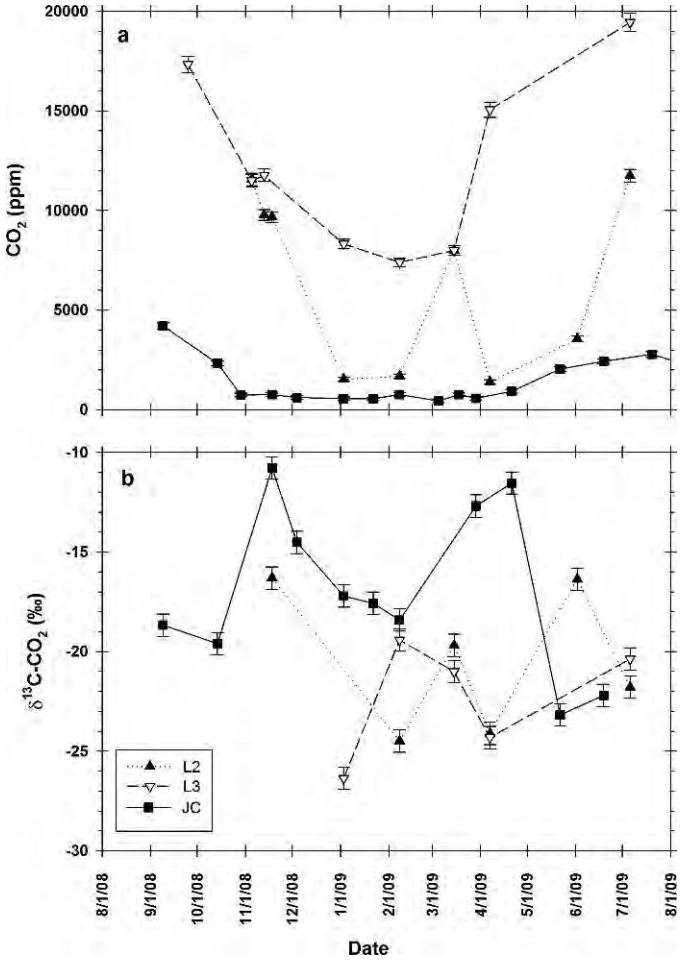

Figure 4. Gaseous soil (L2 and L3) and cave (JC) CO_2 concentration and δ^{13}C-CO_2 from August 2008 to August 2009. Error bars show analytical precision.

began to increase again by June. CO_2 showed a positive, exponential relationship with surface temperature at L3 (r^2 = 0.68) and a weaker relationship at L2 (r^2 = 0.30, Fig. 5a). Soil CO_2 concentration decreased exponentially in L2 with increasing precipitation (r^2 = 0.75), but no such relationship was observed in L3 (Fig. 5b).

Soil δ^{13}C-CO_2 ranged between −16.3‰ and −26.4‰ at both soil sites (Fig. 4b). δ^{13}C-CO_2 became lighter with increasing precipitation in L2 only (r^2 = 0.51, Fig. 5d). Samples from June to November (summer through fall) at L2 and L3 generally had greater CO_2 concentrations and the δ^{13}C-CO_2 values became more negative with increasing CO_2, but the relationship was not statistically significant (Table 1). The concentration of CO_2 decreased between January and April (winter through spring), but did not clearly correlate with isotopic composition.

Atmospheric CO_2 concentrations at in-cave site JC ranged from 440 to 4,210 ppm (Table 2). Average CO_2 was 662 ppm from November to April and 2,668 ppm from May to October. CO_2 changed rapidly between seasons; CO_2 decreased by 1,570 ppm between October and November and increased by 1,120 ppm between April and May (Fig. 4a). CO_2 was lowest during the colder months and increased exponentially with increasing surface temperature (r^2 = 0.83; Fig. 5a). No relationship was observed between precipitation and CO_2 in the cave (Fig. 5b).

Cave δ^{13}C-CO_2 ranged between −10.8‰ and −23.2‰ (Table 2). The heaviest δ^{13}C-CO_2 compositions occurred in November and April (Fig. 4b). In the cave, δ^{13}C-CO_2 generally became lighter with increasing surface temperature (Fig. 5c) and no relationship with precipitation was observed (Fig. 5d). Higher CO_2 concentration generally corresponded with lighter isotopic composition (Fig. 6), but the relationship was not statistically significant.

CO_2 concentration was significantly different among all sites; CO_2 was highest at L3 and lowest at JC ($F(2, 31) = 31.42$, $p < 0.01$). The isotopic composition of CO_2 was significantly heavier at JC than L3 ($F(2, 19) = 3.98$, $p < 0.05$). CO_2 concentration was generally lowest in the cave, and the δ^{13}C-CO_2 was lightest in the soil (Fig. 6).

The δ^{13}C-CO_2 compositions observed in the soil and cave were constrained by mixing between atmospheric CO_2 (approximately 380 ppm and −7.7‰) and two lighter end-member sources with δ^{13}C-CO_2 compositions of −14‰ and −30‰, based on iterative calculations using equations 1 through 4 (Fig. 6). Note that the isotopic compositions of −14‰ and −30‰ bracket all the δ^{13}C-CO_2 values observed in the soil at L2 and L3 and all but two values observed in the cave at JC (January and February samples). For comparison, if the minimum and maximum observed soil δ^{13}C-CO_2 compositions were used in the mixing model (i.e., −16.3‰ and −26.4‰), then more of the observed isotopic compositions from this study would lie outside of the mixing lines.

DISSOLVED INORGANIC CARBON

Dissolved inorganic carbon concentrations ranged between 3.5 and 33.6 mg L^{-1} in soil-water samples (Table 1). L2 consistently had higher DIC concentrations than L3, and both soil sites showed a decrease in concentration between September and January (Fig. 7a). DIC concentration was exponentially correlated with surface temperature in L3 (r^2 = 0.85; Fig. 8a), similar to the observations of CO_2. DIC at L2 did not show a correlation with surface temperature. No relationship between DIC in the soil and precipitation was observed (Fig. 8b).

Soil δ^{13}C-DIC ranged between −22.9‰ and −16.3‰ (average −21.1‰) and was lighter than average cave water DIC (−17.3‰, Fig. 7b). In L2, δ^{13}C-DIC became lighter with increasing precipitation (r^2 = 0.40; Fig. 8d), similar to changes in δ^{13}C-CO_2 at L2. An inverse relationship between seasonal DIC concentration and isotopic composition was observed in the soil in the combined data from L2 and L3 (Fig. 9); as DIC concentration increased, δ^{13}C-DIC values became more negative for samples from June

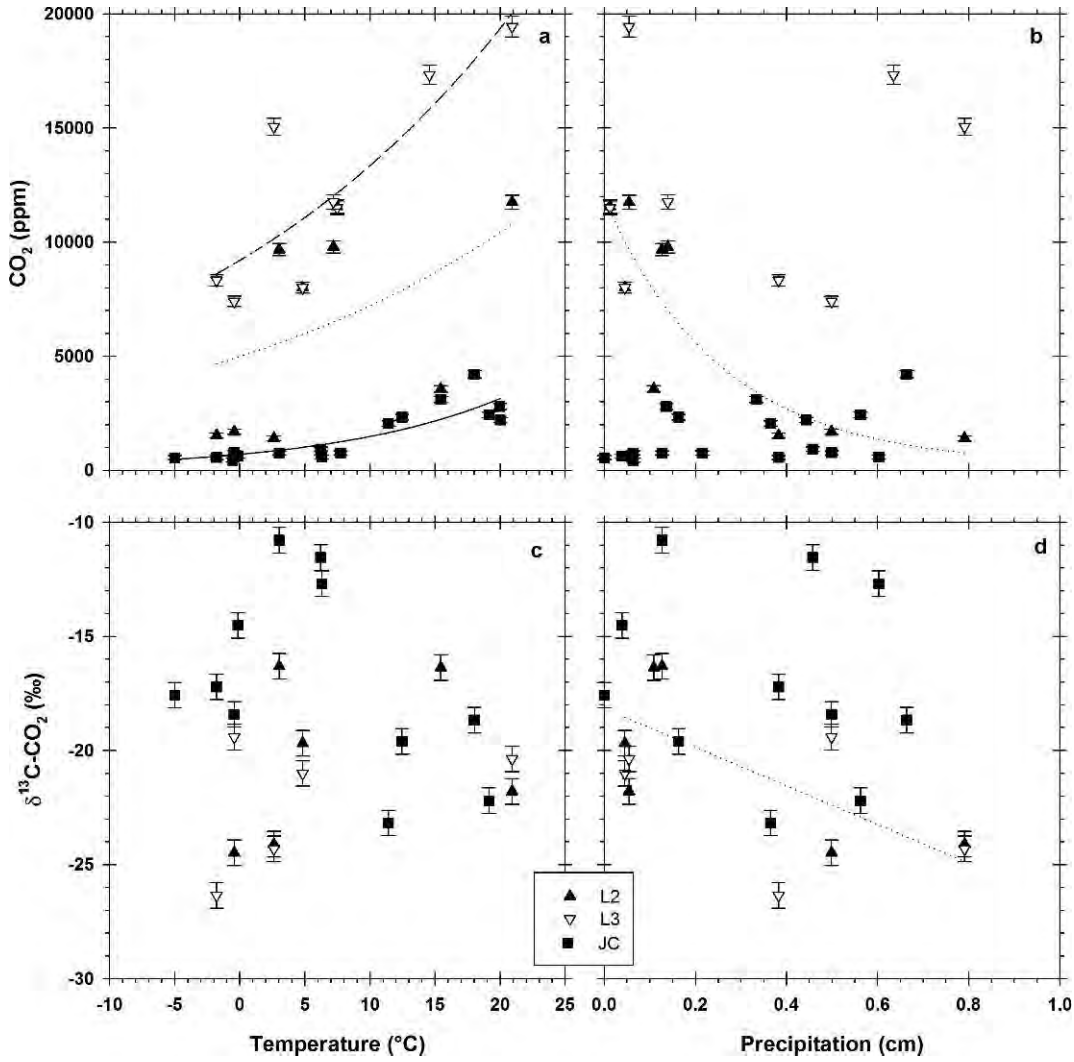

Figure 5. Gaseous soil (L2 and L3) and cave (JC) CO_2 concentration and δ^{13}C-CO_2 compared to surface temperature and precipitation. Regression lines: L2 = short-dash line; L3 = long-dash line; JC = solid line. See text for r^2 values. Error bars show analytical precision.

to November ($r^2 = 0.54$, $p < 0.05$) and January to April ($r^2 = 0.73$, $p < 0.01$) for all soil data.

DIC concentrations in the cave drip-water pool at site JC ranged between 2.0 and 21.7 mg L^{-1} (Table 2) and were generally lower than concentrations observed in the soil (Fig. 7a). Cave water DIC generally decreased from October to March, except for a high value of 21.7 mg L^{-1} in December (Fig. 7a). Cave water DIC increased exponentially with increasing surface temperature ($r^2 = 0.50$), excluding the high DIC value of 21.7 mg L^{-1} (Fig. 8a) that was excluded using the Grubb's outlier test (Z (13) = −2.86, $p < 0.05$). No relationship between DIC in the cave and precipitation was observed (Fig. 8b).

The δ^{13}C-DIC values in the cave ranged between −9.5‰ and −24.2‰ (Fig. 7b). Isotopic compositions in the fall and spring were typically lighter, with the September to November average −19.7‰ and the April to June average −20.9‰, than in winter, with the December to early March average −13.9‰. No relationship between δ^{13}C-DIC in the cave and air temperature (Fig. 8c) was observed. In the cave pool, δ^{13}C-DIC became lighter with increasing precipitation ($r^2 = 0.41$, Fig. 8d).

DIC concentration was significantly higher at L2 than JC or L3 (F (2, 25) = 8.72, $p < 0.01$), although not significantly different between L3 and JC. The isotopic composition of DIC was significantly heavier at JC than at L2 (F (2, 25) = 5.58, $p < 0.01$). DIC concentration was generally lowest in the cave and the δ^{13}C-DIC was lightest in the soil (Fig. 9).

The $\Delta^{13}C_{DIC\text{-}CO_2(g)}$ values in the cave, which are an approximation of gross isotopic enrichment, were between −12.7 and +5.1‰ (Fig. 10). Values for $\varepsilon^{13}C_{HCO_3\text{-}CO_2(g)}$ ranged from 8.9 to 9.3‰ and averaged 9.1‰ (Table 2), as controlled by cave water temperature (Clark and Fritz, 1997). Between pH of 6.4 and 10.3, DIC is dominated by HCO_3^- (Clark and Fritz, 1997). For example, HCO_3^-

Table 2. Geochemical and isotopic data for carbon species in the cave including carbon dioxide (CO_2) and dissolved inorganic carbon (DIC).

Date	Water Temperature (°C)	pH	$\delta^{13}C-CO_2$ (‰)	CO_2 (ppm)	$\delta^{13}C-DIC$ (‰)	DIC (mg L^{-1})	Calcium (mg L^{-1})	Magnesium (mg L^{-1})	Calcite Saturation	$\varepsilon^{13}C_{HCO_3\text{-}CO_2(g)}$ (‰)	Surface Temperature[a] (°C)	Precipitation[b] (cm)
09/09/08	…	…	−18.7	4,210	−21.8	4.7	…	…	−2.8[c]	9.0[c]	18.0	0.66
09/11/08	17.0	7.2	…	…	…	…	1.7	1.01	…	…	17.9	0.66
10/14/08	16.0	7.4	−19.6	2,330	−19.6	6.9	3.6	2.21	−2.2	8.9	12.5	0.16
10/29/08	…	…	…	750	…	…	…	…	…	…	6.2	0.21
11/18/08	14.9	7.9	−10.8	760	−17.7	5.7	11.9	5.94	−1.3	9.1	3.0	0.13
12/04/08	…	8.3	−14.5	620	−9.5	21.7	…	…	…	9.1	−0.2	0.04
01/03/09	14.9	7.7	−17.2	560	−15.2	2.6	1.9	1.17	−2.6	9.1	−1.8	0.38
01/22/09	14.5	7.0	−17.6	550	−15.8	2.6	…	…	…	9.1	−5.0	0.00
02/08/09	14.5	7.5	−18.4	770	−15.8	4.4	1.9	1.19	−2.6	9.1	−0.4	0.50
03/05/09	13.4	9.3	…	440	−13.4	2.0	…	…	…	9.2	−0.6	0.06
03/18/09	…	…	…	760	…	…	…	…	…	…	7.7	0.06
03/29/09	12.9	8.4	−12.7	580	−19.1	3.4	1.2	0.79	−2.0	9.3	6.3	0.60
04/21/09	13.0	9.8	−11.5	930	−24.2	4.2	1.1	0.86	−0.7	9.3	6.2	0.46
05/22/09	13.4	8.0	−23.2	2,050	−19.6	4.5	1.5	1.13	−2.2	9.2	11.4	0.36
06/19/09	14.1	9.4	−22.2	2,430	−18.9	4.3	12.2	4.70	0.1	9.2	19.1	0.56
07/20/09	14.4	8.9	…	2,790	−14.3	13.0	21.0	10.80	0.3	9.1	20.0	0.14
08/13/09	15.4	9.0	…	2,200	…	…	…	…	…	…	20.0	0.44
09/12/09	…	…	…	3,100	…	…	…	…	…	…	15.4	0.33

[a] Minimum daily temperature data at the surface were averaged over the 14-day period prior to and including the date of sample collection.
[b] Daily precipitation data were averaged over the 14-day period prior to and including the date of sample collection.
[c] To calculate calcite saturation and isotopic enrichment on 09/09/08, temperature and pH from 09/11/08 were used.
Note: CO_2 data are from the cave atmosphere and all other data are aqueous species in the cave pool.

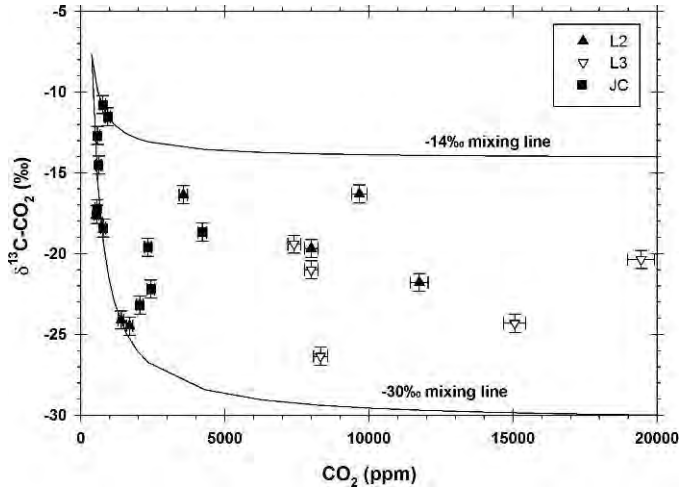

Figure 6. Gaseous soil (L2 and L3) and cave (JC) $\delta^{13}C$-CO_2 versus CO_2 concentration. The mixing lines represent mixing of atmospheric CO_2 (380 ppm and −7.7‰) with two lighter end-member sources calculated to be −14‰ and −30‰. Error bars show analytical precision.

composed 83 to 98% of DIC at JC. The $\varepsilon^{13}C_{DIC\text{-}CO_2(g)}$ (not shown) at JC ranged from 7.5 to 9.1‰ and averaged 8.4‰, based on pH, temperature, and carbonate equilibria (Clark and Fritz, 1997; Peyraube et al., 2013). The observed $\Delta^{13}C_{DIC\text{-}CO_2(g)}$ values were outside the range of equilibrium fractionation for either $\varepsilon^{13}C_{HCO_3\text{-}CO_2(g)}$ or $\varepsilon^{13}C_{DIC\text{-}CO_2(g)}$; and therefore, the simpler $\varepsilon^{13}C_{HCO_3\text{-}CO_2(g)}$ values were used to assess the degree of isotope disequilibrium between aqueous DIC and gaseous CO_2.

Cations and Physical Parameters

Soil water geochemistry data are discussed for L2 only, because L3 generally provided insufficient volume for full analyses. Generally, soil moisture was higher at L2, the downslope lysimeter, as compared to L3 upslope, based on field observations and the difficulty in collecting soil water samples from L3. In the soil water, Ca ranged between 5.6 and 8.6 mg L^{-1} and Mg from 0.62 to 0.97 mg L^{-1} (Table 1), and Mg to Ca ratios were mostly invariant at approximately 0.1.

In the cave, water in the pool at JC temperature averaged 14.6 °C ± 1.4 and pH averaged 8.2 ± 0.9 (Table 2). Ca and Mg concentrations changed seasonally, with the lowest concentrations between January and May. Cave water was generally undersaturated with respect to calcite as the saturation indices ranged from −2.8 to 0.3, with a median value of −2.1. Precipitation of calcite in the cave pool was not observed during the course of this study. Mg to Ca ratios ranged from 0.4 to 0.8 in the cave water.

Bedrock

The $\delta^{13}C$ isotopic composition of bedrock samples from the St. Joe Limestone Member of the Boone Formation

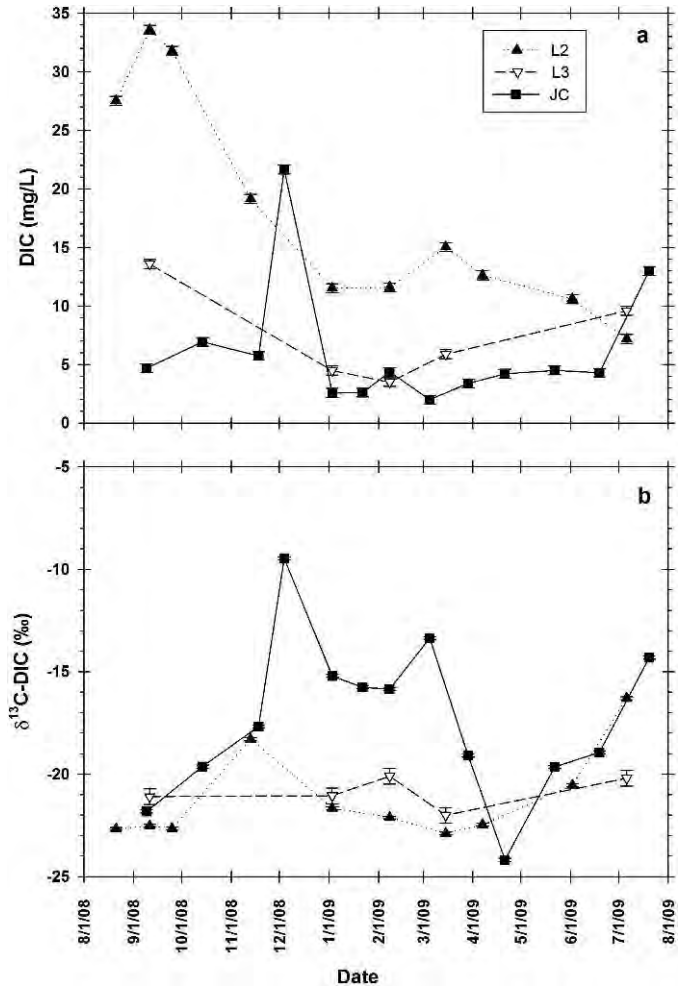

Figure 7. Aqueous soil (L2 and L3) and cave (JC) DIC concentration and $\delta^{13}C$-DIC composition from August 2008 to August 2009.

and from the Everton Formation averaged −1.4‰ (n = 2) and −3.7‰ ± 0.4 (n = 4), respectively. Samples collected previously from the Boone Formation in northwestern Arkansas ranged from 2.5 to 4.9‰ (Pollock, pers. comm.). Therefore, carbonate units in the Ozarks tend to be heavier, within the range of marine carbonates (Clark and Fritz, 1997).

Discussion

In a conceptual model of carbon inputs and transformations at the study site, aqueous DIC and gaseous CO_2 are transported into Jack's Cave from the soil zone, as represented by data from L2 and L3, with cave-atmosphere CO_2 also being sourced directly from the surface atmosphere (Fig. 11). The magnitude of different source inputs to the cave changed seasonally, as evidenced by the month-to-month variability of CO_2 and DIC concentrations and isotopic compositions during the study period (Figs. 4 and 7). The details of the conceptual model for carbon sources

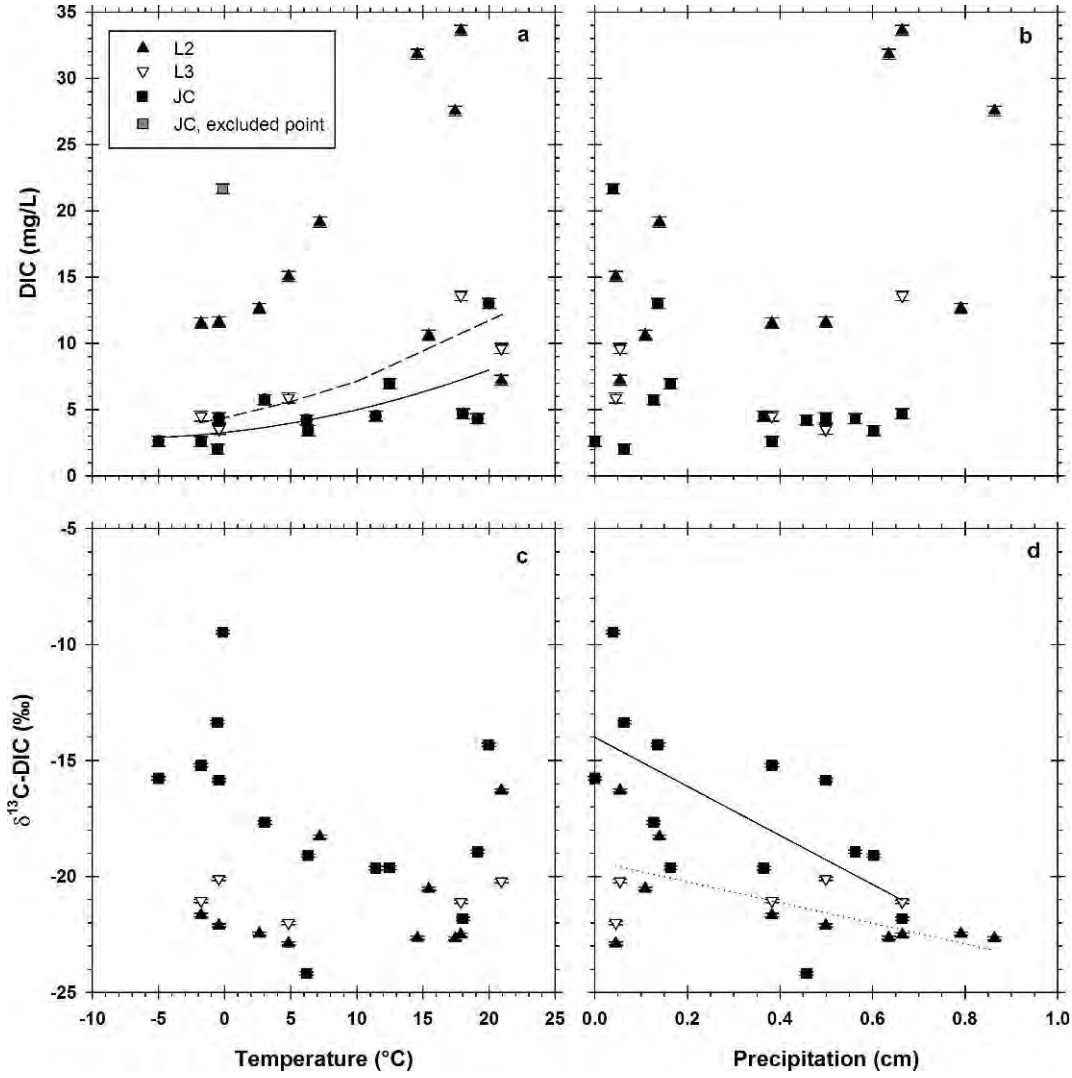

Figure 8. Aqueous soil (L2 and L3) and cave (JC) DIC concentration and δ^{13}C-DIC composition compared to surface temperature and precipitation. Regression lines: L2 = short-dash line; L3 = long-dash line; JC = solid line. See text for r^2 values. In 8a, one data point (gray) was excluded from the JC regression.

and transformations in this shallow karst system are discussed below.

SOIL

Qualitative differences in soil moisture between L2 and L3 contributed to how soil CO_2 was affected by changes in surface temperature and precipitation at the two locations. For example, L3 was generally drier, and CO_2 was more influenced by changes in surface temperature than at L2 (Fig. 5a). Surface temperature is a proxy for soil respiration; plants and microbes have greater respiration rates during the warmer months of the growing season (Davidson et al., 1998). Increased soil temperature explained 47% to 80% of the variation in soil respiration rate at a forested site in Massachusetts (Borken et al., 2003; Davidson et al., 1998), and in this study, surface temperature explained 68% of the variation in CO_2 concentration at L3, the drier of the two soil sites.

Soil temperature and water content can be confounding factors influencing seasonal variation in soil respiration rates because the two factors may covary (Davidson et al., 1998). L2 was often wetter following precipitation events, and soil CO_2 was influenced by the timing of precipitation (Fig. 5b and 5d). Increasing soil moisture may increase CO_2 flux due to oxidation of labile organic carbon following soil wetting, although the exact mechanism of carbon release is debated (Sponseller, 2007). Soil moisture can also decrease CO_2 flux at high water contents as diffusion of oxygen (and subsequent respiration) is slowed (Davidson et al., 1998). If precipitation, and a resulting increase in soil moisture, was stimulating root or microbial respiration, an increase in CO_2 concentration and lighter soil δ^{13}C-CO_2 would be expected (Šantrůčková et al., 2000). Lighter δ^{13}C-CO_2 compositions were observed at L2 with increasing precipitation (Fig. 5d), but an increase in

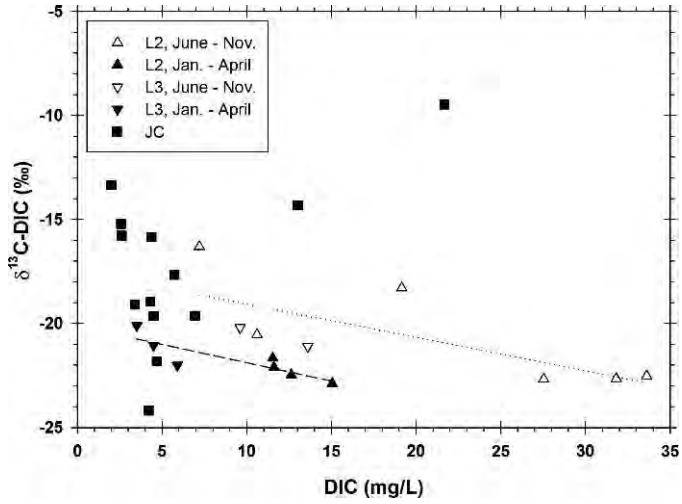

Figure 9. Aqueous soil (L2 and L3) and cave (JC) DIC isotopic composition versus concentration. Note meaning of regression lines differs from that in Figures 5 and 8. Here: June to November samples (L2 and L3) = short-dash line; January to April samples (L2 and L3) = long-dash line. See text for r^2 values.

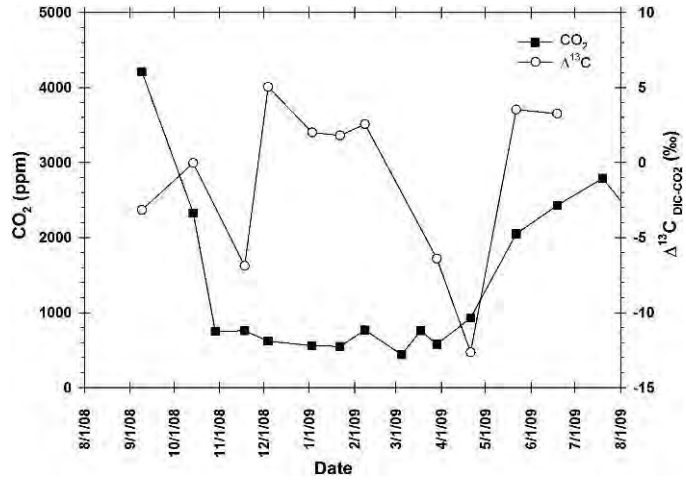

Figure 10. Temporal variability of the difference between the isotopic composition of aqueous DIC in the cave pool and gaseous CO_2 in the cave atmosphere ($\Delta^{13}C_{DIC\text{-}CO_2}$) compared to CO_2 concentration from August 2008 to August 2009.

CO_2 concentration following precipitation was not observed (Fig. 5b). Although this study did not directly measure soil temperature and soil moisture, increasing precipitation decreased CO_2 concentration in L2, similar to findings of Davidson et al. (1998), in which respiration rates and CO_2 decreased at higher soil water contents. Alternatively, CO_2 pulses from soils following precipitation have been shown to decrease to background levels within hours to days (Borken et al., 2003; Sponseller, 2007), so the sampling frequency during this study may have missed rapid increases in soil CO_2.

Using precipitation as a proxy for soil moisture does not account for loss of water by evapotranspiration (ET). PET is highest during the warmer months, when rainfall is typically lower in northwestern Arkansas. The PET estimates from Brye et al. (2004) in Figure 1 are monthly totals, and calculating ET over shorter timescales from daily observations can be difficult due to the diurnal cycle of ET (Fisher et al., 2011). Additionally, actual evapotranspiration (AET) is considered in water-flux calculations, not PET, because PET represents potential energy (Fisher et al., 2011). Without measuring AET at the study site and without the additional climate data required to calculate the PET, accurately quantifying the effect of ET on water flux through the soil zone is difficult. Therefore, daily precipitation data were averaged over the preceding 14 days to represent the cycle of wetting and drying in the soil prior to sample collection.

The increase in concentration of DIC with increasing surface temperature observed in L3 (Fig. 8a) is consistent with the assumption that temperature serves as a proxy for soil respiration. Respired CO_2 exchanges with soil water and through hydration and dissociation of carbonic acid yields the various DIC species, depending on pH (Clark and Fritz, 1997). Decreasing DIC concentration during the winter has been observed elsewhere in karst environments and attributed to decreased rates of respiration (Winston, 2006). Combined data from both soil sites in this study showed a negative correlation between DIC concentration and δ^{13}C-DIC during both the periods June to November and January to April (Fig. 9), indicating an organic carbon source for a component of DIC and further corroborating soil DIC as a proxy for respiration. Additionally, the inverse relationship between DIC concentration and δ^{13}C-DIC occurred during roughly seasonal blocks of time (summer to fall and winter to spring). Similar to δ^{13}C-CO_2 (Fig. 5d), δ^{13}C-DIC decreased at L2 with increasing precipitation (Fig. 8d), illustrating the exchange of carbon species between gaseous and aqueous phases in the soil zone (Fig. 11). Therefore, the isotopic composition of DIC in this shallow karst system has picked up the isotopic signature of respired soil CO_2 prior to entering the cave environment (Fig. 11), and this isotopic signal is affected by changes in temperature and precipitation.

Cave

In the cave, CO_2 concentration was lowest from November to April (Fig. 4a), which is roughly winter through spring for northwestern Arkansas. A decrease in CO_2 concentration during periods of cooler surface temperatures has been observed in caves from other areas (Baldini et al., 2008; Spötl et al., 2005), because changes in surface temperature create density contrasts with cave air, resulting in ventilation patterns that alternate seasonally (Palmer, 2007). Lower soil temperatures also decrease rates of soil respiration (Borken et al., 2003; Davidson et al.,

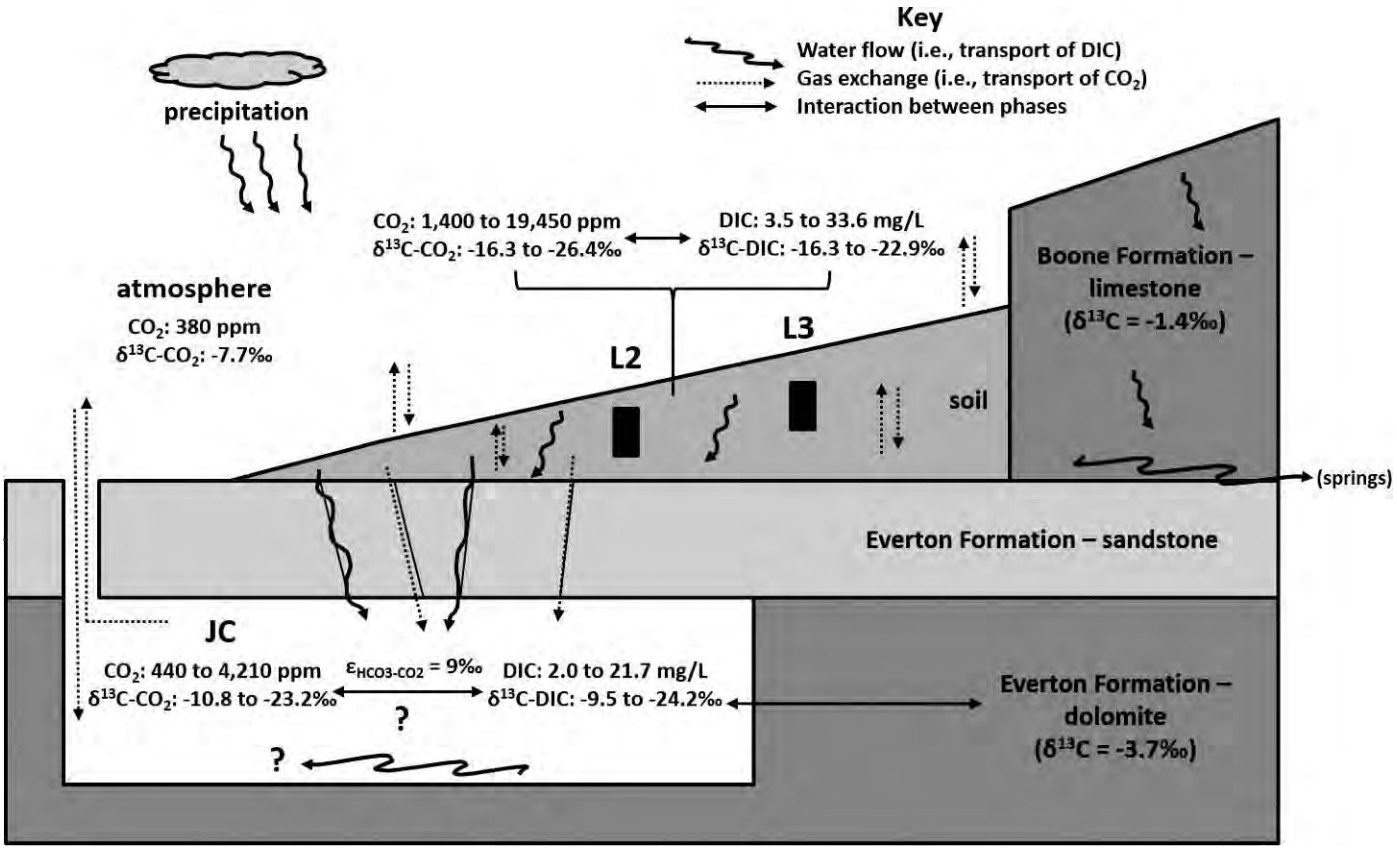

Figure 11. Conceptual model of carbon inputs to Jack's Cave and potential transformations. Groundwater flows from the soil zone, through fractures in the sandstone unit of the Everton Formation, and into the cave, transporting aqueous DIC into the cave. Gaseous CO_2 in the cave is a mix between atmospheric CO_2 and lighter end-member sources, likely from the soil zone.

1998), which would result in lower soil CO_2 concentrations during winter and early spring in northwestern Arkansas (Fig. 4a). Minimum daily surface temperature explained 83% of the variation in cave CO_2 at the Jack's Cave sampling site (Fig. 5a), indicating that surface temperature variation is an important ventilation control in Jack's Cave. Air pressure was not measured during this study, but air pressure has been found to be an important control on cave ventilation in other systems (Palmer, 2007). From November to April, the surface atmosphere is relatively cooler and denser than the cave atmosphere, causing movement of air with lower CO_2 concentration and heavier δ^{13}C-CO_2 into the cave. Cave ventilation is complex, and there are examples where temperature-controlled density gradients do not cause ventilation (Baldini et al., 2008), but the seasonal change in CO_2 concentration at site JC follows closely with changes in surface temperature (Fig. 5a). Additionally, substantial amounts of surface atmosphere can be driven through fractures and pores and into caves (Palmer, 2007), especially caves overlain by fractured sandstone caprock such as Jack's Cave.

As surface temperature warms from May to October, the relatively cooler cave atmosphere is denser than the surface atmosphere, allowing little exchange, and resulting in CO_2 build-up in the cave (Fig. 4a). Soil gas is proposed to contribute a substantial component of the cave atmosphere during this time, resulting in higher CO_2 concentration and lighter δ^{13}C-CO_2 (Fig. 11). The isotopic composition of cave atmosphere CO_2 was mostly constrained by mixing between atmospheric CO_2 (approximately 380 ppm and −7.7‰) and two lighter end-member sources with isotopic compositions of −14‰ and −30‰ (Fig. 6). Note that soil CO_2 represents a mixture of atmospheric CO_2 and soil-respired CO_2 (Davidson, 1995), and CO_2 respired from C3 plants, which dominate plants species, can range from −24‰ to −30‰ (Clark and Fritz, 1997; Šantrůčková et al., 2000). Therefore, the end-member compositions for the two mixing lines (−14‰ and −30‰) may represent two different soil CO_2 isotopic compositions, depending on the degree of mixing between respired CO_2 and atmospheric CO_2 in the soil zone (Fig. 11). Although the concentration and isotopic composition of CO_2 in the soil did vary month-to-month (Fig. 4), the end-member compositions of −14‰ and −30‰ do not clearly represent two distinct seasonal pools of soil CO_2, such as a winter versus a summer soil CO_2 source to Jack's Cave. The variability of CO_2 in the soil zone, prior to entering the cave, may need to be investigated on shorter timescales

than monthly to further constrain these two lighter end-member sources for CO_2.

Although a seasonal pattern in CO_2 concentration was observed in the cave, $\delta^{13}C$-CO_2 did not follow this same pattern throughout the winter (Fig. 4b). An excursion towards lighter $\delta^{13}C$-CO_2 was observed between January and February, and this pattern was also observed in cave $\delta^{13}C$-DIC (Fig. 7b). The January and February CO_2 isotopic compositions lie just outside of the mixing line between atmospheric CO_2 and the possible soil CO_2 source with $\delta^{13}C$-CO_2 of −30‰ (Fig. 6), indicating omission of an apparently minor source of carbon in the mixing model. However, the source of the lighter end member CO_2 in the cave during the winter, when soil respiration rates were lowest, is not fully understood. Therefore, in Jack's Cave, the pattern of CO_2 concentration is proposed to be driven by changes in surface temperature, but the isotopic composition of winter CO_2 requires further investigation.

Similarly to the relationship observed in soil, the increase in DIC concentration at sample site JC with higher surface temperature (Fig. 8a) represents an increased contribution of CO_2 derived from soil respiration being transferred to the cave environment via the aqueous phase (Fig. 11). As groundwater interacts with carbonate bedrock, the organic signature from the soil is diluted, because inorganic carbon is added by carbonate dissolution, as evidenced by the heavier $\delta^{13}C$-DIC in the cave water than soil water (Fig. 9). Calcium carbonate dissolution is also temperature dependent, as greater dissolution can be driven by higher soil CO_2 inputs in open systems, but a greater degree of dissolution contributes more carbon from $CaCO_3$, which is isotopically heavier. For example, dissolution of the carbonate bedrock from the Boone and Everton Formations, which averaged −1.4‰ and −3.7‰, respectively, could provide relatively heavier $\delta^{13}C$-DIC to cave waters, so the correlation between DIC concentration and surface temperature is not as strong in the cave as in the soil (Fig. 8a).

Values for isotopic enrichment $\varepsilon^{13}C_{HCO_3\text{-}CO_2(g)}$, assuming isotopic equilibrium conditions in the cave environment, were 9.1‰ ± 0.1, based on the range of temperature and pH values at site JC (Table 2). The observed $\Delta^{13}C_{DIC\text{-}CO_2}(g)$ values in the cave were between −12.7‰ and +5.1‰ (Fig. 10), indicating that DIC and CO_2 were not in isotopic equilibrium. Isotopic disequilibrium between carbon species was also observed in an Austrian cave and attributed to kinetically induced fractionation due to CO_2 degassing from infiltrating drip water that was supersaturated with aqueous CO_2 compared to the low CO_2 cave atmosphere during the winter (Spötl et al., 2005). The degree of DIC-CO_2 isotopic disequilibrium changed seasonally in Jack's Cave (Fig. 10). From December to February and again in May to June, $\Delta^{13}C_{DIC\text{-}CO_2}(g)$ values were positive, with DIC isotopically heavier than CO_2, and closer to the equilibrium value of 9.1‰ (Clark and Fritz, 1997). This is opposite to what Spötl et al. (2005) described, where isotopic disequilibrium was greatest during the winter because of kinetic fractionation via CO_2 degassing. In Jack's Cave, the extent of possible degassing is not known. However, the $\Delta^{13}C_{DIC\text{-}CO_2(g)}$ values transitioned between positive and negative during November/December and March/April when the CO_2 in the cave was changing (Fig. 10), indicating that ventilation was likely driving changes in isotopic disequilibrium. Therefore, the rapid addition or removal of CO_2 via cave atmospheric exchange between the cave and the surface appears to lead to isotopic disequilibrium between gaseous CO_2 and aqueous DIC. During periods of more stable air, when CO_2 concentration was not rapidly increasing or decreasing, the aqueous DIC in the cave water and gaseous CO_2 in the cave atmosphere were closer to isotopic equilibrium (Fig. 10).

In cave water, Ca and Mg concentrations can be controlled by the degree of rock-water interaction, CO_2 concentration in the soil and cave, and dilution via meteoric water (Spötl et al., 2005; Tooth and Fairchild, 2003; Wong et al., 2011). Between December and March precipitation was low (Fig. 3) and water flow into Jack's Cave decreased, so an increase in Ca and Mg concentrations would be expected due to greater rock-water interaction. However, Ca and Mg concentrations remained low in the cave during the winter and spring, following the same pattern as DIC. Prior calcite precipitation could account for the observed pattern in Ca, but the lack of secondary calcite in the cave pool, rapid infiltration of meteoric water due to direct hydrologic connections between the soil zone and the shallow cave (Knierim et al., 2011), and lower Mg/Ca ratios during the winter make prior calcite precipitation an unlikely mechanism. The seasonal change in cave CO_2 is interpreted as retarding carbonate-rock dissolution during winter periods of low CO_2 concentration, but did not result in calcite supersaturation and enhanced precipitation of calcite. If calcite precipitation versus dissolution is considered on a continuum of $CaCO_3$ solubility, as controlled by CO_2 input, then these results are consistent with other studies that found cave CO_2 correlated with Mg and Ca concentrations in cave water (Spötl et al., 2005; Wong et al., 2011), but they illustrate that Jack's Cave is dominated by varying degrees of dissolution.

Conclusions

Heterogeneity in soil properties within small areas can greatly affect interpretations of carbon transfer and is especially important in shallow karst systems. For example, CO_2 in L3—drier soil site—increased exponentially with increasing surface temperature, whereas at L2—wetter soil site—soil CO_2 decreased exponentially and $\delta^{13}C$-CO_2 became relatively lighter with increasing precipitation. Qualitative differences in soil moisture between the two sites contributed to how soil CO_2 from soil respiration was

affected by changes in surface temperature and precipitation.

Both soil sites showed a seasonal correlation between aqueous DIC concentration and isotopic composition, indicating an organic carbon source for a component of DIC and corroborating soil DIC as a proxy for soil respiration. In the cave, the positive correlation between DIC and surface temperature was also due to increased soil respiration as organic carbon was oxidized in the soil zone and transferred to the cave environment via the aqueous phase. However, aqueous δ^{13}C-DIC was heavier in the cave than in the soil, because the organic signature from soil respiration was diluted by a portion of the inorganic carbon being derived from carbonate dissolution.

Cave atmosphere CO_2 at site JC increased exponentially with increasing surface temperature, possibly due to changing ventilation patterns between the surface and cave atmospheres. The winter period of low CO_2 concentration in the cave is interpreted to mean that carbonate dissolution was reduced, thus lowering the concentration of Ca and Mg in cave water. Therefore, in some environments, such as a shallow karst system capped by sandstone, cave-atmosphere composition can provide information about controls on the geochemistry of small cave streams fed by drip water.

Isotopic disequilibrium between CO_2 and DIC in the cave was greatest when ventilation patterns were presumably changing in the spring and fall, with the associated rapid addition or removal of gaseous CO_2. The isotopic disequilibrium between DIC and CO_2 provided evidence that cave CO_2 was a mixture of carbon from several sources, which was mostly constrained to mixtures between atmospheric CO_2 and soil CO_2. The isotopic composition of cave CO_2 did not follow the same pattern as CO_2 concentration, and an excursion towards lighter δ^{13}C-CO_2 during the winter is not fully understood. The winter CO_2 compositions lay just outside of the mixing line between atmospheric CO_2 and soil CO_2, indicating omission of an apparently minor source of carbon in the mixing model.

In a conceptual model of carbon inputs and transformations at the study site, aqueous DIC and gaseous CO_2 are transported into the cave from the soil zone, with variable amounts of the cave atmosphere CO_2 also being sourced directly from the surface atmosphere. The magnitude of different source inputs to the cave changed seasonally, as evidenced by the month-to-month variability of CO_2 and DIC concentrations and isotopic compositions during the study period. Characterizing the carbon species over time in the unsaturated zone of a mantled karst setting, although challenging, was important for understanding the variability of carbon species observed in the underlying cave. Additionally, isotopic disequilibrium between carbon species provided insight into the sources of carbon in the cave environment. Stable carbon isotope ratios provided an effective tool to explore carbon transfer from the soil zone into the cave, identify carbon sources in the cave, and investigate how seasonality affected the transfer of carbon in a shallow karst system. Jack's Cave in northwestern Arkansas provides a representative example of mechanisms for inorganic carbon transfer in a shallow karst system covered by a regolith mantle.

ACKNOWLEDGEMENTS

Funding was provided by the Arkansas Water Resources Center through the U.S. Geological Survey 104b Program. Any use of trade, firm, or product names is for descriptive purposes only and does not imply endorsement by the U.S. Government. Comments from two anonymous reviewers and the associate editor greatly improved this manuscript. Special thanks to the Carroll family for use of their property.

REFERENCES

Adamski, J.C., Petersen, J.C., Freiwald, D.A., and Davis, J.V., 1995, Environmental and Hydrologic Setting of the Ozark Plateaus Study Unit, Arkansas, Kansas, Missouri, and Oklahoma: U.S. Geological Survey, Water-Resources Investigations Report, 94-4022, 69 p.

Baldini, J.U.L., Baldini, L.M., McDermott, F., and Clipson, N., 2006, Carbon dioxide sources, sinks, and spatial variability in shallow temperate zone caves: Evidence from Ballynamintra Cave, Ireland: Journal of Cave and Karst Studies, v. 68, p. 4–11.

Baldini, J.U.L., McDermott, F., Hoffman, D.L., Richards, D.A., and Clipson, N., 2008, Very high-frequency and seasonal cave atmosphere P_{CO2} variability: Implications for stalagmite growth and oxygen isotope-based paleoclimate records: Earth and Planetary Science Letters, v. 272, p. 118–129. doi:10.1016/j.epsl.2008.04.031.

Borken, W., Davidson, E.A., Savage, K., Gaudinski, J., and Trumbore, S.E., 2003, Drying and wetting effects on carbon dioxide release from organic horizons: Soil Science Society of America Journal, v. 67, p. 1888–1896. doi:10.2136/sssaj2003.1888.

Boyer, D.G., and Pasquarell, G.C., 1999, Agricultural land use impacts on bacterial water quality in a karst groundwater aquifer: Journal of the American Water Resources Association, v. 35, p. 291–300. doi:10.1111/j.1752-1688.1999.tb03590.x.

Breecker, D.O., Payne, A.E., Quade, J., Banner, J.L., Ball, C.E., Meyer, K.W., and Cowan, B.D., 2012, The sources and sinks of CO_2 in caves under mixed woodland and grassland vegetation: Geochimica et Cosmochimica Acta, v. 96, p. 230–246. doi:10.1016/j.gca.2012.08.023.

Brye, K.R., West, C.P., and Gbur, E.E., 2004, Soil quality differences under native tallgrass prairie across a climosequence in Arkansas: The American Midland Naturalist, v. 152, p. 214–230.

Clark, I.D., and Fritz, P., 1997, Environmental Isotopes in Hydrogeology: Boca Raton, New York, Lewis Publishers, 352 p.

Coplen, T.B., 1996, New guidelines for reporting stable hydrogen, carbon, and oxygen isotope-ratio data: Geochimica et Cosmochimica Acta, v. 60, p. 3359–3360. doi:10.1016/0016-7037(96)00263-3.

Davidson, E.A., Belk, E., and Boone, R.D., 1998, Soil water content and temperature as independent or confounded factors controlling soil respiration in a temperate mixed hardwood forest: Global Change Biology, v. 4, p. 217–227. doi:10.1046/j.1365-2486.1998.00128.x.

Davidson, G.R., 1995, The stable isotopic composition and measurement of carbon in soil CO_2: Geochimica et Cosmochimica Acta, v. 59, p. 2485–2489. doi:10.1016/0016-7037(95)00143-3.

Davis, R.K., Brahana, J.V., and Johnston, J.S., 2000, Ground Water in Northwest Arkansas: Minimizing Nutrient Contamination from Non-Point Sources in Karst Terrane: Fayetteville, Arkansas Water Resources Center, Publication Number MSC-288, 173 p.

Doctor, D.H., Alexander, E.C. Jr., Petrič, M., Kogovšek, J., Urbanc, J., Lojen, S., and Stichler, W., 2006, Quantification of karst aquifer discharge components during storm events through end-member mixing analysis using natural chemistry and stable isotopes as tracers:

Hydrogeology Journal, v. 14, p. 1171–1191. doi:10.1007/s10040-006-0031-6.

Fairchild, I.J., Smith, C.L., Baker, A., Fuller, L., Spötl, C., Mattey, D., McDermott, F., and E.I.M.F., 2006, Modification and preservation of environmental signals in speleothems: Earth-Science Reviews, v. 75, p. 105–153. doi:10.1016/j.earscirev.2005.08.003.

Faure, G., 1986, Principles of Isotope Geology, second edition: New York, John Wiley & Sons, Inc., 608 p.

Faure, G., and Mensing, T.M., 2005, Isotopes: Principles and Applications: Hoboken, N.J., John Wiley and Sons, Inc., 928 p.

Fetter, C.W. Jr., 2001, Applied Hydrogeology, fourth edition: Upper Saddle River, New Jersey, Prentice Hall, 598 p.

Fisher, J.B., Whittaker, R.J., and Malhi, Y., 2011, ET come home: Potential evapotranspiration in geographical ecology: Global Ecology and Biogeography, v. 20, p. 1–18. doi:10.1111/j.1466-8238.2010.00578.x.

Graening, G.O., and Brown, A.V., 2000, Trophic Dynamics and Pollution Effects in Cave Springs Cave, Arkansas: Fayetteville, Arkansas Water Resources Center, Publication Number MSC-285, 46 p.

Johnson, T.C., 2008, Geologic map of Forum Quadrangle with a karst inventory, Madison County, Arkansas [M.S. Thesis]: Fayetteville, The University of Arkansas, 188 p.

Katz, B.G., Coplen, T.B., Bullen, T.D., and Davis, J.H., 1997, Use of chemical and isotopic tracers to characterize the interactions between ground water and surface water in mantled karst: Ground Water, v. 35, p. 1014–1028. doi:10.1111/j.1745-6584.1997.tb00174.x.

Kendall, C., 1998, Tracing nitrogen sources and cycling in catchments, *in* Kendall, C., and McDonnell, J.J., eds., Isotope Tracers in Catchment Hydrology: Amsterdam, Elsevier Science, p. 519–576.

Knierim, K.J., 2009, Seasonal variation of carbon and nutrient transfer in a northwestern Arkansas cave [M.S. Thesis]: Fayetteville, University of Arkansas, 141 p.

Knierim, K.J., Pollock, E.D., and Hays, P.D., 2011, Using labeled isotopes to trace groundwater flow paths in a northwestern Arkansas cave, *in* Kuniansky, E.L., ed., U.S Geological Survey Karst Interest Group Proceedings, Fayetteville, Arkansas, April 26–29, 2011: U. S. Geological Survey, Scientific Investigations Report 2011-5031, p. 67–73.

Kowalczk, A.J., and Froelich, P.N., 2010, Cave air ventilation and CO_2 outgassing by radon-222 modeling: How fast do caves breathe?: Earth and Planetary Science Letters, v. 289, p. 209–219. doi:10.1016/j.epsl.2009.11.010.

Lee, Eung Seok, and Krothe, N.C., 2001, A four-component mixing model for water in a karst terrain in south-central Indiana, USA: Using solute concentration and stable isotopes as tracers: Chemical Geology, v. 179, p. 129–143. doi:10.1016/S0009-2541(01)00319-9.

Lohse, K.A., Brooks, P.D., McIntosh, J.C., Meixner, T., and Huxman, T.E., 2009, Interactions between biogeochemistry and hydrologic systems: Annual Review of Environment and Resources, v. 34, p. 65–96. doi:10.1146/annurev.environ.33.031207.111141.

National Cooperative Soil Survey, 2008, Custom Soil Report for Madison County, Arkansas: United States Department of Agriculture, Natural Resources Conservation Service, 16 p.

National Oceanic and Atmospheric Administration, 2009, Arkansas Northwest Division 01, 1895-2009, http://www7.ncdc.noaa.gov/CDO/CDODivisionalSelect.jsp [date accessed March 3, 2010].

Palmer, A.N., 2007, Cave Geology: Dayton, Ohio, Cave Books, 454 p.

Peyraube, N., Lastennet, R., Denis, A., and Malaurent, P., 2013, Estimation of epikarst air P_{CO2} using measurements of water $\delta^{13}C_{TDIC}$, cave air P_{CO2} and $\delta^{13}C_{CO2}$: Geochimica et Cosmochimica Acta, v. 118, p. 1–17. doi:10.1016/j.gca.2013.03.046.

Phillips, D.L., and Koch, P.L., 2002, Incorporating concentration dependence in stable isotope mixing models: Oecologia, v. 130, p. 114–125. doi:10.1007/s004420100786.

Pronk, M., Goldscheider, N., and Zopfi, J., 2006, Dynamics and interaction of organic carbon, turbidity and bacteria in a karst aquifer system: Hydrogeology Journal, v. 14, p. 473–484. doi:10.1007/s10040-005-0454-5.

Révész, K.M., and Landwehr, J.M., 2002, $\delta^{13}C$ and $\delta^{18}O$ isotopic composition of $CaCO_3$ measured by continuous flow isotope ratio mass spectrometry: Statistical evaluation and verification by application to Devils Hole core DH-11 calcite: Rapid Communications in Mass Spectrometry, v. 16, p. 2102–2114. doi:10.1002/rcm.833.

Šantrůčková, H., Bird, M.I., and Lloyd, J., 2000, Microbial processes and carbon-isotope fractionation in tropical and temperate grassland soils: Functional Ecology, v. 14, p. 108–114. doi:10.1046/j.1365-2435.2000.00402.x.

Sponseller, R.A., 2007, Precipitation pulses and soil CO_2 flux in a Sonoran Desert ecosystem: Global Change Biology, v. 13, p. 426–436. doi:10.1111/j.1365-2486.2006.01307.x.

Spötl, C., Fairchild, I.J., and Tooth, A.F., 2005, Cave air control on dripwater geochemistry, Obir Caves (Austria): Implications for speleothem deposition in dynamically ventilated caves: Geochimica et Cosmochimica Acta, v. 69, p. 2451–2468. doi:10.1016/j.gca.2004.12.009.

St-Jean, G., 2003, Automated quantitative and isotopic (^{13}C) analysis of dissolved inorganic carbon and dissolved organic carbon in continuous-flow using a total organic carbon analyser: Rapid Communications in Mass Spectrometry, v. 17, p. 419–428. doi:10.1002/rcm.926.

Taylor, D.S., Goodwin, D.P., Bitting, C.J., Handford, R., and Slay, M., 2009, The Ozark Plateaus: Arkansas, *in* Palmer, A.N., and Palmer, M.V., eds., Caves and Karst of the USA: Huntsville, Alabama, National Speleological Society, Inc., p. 172–174.

Tooth, A.F., and Fairchild, I.J., 2003, Soil and karst aquifer hydrologic controls on the geochemical evolution of speleothem-forming drip waters, Crag Cave, southwest Ireland: Journal of Hydrology, v. 273, p. 51–68. doi:10.1016/S0022-1694(02)00349-9.

Trautz, R.C., Pugh, J.D., Varadharajan, C., Zheng, Liang, Bianchi, M., Nico, P.S., Spycher, N.F., Newell, D.L., Esposito, R.A., Wu, Yuxin, Dafflon, B., Hubbard, S.S., and Birkholzer, J.T., 2013, Effect of dissolved CO_2 on a shallow groundwater system: A controlled release field experiment: Environmental Science and Technology, v. 47, p. 298–305. doi:10.1021/es301280t.

United States Department of Agriculture, 2002, State Fact Sheets: Arkansas, http://www.ers.usda.gov/data-products/state-fact-sheets/state-data.aspx?StateFIPS=05&StateName=Arkansas#.VEgT9xY00jZ, [date accessed July 1, 2009].

United States Department of Agriculture, 2007, Quick Stats, http://www.nass.usda.gov/ [date accessed July 1, 2009].

Winston, B., 2006, The biogeochemical cycling of nitrogen in a mantled karst watershed [M.S. Thesis]: Fayetteville, University of Arkansas, 98 p.

Wong, C., and Banner, J.L., 2010, Response of cave air CO_2 and drip water to brush clearing in central Texas: implications for recharge and soil CO_2 dynamics: Journal of Geophysical Research: Biogeosciences, v. 115, article G04018, 13 p. doi:10.1029/2010JG001301.

Wong, C.I., Banner, J.L., and Musgrove, M., 2011, Seasonal dripwater Mg/Ca and Sr/Ca variations driven by cave ventilation: Implications for and modeling of speleothem paleoclimate records: Geochimica et Cosmochimica Acta, v. 75, p. 3514–3529. doi:10.1016/j.gca.2011.03.025.

G. Iskali and Y. Zhang – Guano subsidy and the invertebrate community in Bracken Cave: the world's largest colony of bats. *Journal of Cave and Karst Studies,* v. 77, no. 1, p. 28–36. DOI: 10.4311/2013LSC0128

GUANO SUBSIDY AND THE INVERTEBRATE COMMUNITY IN BRACKEN CAVE: THE WORLD'S LARGEST COLONY OF BATS

Goniela Iskali* and Yixin Zhang
Texas State University-San Marcos, 220 E. Sessoms Dr., San Marcos, TX 78666

Abstract: Fluxes of resource subsidy across ecosystems can affect consumer-community dynamics in recipient systems. Bracken Cave is an unusual ecosystem because of the magnitude of allochthonous input of guano that is produced by the largest bat population in the world—a colony of more than 20 million Mexican free-tailed bats (*Tadarida brasiliensis*). Research on the guano-subsidy ecosystems dynamics of Bracken Cave is limited, but imperative to our understanding and conservation of this extraordinary ecosystem. The objectives of this study are to determine the quantity and quality of guano deposition across seasons and its effect on the macroinvertebrate community and to examine the effect of the cave's habitat characteristics, such as distance from entrances and depth within the guano substrate, on the macroinvertebrate abundance and taxon richness at Bracken Cave. Core samples of guano and macroinvertebrates were collected at increasing distances within the cave on a monthly basis. Guano from the core samples was analyzed with respect to C, N, and P to determine guano quality variations. In addition, pitfall trap sampling was employed to supplement the macroinvertebrate core sampling. An estimated dry weight total of 50,500 kg of guano was deposited on the 3078 m^2 of floor from August 2009 to August 2010, with the highest rate recorded in September 2009 and the lowest in January–March 2010. Variations in guano deposits with respect to seasonality do not have a significant effect on macroinvertebrate abundance and richness. On the other hand, habitat characteristics significantly affected the macroinvertebrate abundance and richness in the cave. Macroinvertebrate abundance decreased with increasing depth within the guano substrate. Carbon concentrations were significantly higher in the top layers of guano, while nitrogen and phosphorous concentrations were not significantly different with respect to guano depth. Results from pitfall-trap sampling indicated that macroinvertebrate richness was significantly higher near cave entrances. This study indicates that the invertebrate community at Bracken Cave was relatively stable and experienced few seasonal fluctuations, but was shaped by the micro-habitat characteristics of distance from entrances and depth within the guano substrate. The bats and the nutrients that they contribute play a central role as productivity donors to the bottom-up dynamics of one of the most unusual cave ecosystems in the world.

Introduction

Fluxes of energy, nutrients, and materials across ecosystems can affect consumer-community dynamics in the recipient systems and produce a variety of ecosystem dynamic outcomes (Polis and Strong, 1996). The rate of input depends on many environmental and organismal attributes and can determine the magnitude of subsidy effects on the recipient ecosystems. Generally, allochthonous inputs increase primary productivity; and consequently, prey and predator populations (Polis et al., 1997). However, large quantities of allochthonous input can destabilize trophic interactions by stimulating the growth of higher consumers, diminishing prey populations. Although in some recipient systems, ample allochthonous input can represent a constant energy supply that cannot be overexploited, and thus, stabilizes ecosystem interactions (Anderson and Polis, 2004). This is especially true in unproductive systems, such as caves, that receive regular inputs of subsidies (Schneider et al., 2011; Polis et al., 1997).

Due to light limitation, cave ecosystems rely almost entirely upon allochthonous energy fluxes originating from surface ecosystems (Culver, 1985, 1982). Therefore, communities in caves are profoundly impacted by the resource subsidies that they receive. The types of resources that enter caves vary in terms of regularity, duration, and usability (Schneider et al., 2011). The most prevalent resource inputs to caves are decaying leaf and woody debris that has fallen or washed into caves and carcasses of animals that fall into pit entrances or get lost within the cave (Culver, 1982, Poulson, 2005, Schneider et al., 2011).

* Corresponding Author: goniela_iskali@yahoo.com

Fecal matter deposited by cave inhabitants, such as crickets and bats, also represents an important, nutrient-rich energy resource for oligotrophic cave ecosystems (Poulson, 2005; Ferreira et al., 2007; Fagan et al., 2007). Bat guano consists of the egested waste and nitrogenous materials of animal metabolism, which are rich in inorganic and organic nutrients (Hutchinson, 1950).

Some caves are inhabited by high-density populations of bats and receive large quantities of nutrient-rich guano. In limestone caves of the southern United States and Mexico, considerable quantities of bat guano have been observed (Hutchinson, 1950). The guano acts as the resource base of their food webs and can support relatively large populations of detrivorous species such as invertebrates, fungi, bacteria, and other microorganisms. These types of caves differ from other cave ecosystems in the sense that they are not oligotrophic. However, our knowledge of the effects of the guano-subsidy input on cave-community dynamics is limited. In general, caves are regarded as some of the least explored, but most fragile, ecosystems in the world (Clements et al., 2006; Vermeulen and Whitten, 1999; Dennis and Aldhous, 2004). The purpose of our study is to examine the effects of guano input on the macroinvertebrate-community dynamics of Bracken Cave, which is a very unusual cave ecosystem in terms of the amount of allochthonous input and a valuable conservation resource in terms of housing the largest population of bats in the world.

Along with energy fluxes, cave-habitat characteristics can play an important role in influencing cave-community dynamics. A multitude of factors such as lithology, cave climate, and proximity to cave entrance define cave habitats and can influence the distribution of organisms that occur within them (Souza-Silva et al., 2011; Biswas, 2010; Lavoie et al., 2007; Ferreira et al., 2007). For example, distance from the cave entrances and depth within the guano create varying microhabitat conditions that may translate to variations in the macroinvertebrate abundance and richness. Cave entrances also provide an opportunity for surface organisms to enter the cave, either accidentally or intentionally, and this may also affect macroinvertebrate community assemblages in the cave (Ferreira et al., 2007). Interactions between energy availability and habitat characteristics create unique microhabitats and ecological niches within a cave. Ferreira et al. (2007) found that organisms in a guano-subsidy cave were more dependent upon their microhabitat than the overall cave conditions. Thus, the variability of energy input and habitat conditions and their interactions must be taken into consideration to gain an understanding of the factors that influence cave communities.

This study focused on the ecosystem interactions at Bracken Cave and tested three hypotheses, 1) that seasonal changes in bat-population densities and the quantity of guano input influence cave invertebrate abundance and taxon richness, 2) that cave-invertebrate abundance and richness will significantly vary with habitat characteristics such as distance from the cave entrances and depth within the guano substrate, and 3) that differences in the carbon, nitrogen, and phosphorous nutrient composition in the guano will indicate guano quality variability and its effect on the macroinvertebrate community. Through this study we gain a greater understanding on the role of guano subsidy input and its effect on the community dynamics of Bracken Cave.

Materials and Methods

Bracken Cave

Bracken Cave is located in a suburban setting near San Antonio, Texas. The cave and the 282 hectares surrounding it are managed by Bat Conservation International. The cave consists of two rooms that comprise an estimated 3078 m^2 (Fig. 1). A maternity colony of more than 20 million Mexican free-tailed bats (*Tadarida brasiliensis*) inhabits Bracken Cave (BCI, 2013a) during March through October. In addition, the cave is occupied by a significantly smaller overwintering population of Mexican free-tailed bats. Due to the prolonged use of the cave by bats, it is estimated that guano fills about half of the cave volume (Fran Hutchins, pers. comm., February 2011).

Mexican Free-Tailed Bats

Mexican free-tailed bats (*Tadarida brasiliensis*; BCI, 2013b) occupy a wide variety of habitats and can be found throughout the southern portion of the United States, but the densest concentrations of this species are found in Texas, where they form maternity colonies numbering in the millions. The majority of the maternity colonies are in limestone caves, in abandoned mines, under bridges, or in buildings. It is estimated that 100 million Mexican free-tailed bats come to central Texas each year to raise their young (BCI, 2013b, Cleveland et al., 2006). Nursing females require large quantities of insects that are high in fat, which they obtain by consuming egg-laden moths. The 100 million free-tailed bats living in central Texas caves consume approximately 1,000 tons of insects nightly, a large proportion of which are agricultural pests. Therefore, the ecological and economic impacts of these large bat colonies are highly significant (BCI, 2013b).

Macroinvertebrate Abundance and Taxon Richness

In order to monitor macroinvertebrate population differences with respect to cave entrances, the cave was divided into three regions of relatively equal area at increasing distance from the natural entrance: entrance zone, twilight zone, and dark zone. However, a smaller artificial man-made ceiling entrance exists in the dark zone of the cave (Fig. 1). Each region was approximately 45 m in length, with an average width of 30 m.

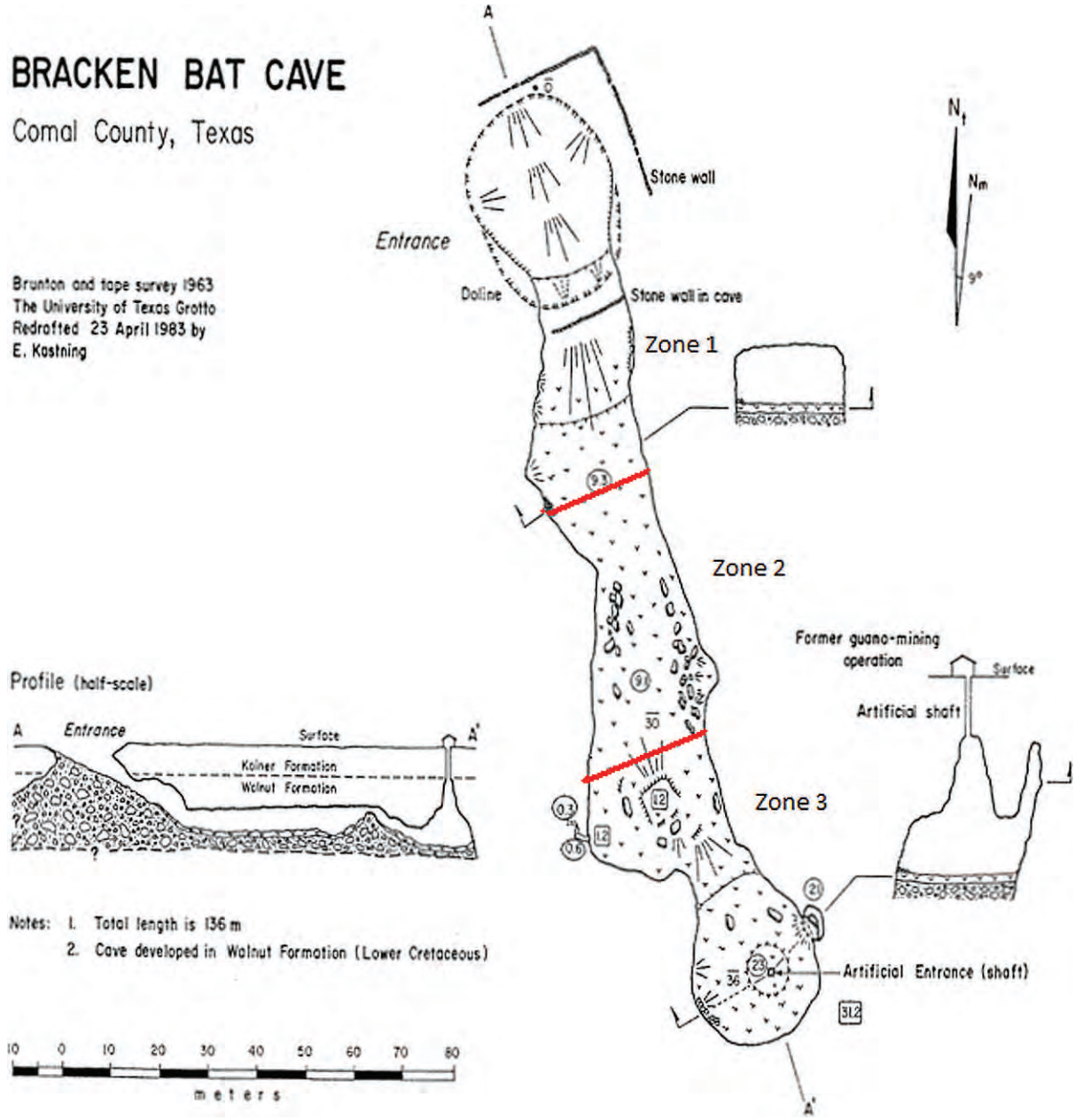

Figure 1. Map of Bracken Cave, Garden Ridge, Texas (modified from Kastning, 1983). The map includes the division of the cave into zones of 45 m in length.

We collected three core samples from each region on a monthly basis for five months (August–December 2009). This was accomplished by randomly inserting a PVC pipe sampler 0.08 m in diameter and 0.91 m long into the cave floor and determining the taxa richness and abundance of organisms present between the surface and 0.91 m of guano depth. The method for extracting stratified guano for this study is one that was used by Altenbach and Petit (1972) to study the effects of pollution and heavy metals on the environment. This involved inserting a pipe into the guano, digging a trench around it in order to place a stopper at the bottom, and then extracting the pipe or core sampler. As soon as the sample was collected, three plastic dividers were inserted into the PVC pipe to divide the guano into four 0.23 m layers and prevent guano and organism displacement during the extraction. The length of the layers and length of the pipe used were determined through preliminary data collection, where 0.91 m depth of guano was examined using the same pipe-trench method, which showed that guano layers were significantly different in texture and color at approximately every 0.23 m in depth. These layers roughly correlate to a yearly deposit of guano (Wurster et al., 2007). During this study, we examined the top four apparently distinctive layers of guano and the macroinvertebrates

within each of these layers. Macroinvertebrates in each core sample layer were separated in the lab from the guano mixture using a 1 mm sieve, picked and placed in 70% ethanol for preservation, and later identified to the lowest taxonomic level possible (typically family or genus level).

In addition to core sampling, we also employed pitfall trap sampling to measure macroinvertebrate abundance and richness. The pitfall traps were used to supplement the invertebrate core-sampling method and ensure that our samples contained a more comprehensive representation of the cave organisms. Three pitfall traps 0.06 m in diameter with a volume of 236.59 cm^3 were installed in each zone of the cave for 48 hours in November 2009, April 2010, and July 2010. The pitfall traps were filled with 50% water and 50% of a 70% ethanol solution. Ethanol has been shown to be an effective pitfall trap preservative, and we mixed it with water to reduce evaporation (Aristophanous 2010). Pitfall-trap specimens were preserved in 70% ethanol and identified to the lowest possible taxonomic level. In addition, pitfall-trap samples were sub-sampled to one-fourth for macroinvertebrates larger than 1 mm and one-twelfth for macroinvertebrates smaller than 1 mm. Sub-sampling was conducted because of the large number of macroinvertebrates contained in each pitfall trap.

Guano Deposition Rate

Guano is the base food resource for the food web in Bracken Cave. Therefore, determining the quantity and quality of the guano is essential to understanding this ecosystem. Guano deposition samples were collected in six plastic containers 0.34 m by 0.21 m by 0.12 m. Each cave zone (Fig. 1) had two randomly placed containers that were collected every month from September 2009 to August 2010. This was conducted to assess the quantity and seasonal variation of the guano being deposited. The guano was then dried at 60 °C for 72 hours and weighed to the nearest 0.1 g.

Guano Nutrient Analyses

Guano collected during core sampling was also examined with respect to nutrient composition. Thirty-six samples (9 replicates × 2 seasons × 2 guano depth layers) were analyzed to determine the concentrations of carbon, nitrogen, and phosphorous in guano samples from summer and winter bat-population seasons and top and bottom guano depths. To determine carbon and nitrogen concentrations, samples were processed using the Flash EA 1112 Elemental analyzer. Samples were analyzed for phosphorous content by the Soil Testing Services at the University of Missouri. The samples were dry-ashed using an adaptation of AOAC 985.01 (Isaac, 2009), and phosphorous content was determined through inductively coupled plasma-atomic emission spectroscopy (US EPA 1992).

Statistical Analyses

An unbalanced ANOVA was used to estimate if there were any significant differences between the guano deposit rates, where weight of the samples was the response variable and the distance from the entrances and seasonality were the two predicting factors. To investigate the variability in macroinvertebrates from the core-sample data with respect to distance from the entrances, guano depth, and seasonality, we employed two linear mixed-effects models. Seasonality was the random predictor variable, and cave zone and guano depth were the fixed predictor variables in the models. The guano depth data were organized to compare the two top layers of guano with the two bottom layers of guano. Macroinvertebrate abundance, as number of macroinvertebrates per sample per month, was the response variable in one of these regression models, and macroinvertebrate richnes, as number of taxa per sample per month, was the response variable in the other model. The abundance data were $\log_{10}$ (n+1) transformed to meet the normality and homoscedasticity assumptions. The pitfall traps were analyzed using unbalanced ANOVAs with macroinvertebrate abundance (number per sample) and richness (taxa per sample) as the response variables and seasonality and cave zone as the predicting factors for both ANOVAs. The macroinvertebrate abundance data from these pit-fall samples was natural-log (ln) transformed to achieve normality and homoscedasticity. Finally, we used two-way balanced ANOVAs to compare the C, N, and P content in the samples, and we used one ANOVA for each C, N, and P where seasonality and guano depth were used as factors for each of the tests. All analyses were performed using the statistical programming language, R.

Results

Seasonal Guano Deposit Comparisons

We determined that the amount of guano deposition per month ranged from the highest of 11,337 ± 637 kg (September 2009) to the lowest of 66 ± 50 kg (January–March 2010) when extrapolating to the total cave area (Fig. 2). The average guano deposition in Bracken Cave was approximately 4,210 ± 989 kg per month. The deposition of guano varied significantly between months ($F_{1,27} = 16.87$, $P < 0.001$), (Fig. 2) but did not differ with respect to distance from the entrances when comparing the three cave zones ($F_{2,27} = 2.68$, $P = 0.09$) . Lastly, the total estimated guano deposition in the cave was 50,521 ± 11,868 kg for August 2009 through August 2010.

Macroinvertebrate Community Structure

The macroinvertebrate sampling at Bracken Cave collected and identified 754,265 individual macroinvertebrates. Invertebrates were classified in eight orders of at least ten families. Acarina was by far the most abundant order, containing 95.91% of the macroinvertebrates observed. The second most abundant order was Coleoptera, containing 4.01% of the macroinvertebrates, and the most

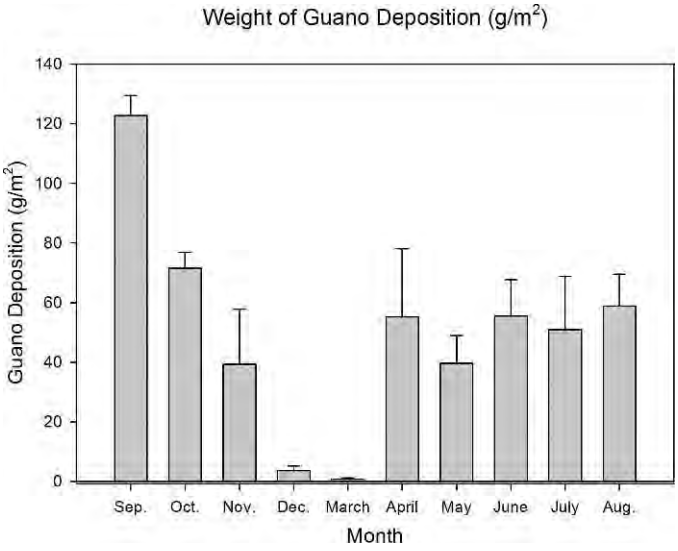

Figure 2. Mean weight in six locations of guano deposition (g m^{-2}) per month (September 2009 through August 2010). Error bars are standard error. The guano deposition observed throughout the months varied significantly ($F_{1,27} = 16.87$, $P < 0.001$).

abundant families of this order were Dermestidae and Tenebrionidae (Table 1).

Linear mixed-effect model analyses revealed that monthly seasonality only explained 28% of the variation in macroinvertebrate abundance and 2.4% of the variation in macroinvertebrate taxa richness from the core samples collected August through December 2009. The highest abundance (14,216.87 ± 3,633.73 number per cubic meter per month ± SE) and richness (2.22 ± 0.09 number of taxa per month) were encountered during the month of September, while the months of August, October, November, and December displayed similar, but lower, values in macroinvertebrate abundance and richness (Fig. 3). In addition, cave zones or distance from entrances did not significantly affect macroinvertebrate abundance ($F_{1, 115} = 1.66$, $P = 0.19$) and richness ($F_{1, 117} = 0.17$, $P = 0.67$). Zone 2, or the twilight zone, displayed the highest abundance of 7,351.81 ± 187.95 and richness of 1.82 ± 0.02, but this was not significantly higher than zone 1 or 3. Guano depth was significantly correlated with macroinvertebrate abundance ($F_{1, 117} = 8.56$, $P = 0.004$*) but not richness ($F_{1, 117} = 3.46$, $P = 0.07$) (Fig. 4). The top two layers of guano displayed significantly higher abundance (5,431.33 ± 110.84) when compared to the bottom two layers of guano (3,549.40 ± 156.63). Richness of taxa was slightly higher, but not significantly different, in the top layers of guano (1.80 ± 0.01) versus the bottom layers of guano (1.57 ± 0.02).

The abundance of organisms found during pitfall-trap sampling was not significantly correlated to seasonality ($F_{2,13} = 3.17$, $P = 0.07$) or cave zones ($F_{2,13} = 3.16$, $P = 0.07$). The highest abundance of macroinvertebrates was collected during the month of July ($2.39 \times 10^8 \pm 1.14 \times 10^8$) (number of organisms per cubic meter per month), compared to the average seasonality abundance ($1.24 \times 10^8 \pm 0.62 \times 10^8$). In addition, the highest abundance of macroinvertebrates was collected in zone 3, $2.32 \times 10^8 \pm 1.16 \times 10^8$, compared to the average zone abundance of $1.35 \times 10^8 \pm 0.71 \times 10^8$. However, a significant correlation was found between taxon richness and cave zones ($F_{1,13} = 8.91$, $P = 0.004$) (Fig. 5), but not seasonality ($F_{1,13} = 3.48$, $P = 0.06$). Zone 2 (4.75 ± 0.37) (number of taxa/month) displayed significantly lower macroinvertebrate richness

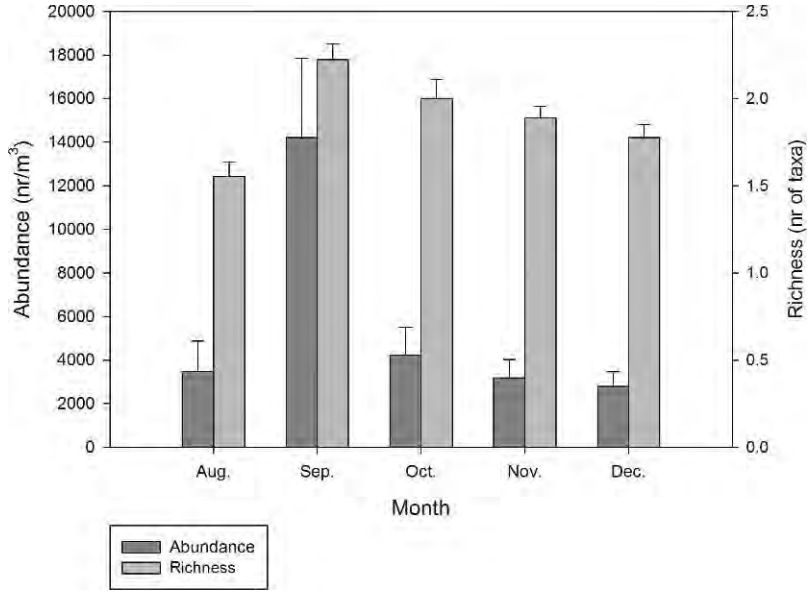

Figure 3. Macroinvertebrate density (number per cubic meter) and richness (number of taxa) ± SE of Bracken Cave encountered in core samples from August through December 2009.

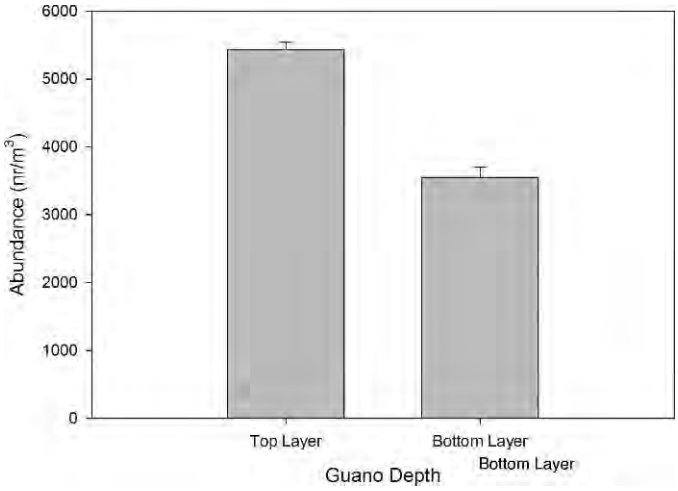

Figure 4. Mean macroinvertebrate density (number per cubic meter) ± SE of Bracken Cave with respect to guano depth encountered in the core samples. The top half of the cores (0–0.45 m) displayed significantly higher macroinvertebrate abundance than the bottom half (0.45–0.91 m) ($F_{1,117} = 8.56$, $P = 0.004$).

than zone 1 (6.50 ± 0.56) and zone 3 (6.63 ± 0.53). The highest macroinvertebrate richness was observed in April 2010 (6.40 ± 0.98), compared to the seasonal average (5.97 ± 0.64).

Guano Nutrient Analyses

Carbon concentrations (moles/g) significantly differed between different layers of guano depth ($F_{1,32} = 7.04$, $P = 0.01$), but did not differ with seasonality ($F_{1,32} = 1.40$, $P = 0.25$). Moles of carbon per gram were significantly higher in the top layer of guano ($0.034 \pm 8.19 \times 10^{-5}$ mol g^{-1}, mean ± SE) versus the bottom layer ($0.031 \pm 3.27 \times 10^{-4}$). The mean overall carbon content found in the samples was 0.033 ± 0.001 mol g^{-1}. Alternatively, nitrogen moles per gram did not differ significantly with respect to guano depth ($F_{1,32} = 0.02$, $P = 0.9$) or seasonality ($F_{1,32} = 2.41$, $P = 0.13$). The mean nitrogen content estimated from the samples was 0.009 ± 0.0002 mol g^{-1}. Similarly, phosphorous in moles per gram did not significantly differ with respect to guano depth ($F_{1,32} = 0.12$, $P = 0.74$) or seasonality ($F_{1,32} = 1.33$, $P = 0.26$) (Fig. 6). The mean phosphorous content estimated from the samples was $0.0005 \pm 2.57 \times 10^{-5}$ mol g^{-1}.

Discussion

We observed a huge flux of cross-ecosystem subsidy and a high abundance of macroinvertebrates in Bracken Cave, a stable microenvironment of unlimited guano supply. By providing energy and nutrients, the bats play a central role as productivity "donors" to the "bottom-up dynamics" of the cave ecosystem. The guano input at Bracken Cave significantly varied with seasonality due to fluctuations in bat population densities. But these variations do not seem to translate into changes in macroinvertebrate population abundance and richness as indicated by the guano core sampling and pitfall-trap sampling. This is contrary to our first hypothesis and other related studies that have shown cave organisms will respond to fluctuations of nutrient supplies delivered to the cave (Humphreys, 1991; Poulson, 2005). However, Bracken Cave differs from most caves in

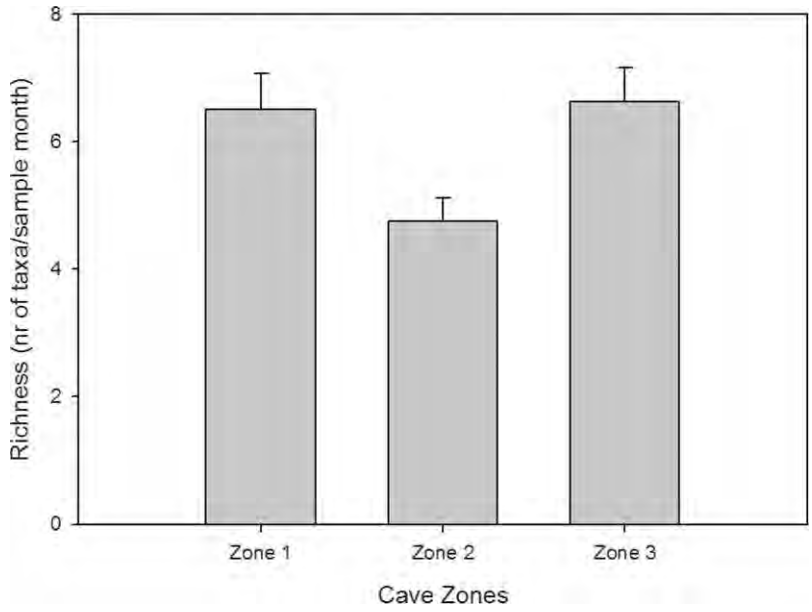

Figure 5. Comparison of mean macroinvertebrate richness ± SE (number of taxa) found in the cave zones (Fig. 1) during pitfall-trap sampling. Richness was significantly different between the three cave zones, since zone 2 had a significantly lower richness when compared to zones 1 and 3 ($F_{1,13} = 8.91$, $P = 0.004$).

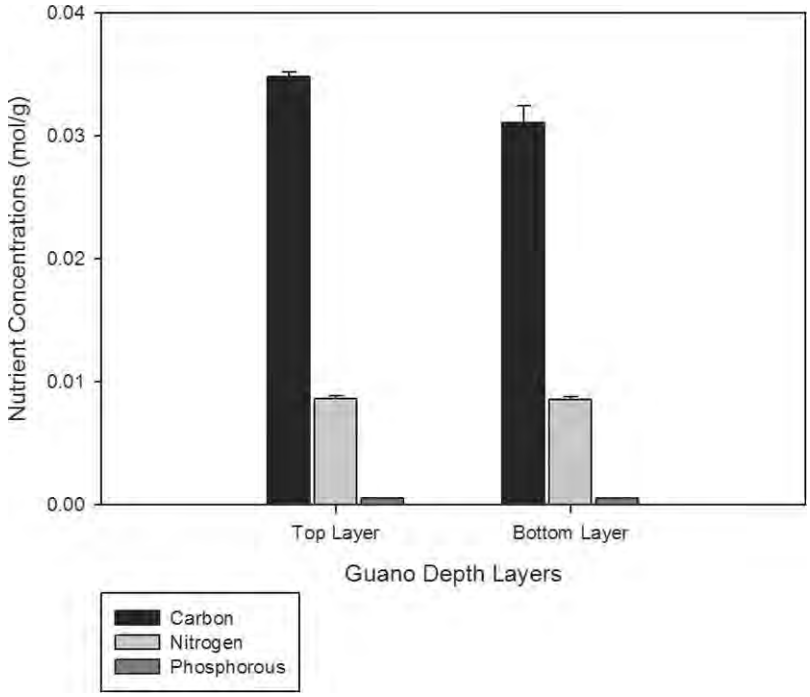

Figure 6. Carbon, nitrogen, and phosphorous concentrations (mol g^{-1}) compared between top (0–0.46 m) and bottom halves of the (0.46–0.91 m) guano cores. Carbon content (mol g^{-1}) was the only nutrient that varied significantly with respect to guano depth ($F_{1,32} = 7.04$, $P = 0.01$).

that there is a constant and plentiful amount of guano available throughout the year, despite the varying densities of bat population and rate of guano deposition. In some places, the guano can reach depths of over 20 meters (Fran Hutchins, pers. comm., February 2011). In addition, nutrient analyses from this study demonstrated that guano contents of carbon, nitrogen, and phosphorous do not differ with respect to seasonality. The constant supply of guano and the lack of seasonal variability in nutrient quality, explains the lack of fluctuations in macroinvertebrate abundance and richness with respect to seasonality.

Secondly, we observed an insignificant difference in macroinvertebrate abundance and taxa richness in the guano core samples at different distances from the entrance. Our results from core samples contradict our second hypothesis and indicate that macroinvertebrate populations are not significantly correlated with the distance from entrances. These findings are supported by our observations that the amount of guano distribution is relatively even throughout the cave and indicate that guano availability, and not distance from the entrance, influenced macroinvertebrate abundance and taxa richness in Bracken Cave. However, we did observe a significant difference in macroinvertebrate richness, but not abundance, from the pitfall trap samples when comparing the three cave zones. The two cave zones with the highest macroinvertebrate richness were near entrances and had a higher incidence of trogloxenes (accidental cave organisms). The negative relationship between cave depth and richness is also supported by other studies (Ferreira and Martins, 1998; Ferreira et al., 2007). Ferreira et al. (2007) also observed a reduction in diversity with increasing distance from the cave entrances in a guano-subsidy cave. It is not surprising that this difference in macroinvertebrate richness was detected from pitfall-trap sampling but not guano-core sampling. Pitfall traps allow for a longer time, and presumably, larger area of sampling, and the probability of capturing rare organisms and actively moving organisms is higher with this method. Additionally, the pitfall trap samples included a higher range of macroinvertebrate sizes, because the guano core samples discriminated against smaller invertebrates (less than 1 mm). Thus, cave entrances play an important role in introducing organisms to cave ecosystems and influencing the cave richness of microhabitats near these entrances. However, the distance from the cave entrance does not correlate with guano availability and does not influence the populations of the predominant organisms found at Bracken Cave.

Lastly, analysis of guano core samples indicated that there was a significant difference in macroinvertebrate abundance, but not taxa richness, when comparing the different layers of guano depth. These results were anticipated and concurred with our third hypothesis, because abiotic conditions such as oxygen concentration, moisture, and temperature (Sanders, 1981), and biotic conditions, such as microbial activity, vary with soil or substrate depth (Fierer et al., 2003). Reduced space among guano particles in the deeper layer can be another limiting

Table 1. Summary of the macroinvertebrates found in Bracken Cave through core sampling and pitfall traps methods (August 2009-July 2009).

Order	Family	Genus	Species
Acarina			
Araneae			
Coleoptera	Dermestidae	*Dermestes*	*carnivorus*
Coleoptera	Histeridae	*Carcinops*	*pumilio*
Coleoptera	Histeridae	*Euspilotus*	*sp. 1*
Coleoptera	Histeridae	*Euspilotus*	*sp. 2*
Coleoptera	Tenebrionidae	*Alphitobius*	*diaperinus*
Hemiptera			
Dermaptera			
Diptera			
Pseudoscorpionida	Chernetidae		
Siphonaptera	Ischnopsyllidae		

factor. These changes in abiotic and biotic conditions may have led to the variation in the abundance of macroinvertebrates. Another explanation for these results could be the decrease of guano quality with increasing depth and time (Hutchinson, 1950). The nutrient analyses from this study demonstrated that top layers of guano had significantly higher levels of carbon, but not nitrogen and phosphorous, when compared to the bottom layers of guano. We also expected macroinvertebrate richness to follow a similar pattern, but this was not the case. However, macroinvertebrate richness (>1 mm invertebrates) at Bracken Cave is relatively low, as the ecosystem is dominated by abundant populations of Dermestidae and Tenebrionidae beetles. These beetles were ubiquitous throughout the 0.91m of guano depth analyzed. Perhaps if greater depths of guano are analyzed we may detect differences in macroinvertebrate richness with respect to substrate depth.

We presume that the abundant quantity, equal-area distribution, and equal nutrient composition of guano with respect to season have created a fairly stable ecosystem supported by a considerable amount of cross-ecosystem subsidy in Bracken Cave. This ecosystem experiences relatively few fluctuations in macroinvertebrate abundance and taxa richness with respect to seasonality. Macroinvertebrate richness also does not vary in the guano depth examined, and abundance is not correlated with the distance from the cave entrances. However, evidence from pitfall-trap sampling suggests that cave entrances do play a role in the introduction of accidental macroinvertebrates to the cave ecosystem. The effect of these trogloxenic animals may be insignificant to the overall community dynamics of this ecosystem due to their low incidence.

Conclusion

This study provides a description of the community and ecosystems dynamics of one of the most unusual, but understudied, ecosystems, Bracken Cave. Our study is the first to focus on the bat-guano subsidy and macroinvertebrate community of this extraordinary cave ecosystem to determine how the habitat characteristics of distance from an entrance and guano depth, guano quantity and quality, and seasonality affect the macroinvertebrate community of Bracken Cave. Our findings indicate that the macroinvertebrate communities of Bracken Cave do not experience large fluxes in abundance or richness with respect to season. But macroinvertebrate populations did fluctuate with respect to distance from the cave entrances and guano depth. Additionally, guano nutrient quality, and not variations in quantity, may also be one factor that influences macroinvertebrate biodiversity in this cave. This study represents an initial but an important and comprehensive view of the Bracken Cave ecosystem. The information gained from this study improves our understanding of the Bracken Cave ecosystem and can aid managers in developing management plans to conserve this distinctive ecosystem.

Concern over cave ecosystems and the cave-limited species that inhabit them has escalated over the last two decades (Schneider et al., 2011). But despite recent advances in cave research, cave ecosystems and the threats that they face remain understudied (Marmonier et al., 1993; Elliott 2000; Hancock et al., 2005). Bracken Cave, located in a suburban setting, is constantly threatened by the effects of urbanization and further development in the growing metropolis of San Antonio (BCI, 2013a). Damages to this extraordinary and not yet fully understood ecosystem would undoubtedly have devastating effects on the bat community, which would, negatively affect the local economy of the region. Cleveland et al. (2006) estimated that pest-control services provided by Mexican free-tailed bats have an average to an annual value of $741,000 per year, with a range of $121,000 to $1,725,000 per year in the south-central Texas area. Therefore, understanding cave ecosystems and their community dynamics is imperative for the preservation of the organisms that occupy them and the benefits gained through the ecosystem services that they provide.

Acknowledgements

We are sincerely grateful to BCI, especially Fran Hutchins and Jim Kennedy, for providing access to the cave, helping us devise and finalize the sampling protocol, aiding in sample collection, and providing necessary information about Bracken Cave and it's bats. We would also like to thank Dr. Benjamin Schwartz and Dr. Weston Nowlin for their helpful suggestions and thesis edits that made this project successful. Lastly, this project would not have been possible without the contribution and endless field and laboratory efforts put forth by the following individuals: Val Yerby, Sam Peterson, Jessica Callery,

Natasha Lehr, Ryan Stewart, Megan Lindsey, Mario Sullivan, Trey Nobles, etc. Funding for this project was partly provided by the National Speleological Society.

References

Altenbach, J.S., and Petit, M.G., 1972, Stratification of guano deposits of the Free-Tailed Bat, *Tadarida brasiliensis*: Journal of Mammalogy, v. 53, p. 890–893.

Anderson, W.B., and Polis, G.A., 2004, Allochthonous nutrient and food inputs: Consequences for temporal stability, *in* Polis, G.A., Power, M.E., and Huxel, G.R., eds., Food Webs at the Landscape Level: Chicago, University of Chicago Press, p. 82–95.

Aristophanous, M., 2010, Does your preservative preserve? A comparison of the efficacy of some pitfall trap solutions in preserving the internal reproductive organs of dung beetles: Zookeys, no. 34, p. 1–16. doi:10.3897/zookeys.34.215.

Bat Conservation International, 2013b, BCI Species Profiles: *Tadarida brasiliensis*, http://www.batcon.org/index.php/all-about-bats/species-profiles.html?task=detail&species=1738&country=43&state=all&family=all&start=25 [accessed March 7, 2013].

Bat Conservation International, 2013a, Bracken Cave, http://batcon.org/index.php/get-involved/visit-a-bat-location/bracken-bat-cave/subcategory.html?layout=subcategory [accessed August 15, 2013].

Biswas, J., 2010, Kotumsar Cave biodiversity: A review of cavernicoles and their troglobitic traits: Biodiversity and Conservation, v. 19, p. 275–289. doi:10.1007/s10531-009-9710-7.

Clements, R., Sodhi, N.S., Schilthuizen, M., and Ng, P.K.L., 2006, Limestone karst of Southeast Asia: Imperiled arks of biodiversity: BioScience, v. 56, no. 9, p. 733–742. doi:10.1641/0006-3568(2006)56[733:LKOSAI]2.0.CO;2.

Cleveland, C.J., Betke, M., Federico, P., Frank, J.D., Hallam, T.G., Horn, J., Lopez, J.D. Jr., McCracken, G.F., Medellin, R.A., Moreno-Valdez, A., Sansone, C.G., Westbrook, J.K., and Kunz, T.H., 2006, Economic value of the pest control service provided by Brazilian free-tailed bats in south-central Texas: Frontiers in Ecology and the Environment, v. 4, p. 238–243. doi:10.1890/1540-9295(2006)004[0238:EVOTPC]2.0.CO;2.

Culver, D.C., 1982, Cave Life: Evolution and Ecology: Cambridge, Massachusetts, Harvard University Press, 189 p.

Culver, D.C., 1985, Trophic relationships in aquatic cave environments: Stygologia, v. 1, p. 43–53.

Dennis, C., and Aldhous, P., 2004, Biodiversity: A tragedy with many players, Nature, v. 430, p. 396–398. doi:10.1038/430396a.

Elliott, W.R., 2000, Conservation of the North American cave and karst biota, *in* Wilkins, H., Culver, D.C., and Humphreys, W.F., eds., Subterranean Ecosystems: Amsterdam, Elsevier, Ecosystems of the World 30, p. 665–689.

Fagan, W.F., Lutscher, F., and Schneider, K., 2007, Population and community consequences of spatial subsidies derived from central-place foraging: The American Naturalist, v. 170, p. 902–915. doi:10.1086/522836.

Ferreira, R.L., and Martins, R.P., 1998, Diversity and distribution of spiders associated with bat guano piles in Morrinho Cave (Bahia State, Brazil): Diversity and Distributions, v. 4, p. 235–241.

Ferreira, R.L., Prous, X., and Martins, R.P., 2007, Structure of bat guano communities in a dry Brazilian cave: Tropical Zoology, v. 20, p. 55–74.

Fierer, N., Schimel, J.P., and Holden, P.A., 2003, Variations in microbial community composition through two soil depth profiles: Soil Biology and Biochemistry, v. 35, p. 167–176. doi:10.1016/S0038-0717(02)00251-1.

Hancock, P.J., Boulton, A.J., and Humphreys, W.F., 2005, Aquifers and hyporheic zones: Towards an ecological understanding of groundwater: Hydrogeology Journal, v. 13, p. 98–111. doi:10.1007/s10040-004-0421-6.

Humphreys, W.F., 1991, Experimental re-establishment of pulse-driven populations in a terrestrial troglobite community: Journal of Animal Ecology, v. 60, p. 609–623. doi:10.2307/5301.

Hutchinson, G.E., 1950, Survey of Existing Knowledge of Biochemistry: 3. The Biochemistry of Vertebrate Excretion: New York, Bulletin of the American Museum of Natural History 96, 554 p.

Isaac, R.A., 2009, AOAC Method 985.01, Metals and other elements in plants, *in* Cunniff, P., ed., Official Methods of Analysis of AOAC International, 16th ed.: Arlington, AOAC International.

Kastning, E.H., Jr., 1983, Geomorphology and hydrogeology of the Edwards Plateau kast, central Texas [PhD thesis]: Austin, University of Texas at Austin.

Lavoie, K.H., Helf, K.L., and Poulson, T.L., 2007, The biology and ecology of North American cave crickets: Journal of Cave and Karst Studies, v. 69, no. 1, p. 114–134.

Marmonier, P., Vervier, P., Gibert, J., and Dole-Olivier, M.-J., 1993, Biodiversity in ground waters: Trends in Ecology and Evolution, v. 8, p. 392–395. doi:10.1016/0169-5347(93)90039-R.

Polis, G.A., Anderson, W.B., and Holt, R.D., 1997, Toward an Integration of landscape and food web ecology: The dynamics of spatially subsidized food webs: Annual Review of Ecology, Evolution, and Systematics, v. 28, p. 289–316. doi:10.1146/annurev.ecolsys.28.1.289.

Polis, G.A., and Strong, D.R., 1996, Food web complexity and community dynamics: The American Naturalist, v. 147, p. 813–846.

Poulson, T.L., 2005, Food sources, *in* Culver, D.C., and White, W.B., eds., Encyclopedia of Caves: Burlington, Vermont, Elsevier, p. 255–264.

Sanders, J.E., 1981, Principles of Physical Geology: New York, John Wiley and Sons, 636 p.

Schneider, K., Christman, M.C., and Fagan, W.F., 2011, The influence of resource subsidies on cave invertebrates: Results from an ecosystem-level manipulation experiment: Ecology, v. 92, no. 3, p. 765–776. doi:10.1890/10-0157.1.

Souza-Silva, M., Martins, R.P., and Ferreira, R.L., 2011, Cave lithology determining the structure of the invertebrate communities in the Brazilian Atlantic Rain Forest: Biodiversity and Conservation, v. 20, no. 8, p. 1713–1729. doi:10.1007/s10531-011-0057-5.

US EPA, 1992, Method 6010A, inductively coupled plasma-atomic emission spectroscopy, *in* Test Methods for Evaluation Solid Waste, Physical/Chemical Methods: United States Environmental Protection Agency SW-846, 3rd Edition.

Vermeulen, J., and Whitten, T., 1999, Biodiversity and Cultural Property in the Management of Limestone Resources: Lessons from East Asia: Washington, World Bank, 144 p.

Wurster, C.M., McFarlane, D.A., and Bird, M.I., 2007, Spatial and temporal expression of vegetation and atmospheric variability from stable carbon and nitrogen isotope analysis of bat guano in the southern United States: Geochimica et Cosmochimica Acta, v. 71, no. 13, p. 3302–3310. doi:10.1016/j.gca.2007.05.002.

D.A. Burney, J.P. Hume, G.J. Middleton, L. Steel, L.P. Burney and N. Porch – Stratigraphy and chronology of karst features on Rodrigues Island, Southwestern Indian Ocean. *Journal of Cave and Karst Studies,* v. 77, no. 1, p. 37–51. DOI: 10.4311/2013PA0132

STRATIGRAPHY AND CHRONOLOGY OF KARST FEATURES ON RODRIGUES ISLAND, SOUTHWESTERN INDIAN OCEAN

David A. Burney[1*], Julian P. Hume[2], Gregory J. Middleton[3], Lorna Steel[4], Lida Pigott Burney[5], and Nick Porch[6]

Abstract: The remote Indian Ocean island of Rodrigues, while largely of volcanic origin, also contains a large body of eolian calcarenite with over thirty surveyed caves and many other karst features. Little is known, however, regarding the age and stratigraphy of the clastic deposits in the caves and the associated fossils of the highly endemic, now mostly extinct, fauna. On the Plaine Caverne and Plaine Corail of the southwestern part of the island, we obtained sediment cores up to 10 m in length and excavated bones of the extinct fauna from caves in the vicinity. Stratigraphic description and radiocarbon dating revealed that sediments in Canyon Tiyel, a collapsed-cave feature, primarily accumulated during the early and middle Holocene. Sedimentation in the canyon and adjacent caves has slowed in recent millennia, with the result that many bones of fauna that went extinct after human arrival in recent centuries are on or near the surface. The chemistry of the sediments and the alternate wet and dry regime of the cave and canyon surfaces are often not conducive to preservation of bone collagen and plant microfossils. Grotte Fougère, with an apparently unique anchialine pond inside a collapsing cave, however, contains over one meter of highly organic sediment with excellent preservation of plant and animal remains.

Introduction

Rodrigues Island is the smallest and most isolated of the three Mascarene Islands. It was one of the last habitable places on earth to be discovered and colonized by humans. Due to its remote location about 600 km east of Mauritius in the southwestern Indian Ocean (Fig. 1) and its lack of a good natural harbor, being instead surrounded by a vast reef that posed a great hazard to curious early navigators, it was not until 1691 that the first small band of men, led by French Huguenot François Leguat, temporarily occupied the island (North-Coombes, 1971). Although the tiny colony was abandoned two years later, other visitors spent many months there at intervals of several decades, and a few French families and their slaves settled there in the late eighteenth century. At roughly thirty-year intervals beginning with Leguat, a succession of literate naturalists provided detailed accounts documenting the conversion of the island within one century from a natural paradise teeming with giant tortoises, the solitaire (*Pezophaps solitaria*), which was a giant pigeon related to the Dodo of neighboring Mauritius, and a host of other endemic birds, reptiles, invertebrates, and plants, to a deforested land lacking most of its native species (Cheke and Hume, 2008). Today this relatively small island supports a population of nearly forty thousand people, many of Creole descent.

With an area of only 108 km^2, it is perhaps surprising that this old volcanic island has a relatively large area of eolian calcarenite on its southwestern side, with over thirty surveyed caves, including a stream cave over a kilometer in length, and numerous surface karst features. Braithwaite (1994) attributes this large formation to the presence of a reef platform and shallow lagoon around the island that is more than twice the island's area. Although this karst area has yielded virtually all the fossils of the extinct and endangered endemic fauna found to date, almost nothing is known of the age and stratigraphic context of the cave sediments that have yielded these bones.

The goal of this project was to make a preliminary investigation of the island's stratigraphic contexts, with particular emphasis on the karst areas, with samples from other coastal sites for comparison. Since no natural lakes or inland marshes are known in this ancient eroded landscape, caves and related karst features offer the best hope for recovering information regarding the late Quaternary dynamics of this interesting and little-known island.

Methods

We have attempted to locate all the potential sites on the island and its offshore islets that might contain a stratigraphic record of the Holocene. Using sediment-coring and

[1] National Tropical Botanical Garden, Kalaheo, HI 96741 USA
[2] Bird Group, Dept. of Life Sciences, Natural History Museum, Akeman St., Tring, HP23 6AP UK
[3] Sydney Speleological Society, Box 269, Sandy Bay, TAS 7006 Australia
[4] Dept. of Earth Sciences, Natural History Museum, London SW7 5BD UK
[5] Makauwahi Cave Reserve, Box 1277, Kalaheo HI 96741 USA
[6] School of Life and Environmental Sciences, Deakin University, Burwood VIC 3125 Australia
*Corresponding author: dburney@ntbg.org

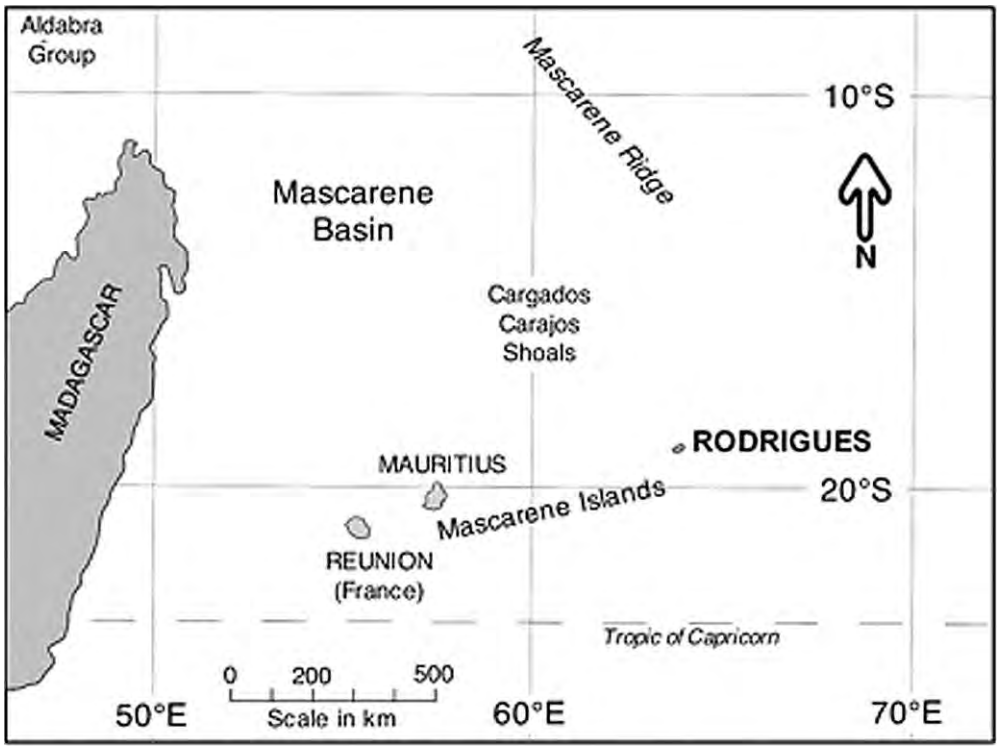

Figure 1. Location of Rodrigues Island in the southwestern part of the Indian Ocean, after Middleton and Burney (2013).

excavating equipment, we sampled sites throughout the most promising area, the caves and karst of the Plaine Corail and Plaine Caverne on the southwest corner of the island. We also sampled deposits of various types throughout the island and on Ile Gombrani, an offshore islet (Table 1, Fig. 2). Site locations were determined via GPS, and elevations were measured when possible within about 5 m using a high-resolution barometric altimeter calibrated to adjacent sea-level sites. All sediments were screened, wet or dry depending on substrate, to 1.5 mm, and all recovered fossils were dried, labeled, and placed in the accessions of the museum collections at the François Leguat Giant Tortoise and Cave Reserve (FLGTCR) near Anse Quitor.

Excavated materials and museum specimens excavated previously were submitted for AMS radiocarbon dating (Table 2). However, with few exceptions, bones selected for potential dating yielded little or no collagen, so that they could not be securely dated. The organic fraction of three key levels in the longest core, a 10 m section from Canyon Tiyel, a karst blind valley in the FLGTCR, yielded suitable material for dating after acid pretreatment to remove carbonates. Sediment samples were examined microscopically for fossil pollen contents and charcoal particles.

RESULTS

CANYON TIYEL CORES

Canyon Tiyel is a karst blind valley (Fig. 3) surrounded by subterranean chambers. The floor contains many boulders likely to be the result of roof and wall collapse. Three cores were collected via bucket auger from the clay floor of the canyon, one from near the center, one from the edge nearby, and one from the lower end of the canyon. The 10.1-m core from the central area, RCT-1, is briefly described in Table 3. The early date at 740 cm in this core probably reflects some reworking of older sediments, a phenomenon that is also apparent at the surface in Canyon Tiyel and the adjacent caves. The sandy and gravelly nature of the sediments around this level suggest higher-energy conditions at this time than in the lower part of the core dated at 9540 to 9460 cal yr BP (Table 2). The latter date is from finer and more organic sediments lacking the gravel in the 740-cm date, and it is therefore likely to be more reliable.

Other cores from Canyon Tiyel, although much shorter, confirmed the stratigraphic trends of the upper unit. In particular, RCT-3, from the slightly lower south end of the site, contained a few bone fragments, including some from the extinct giant tortoise *Cylindraspis* sp. at 70–80 cm, suggesting that sediments near the surface predate the late eighteenth century, when the tortoises were known from historical records to have been driven to extinction by overharvesting (Cheke and Hume, 2008). Of course we cannot rule out the possibility of redeposition in the case of such fragmentary material.

Pollen preservation was generally disappointing, probably owing to the destructive wetting and drying cycle that affects the canyon sediments. Sediments were also examined

Table 1. Sites investigated on Rodrigues Island.

Site in Figure 2	Site Name	Type	Location		Elevation (m ASL)	Samples
			Latitude	Longitude		
1	Canyon Tiyel	Blind Valley	S19°45.357′	E63°22.205′	24	Cores: RCT-1, 1A, 2, 3
2	Grande Caverne	Cave	S19°45.190′	E63°22.232′	52	Cores: RGC-1,2,3
3	Caverne Bambara I	Cave	S19°45.274′	E63°22.186′	37	Excavation: RBA-1
4	Caverne de la Vierge	Cave	S19°45.470′	E63°22.203′	…	Excavation: RCV-1
5	Caverne L'Affouche	Cave	S19°45.428′	E63°22.117′	…	Excavation (previous)
6	Caverne Mapou	Cave	S19°45.277′	E63°22.177′	47	Excavations: RMP-1,2
7	Caverne L'Etrave	Cave	S19°45.254′	E63°22.016′	27	Excavation: RET-1
8	Caverne Solitaire	Cave	S19°45.278′	E63°22.181′	34	Surface collection
9	Caverne Dora	Cave	S19°45.428′	E63°22.217′	…	Surface collection
10	Electricity Pole Cave	Cave	S19°45.681′	E63°22.289′	26	Excavation: REP-1
11	Caverne Papaye	Cave	S19°45.635′	E63°22.314′	22	Surface collection
12	Caverne Poule Rouge	Cave	S19°45.325′	E63°22.189′	…	Excavation (previous)
13	Caverne Monseigneur	Cave	S19°45.559′	E63°22.916′	23	Excavation: RMS-1 Core: RMS-1
14	Caverne d'Ami de Monseigneur	Cave	S19°45.528′	E63°22.910′	23	Surface collection
15	Caverne Mario	Cave	S19°45.669′	E63°23.129′	16	Surface collection
16	Caverne Patate (main entrance)	Cave	S19°45.492′	E63°23.191′	26	No collection
17	Caverne Bouteille	Cave	S19°45.903′	E63°22.443′	14	No collection
18	Grotte Fougère	Cave/Sinkhole	S19°46.090′	E63°22.586′	5	Cores: RGF-1,2 Excavations: RGF-3,4
19	Petit Lac	Pond	S19°46.048′	E63°22.544′	8	Surface collection
20	South Grande Var	Cave	S19°44.984′	E63°23.618′	3	No collection
21	North Grande Var	Cave	S19°44.975′	E63°23.613′	2	No collection
22	Ile Gombrani	Sinkhole	…	…	…	Cores: RGO-1,2
23	Cotton Bay	Estuary	S19°41.297′	E63°29.587′	2	Cores: CBE-1A,1B
24	Plaine Caverne	Quarry	S19°45.212′	E63°22.557′	73	Bulk samples, surface collection
25	Port Sud-Est	Quarry	S19°45.382′	E63°23.718′	13	Bulk samples, surface collection

for charcoal particles, and they were found to generally contain charcoal only in the surficial sediments, no doubt owing to the general absence of fires before human arrival and the low sedimentation rates at the site in recent centuries, as evidenced by the presence of bones of extinct tortoises near the surface.

Cave Deposits

Caves in the eolianite deposits of southwestern Rodrigues were surveyed in detail. Caves were explored and sampled throughout the Plaine Caverne and to lesser degree in the more southern karst area, known as Plaine Corail. These caves vary greatly in size, configuration, and elevation (Table 1), from small caves near sea level to huge caverns with entrances up to around 50 m ASL such as Grande Caverne and Caverne Patate. Vertical profiles were also diverse, ranging from large horizontal passages in the caves that integrate with Canyon Tiyel to more vertical caves such as Monseigneur and Bouteille. Of particular interest for paleoecological potential, were caves such as Grande Caverne and Caverne Bambara that have

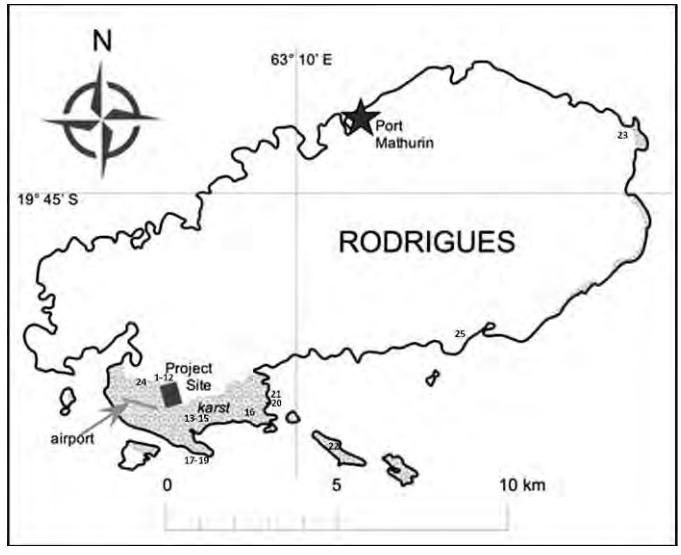

Figure 2. Map of Rodrigues Island showing approximate locations of sites investigated. See Table 1 for a key to numbered locations.

Table 2. AMS ^{14}C dates from Rodrigues Island.

Beta Lab No.	Material	Provenance	Radiocarbon Age (yr ± 1σ)	Calibrated Age Range cal yr BP (2σ)
RCT-1 Core				
309300	sediment	330 cm	6460 ± 30 BP	7430–7320
309301	sediment	740 cm	10020 ± 40 BP	11750–11740, 11720–11320
305254	sediment	990 cm	8490 ± 40 BP	9540–9460
Bones of Extinct Fauna				
305254	bone collagen	*Mascarenotus murivorus*, Caverne Dora RDO 60-75B	2850 ± 30	3060–2870
305257	bone collagen	*Pezophaps solitaria*, Caverne Monseigneur RMS-1: 114 cm	insufficient collagen	…
305255	bone collagen	*Cylindraspis* sp., Canyon Tiyel 70–80 cm in core RCT-3	insufficient collagen	…

significant amounts of clastic fill on their floors. Grande Caverne (Fig. 4), for instance, was cored in several places with the bucket auger, yielding profiles of clay stratigraphy up to 4.4 m thick. However, the chemistry of these sediments was conducive to preservation of neither bones, which were intact only near the surface, nor pollen grains. All cores bottomed out on the limestone floor of the cave. Grande Caverne is the island's most developed show cave (Fig. 5), with electric lighting and a raised walkway that protects the features while permitting appreciative viewing by many of the approximately twenty thousand tourists each year who visit FLGTR.

Other caves, such as Bambara I (Fig. 6), which is part of a cave in the process of collapse, with many skylights and entrances, have extensive breccia deposits on the floors. Excavations at this site yielded bones and shells in distinct layers, often including breakdown and clay lenses. Bones of extinct species, including the solitaire and giant tortoises, were present at the surface, indicating that the site has apparently not accumulated significant amounts of sediment in the last few centuries.

Figure 3. View of the floor of Canyon Tiyel, a karst blind valley where the grass is kept short by the grazing of hundreds of introduced Aldabra tortoises. The canyon and its many associated caves are part of the François Leguat Giant Tortoise and Cave Reserve.

Dating of bones recovered from caves proved extremely problematic. Visual inspection of many specimens at low magnification showed that the bones were generally porous and friable, as is typical of bones subjected to alternate wetting and drying, leading to oxidation and biological diagenesis of collagenous material. It was particularly disappointing that we could not date bones from a large erosion scarp below a skylight in Caverne Monseigneur, where excavation from a face and bucket augering at the foot of the scarp yielded a combined profile of 240 cm. These sediments yielded bones of solitaire and other extinct species, but these proved undatable due to a lack of collagen. Pollen preservation was also poor in these oxidized sediments.

One specimen, sampled from the museum collection, was relatively waxy and lustrous in appearance and yielded sufficient collagen for dating. This was from the extinct Rodrigues owl, *Mascarenotus murivorus*, from Caverne Dora. Although collected from only 60 to 75 cm below surface, it was dated to 2850 ± 30 yr BP (3060 to 2870 cal yr BP; Table 2). Again, as in Canyon Tiyel, this suggests very low sedimentation rates in the late Holocene. Caverne Dora is a small fissure cave (Figs. 7, 8), well above the canyon floor, and has probably been well-drained throughout its existence. The matrix consists primarily of limestone breakdown and alkaline sand, rather than the more acidic clay typical in many parts of the lower caves.

Another cave in the FLGTCR that has yielded many bones of the extinct and endangered fauna is Caverne Poule Rouge, an unusual cave with a downward-spiraling passage (Fig. 9). This cave is heavily decorated with attractive speleothems, including unusually large and

Table 3. Core sample descriptions.

Core Sample	Depth, cm	Color[a]	Notes
Core RCT-1 from Canyon Tiyel	0–50	2.5YR 3/4	Dark reddish brown clayey silt containing a few limestone fragments.
	50–350	5YR 3/4 7.5YR 3/3	Dark reddish brown silty clay, becoming darker and denser downwards.Dark brown silty clay, with fewer rocks and some land snail shell fragments (cf. *Tropidophora*). Sediment organic fraction at 330 cm dated to 6460 ± 30 BP (7430–7320 cal yr BP)
	350–580	7.5YR 3/3	Color and texture as above, becoming sandier at 580.
	580–755	7.5YR 3/2	Dark brown sandy silty humic clay. 740 cm sediment organic fraction dated to 10,020 ± 40 yr BP (11,750–11,740, 11,720–11,320 cal yr BP).
	755–810	7.5YR 3/2	Color as above, but sediments contain gravelly component consisting of basalt pebbles, shell fragments, and calcite.
	810–960	7.5YR 3/2	As above, but lacking gravel.
	960–990	7.5YR 4/3	Becoming lighter, more organic with some pebbles. 990 cm sediment organics dated to 8490 ± 40 yr BP (9540–9460 cal yr BP).
	990–1010	2.5Y 4/4	Olive brown sandy silt with basalt pebbles, calcarenite fragments, and marbling of orange-yellow to bluish-green streaks. Stopped on solid calcarenite rock at 1010 cm.
Core CBE-1B from Cotton Bay	0–30	10YR 3/4	Dark yellowish-brown silty clay loam with estuarine gastropod shells, marine shell fragments, and glass sherds.
	30–55	10YR 3/2	Very dark brown silty clay.
	55–80	10YR 4/6	Dark yellowish brown sandy silty clay.
	80–115	10YR 4/6	Dark yellowish brown silty humic sand, coarsening downward. Water table stood at 100 cm.
	115–160	10YR 4/6	Dark yellowish brown coarse humic sand, with marine shell fragments, seeds, plant fibers, and angular to sub-rounded basalt fragments. Stopped by collapsing loose sand.
Core RGO-1 from Ile Gombrani	0–25	5YR 6/4	Light brown humic clayey sand with calcareous nodules.
	25–50	5YR 6/4	As above, changing gradually to marbled brown clay and yellow sand at ca. 40 cm
	50–60	2.5Y 6/4	Yellow sand, stopped on rocks.
Core RGF-2 from Grotte Fougère	0–20	N 2/0	Black unconsolidated muck, no coarse particles except introduced snails.
	20–40	2.5Y 3/3	Gradual change to 2.5Y 3/3 dark olive brown silty muck.
	40–70	2.5Y 4/4	Olive brown silty muck, including seeds, snails, and bones of endemics.
	70–102	2.5Y 4/4	Olive brown silty sandy muck, with increasing molluscan gravel near bottom.

[a] Munsell color notation, the order is hue, value, and chroma. For example, a designation of 2.5YR 3/4 has hue = 2.5YR, value = 3, and chroma = 4.

grotesque helictites (Fig. 10). Excavations through a pinkish-gray stony silt that is 85 cm thick have yielded many good fossil finds. On the surface of the floor of a distant passage is a unique virtually complete skeleton of an adult solitaire, mantled in flowstone (Fig. 11).

Table 4 is a provisional list of vertebrate taxa identified from bones collected in the caves in and near the FLGTCR (Table 1, sites 2–12). This includes many of the extinct taxa of Rodrigues, notably an associated female solitaire from Caverne L'Affouche, associated Rodrigues night heron (*Nycticorax megacephalus*) and Rodrigues rail (*Erythromachus leguati*) from Caverne Poule Rouge, and even keratinous scutes from the carapace of the extinct tortoise *Cylindraspis peltastes.* These remains, as well as land snail shells and fossil seeds, were labeled and added to the accessions of the museum at FLGTCR for future studies.

Other Deposits

Sites containing Quaternary stratigraphy were sought throughout the island. Although most of the island is

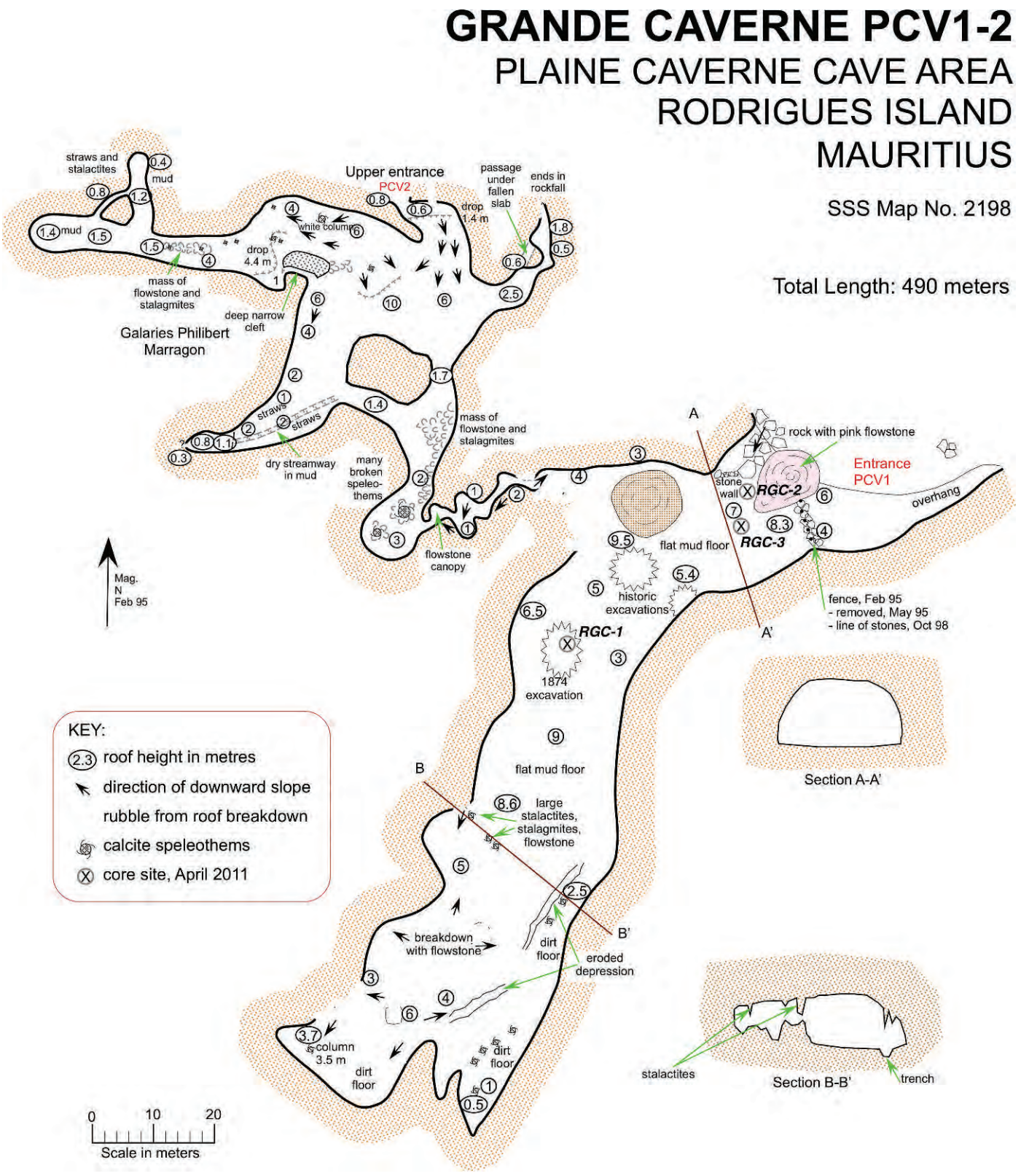

Figure 4. Map of Grande Caverne in the François Leguat Giant Tortoise and Cave Reserve. The sites of sample cores RGC1, 2, and 3 are indicated.

Figure 5. Grande Caverne is Rodrigues's most-developed show cave, with electric lights and raised walkways designed to minimize tourist impacts while affording a good view of the spectacular speleothems.

ancient eroded volcanic rocks with no potential for our research purposes, one distinct possibility is that the inshore parts of the small estuaries formed by the short streams that drain the interior might contain intact stratigraphy. As might be expected, however, the estuarine and stream-bed sediments show evidence for high-energy deposition, with cobbles and gravel mixed into sandy, silty, or clayey deposits. Likewise, organic lenses were generally thin and superficial. The frequent occurrence of storm surges and hard downpours associated with the violent cyclones that occur periodically in the southwestern Indian Ocean at this latitude probably quickly re-mix any stratified deposits in any context that is near sea level or adjacent to the headwalls that are characteristic of the inland side of these small estuaries. Cotton Bay, number 23 in Figure 2 and Table 1, one of the largest and flattest areas inshore from the coast, was judged to be the most promising, and bucket auger cores from this site yielded some distinctive stratigraphy. The description of core CBE-1B is summarized in Table 3.

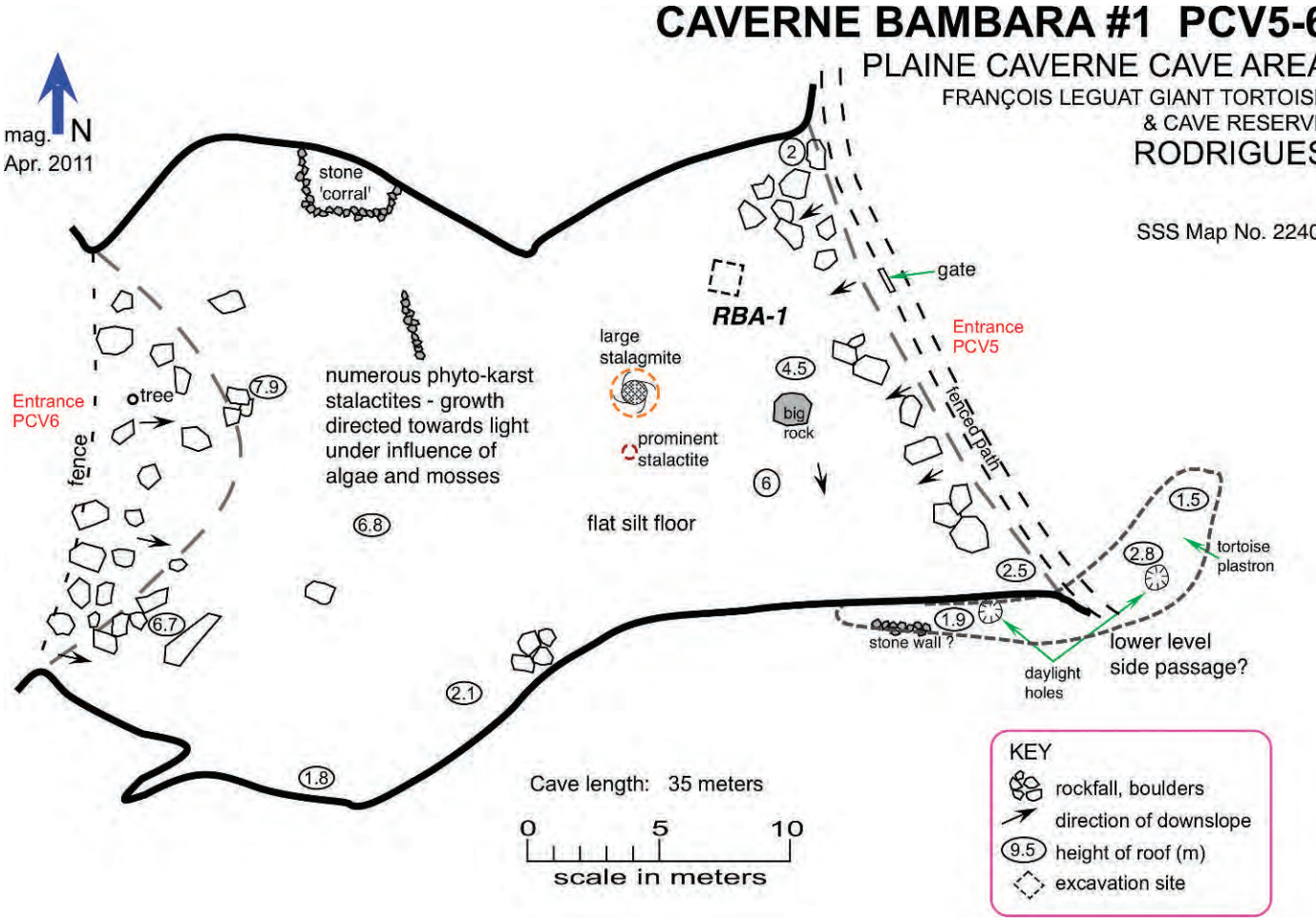

Figure 6. Map of Caverne Bambara I showing location of excavation site RBA-1. This is one of four mapped cave sections in the collapsing Bambara system, characterized by many skylights and entrances and a complex floor stratigraphy including breccias, clay lenses, and breakdown.

Figure 7. In Caverne Dora, one of the fissure caves in the walls of Canyon Tiyel, delicate speleothem growth even near the floor confirms that the higher caves in the system receive little if any water flow during rainy seasons, resulting in better bone preservation.

Another possibility explored was that the small eolian calcarenite limestone quarries that have been excavated on the southwest and southeast sides of the island for building stone might contain late Quaternary fossils. Indeed, the two quarries investigated contained interesting cross-bedded calcarenites, with some associated shells of land snails that appeared to be surficial and fissure-fill deposits. However, these sites were heavily oxidized and subject to water erosion, and were not found to contain organic materials of interest.

Yet another area of investigation was a search for permanent water bodies in the karst that might serve as coring sites. One subterranean pond was previously known: Caverne Bouteille is a small opening on the Plaine Corail that gives access to a water-filled chamber that serves as a water source for local people. A previous descent by author GM confirmed that the small amount of sediment in the bottom was likely to have been disturbed by manual water extraction.

Two other small bodies of water were found in surficial limestones near Pointe Corail, on the extreme southwest corner of the island. One of these was a small pond, which we named Petit Lac, in a natural depression in the surficial calcarenite. This pond contained no significant sediment accumulation, probably owing to deflation at times when the shallow water in this rain-fed pond dried out. The other is a small, partially collapsed cave feature (Fig. 12), which we named Grotte Fougère (Fern Grotto) that contained a small pond (Figs. 13, 14) beneath the cave overhang with measured water-surface elevation within a meter of sea level. This pond is probably hydrologically stable, as its low surface elevation would suggest that it is a hydrographic window, i.e., a groundwater-fed body, and it is isolated from direct marine action by higher land surfaces on all sides. The pond is also under slight tidal influence, a true anchialine pond, as it showed variation over 30 cm during the tidal cycle, but lagging as much as 2 hr behind the much greater tidal variation of 1 m on the day of observation on the adjacent estuary of the Anse Quitor River, which is visible from the rim of the sinkhole.

Fine organic sediment has accumulated inside the small cave. Two 5-cm diameter piston cores were obtained from the area of the pool that probing showed to have the thickest sediment package, about 1.2 m to the rock bottom. The sediments are a fine dark muck containing well-preserved bones, terrestrial and freshwater gastropod shells, and microfossils that include pollen, spores, and algal skeletons. Core RGF-2 is summarized in Table 3.

Three bucket auger cores were collected next to the continuous gravity cores and wet-screened on site in 30-cm increments. Among the findings was a radius of an adult female solitaire that had a healed break mid-shaft. A 1.2 by 0.4 m test pit, RGF-4, was excavated about 15 m north-northwest of the coring site, along the western wall of the cave, to a depth of 50 cm. It yielded, at the surface, a tibial epiphysis of the extinct giant saddle-backed tortoise *Cylindraspis vosmaeri.*

An effort was made to visit as many offshore islets as possible, as we have noted previously that small islets may sometimes harbor depressions fed by fresh or brackish groundwater, and sedimentation rates may be quite low, owing to the lack of human activities and terrestrial sediment sources on these uninhabited islands. We were able to procure a small boat and visit the following islets: Chat (Pierrot), Gombrani, Hermitage, and Crabe. Only Gombrani, site 22 in Figure 2, showed any promise. On this islet, near the center, were some very small solution features in calcarenite, tiny depressions with brackish water at depth and some soft sediment. A sounding with the bucket auger revealed 60 cm of soft sediment down to rock (Table 3).

DISCUSSION

As is often the case with small islands, it has been difficult to find suitable sites for our paleoecological investigations. However, we have made significant progress on several fronts. First, we now have, thanks to a thorough review of the historical literature for Rodrigues (see Cheke and Hume, 2008), a good understanding of the transformation there in the wake of human arrival. Second, our intensive survey of the island's paleoecological potential has shown what will and will not work in terms of future research efforts. Caves there hold great promise for further elucidating the past faunal diversity of the island, which clearly has one of the highest percentages of endemism

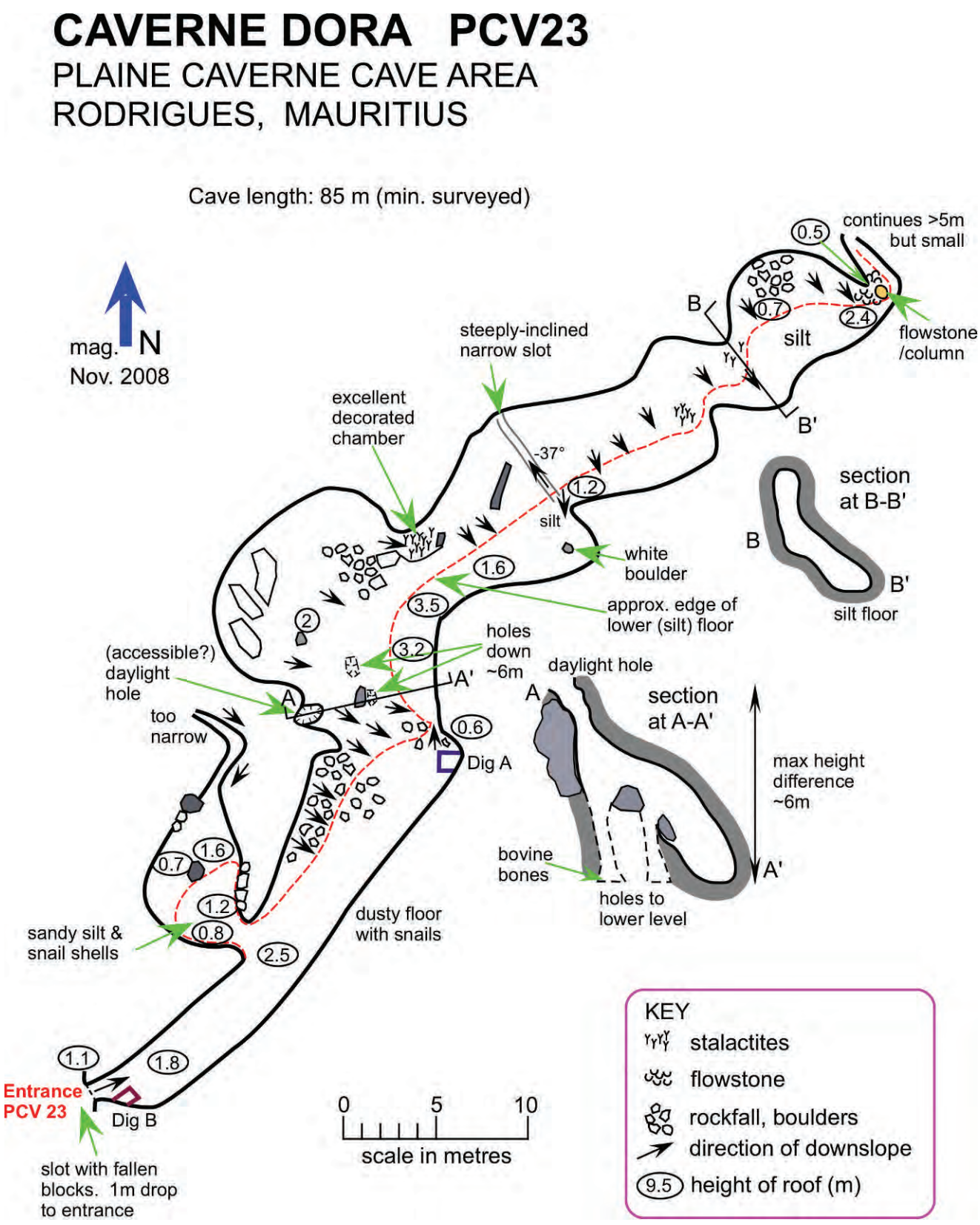

Figure 8. Map of Caverne Dora, showing the locations of the two excavations, Dig A and Dig B, conducted by authors JH and LS and others in past field seasons.

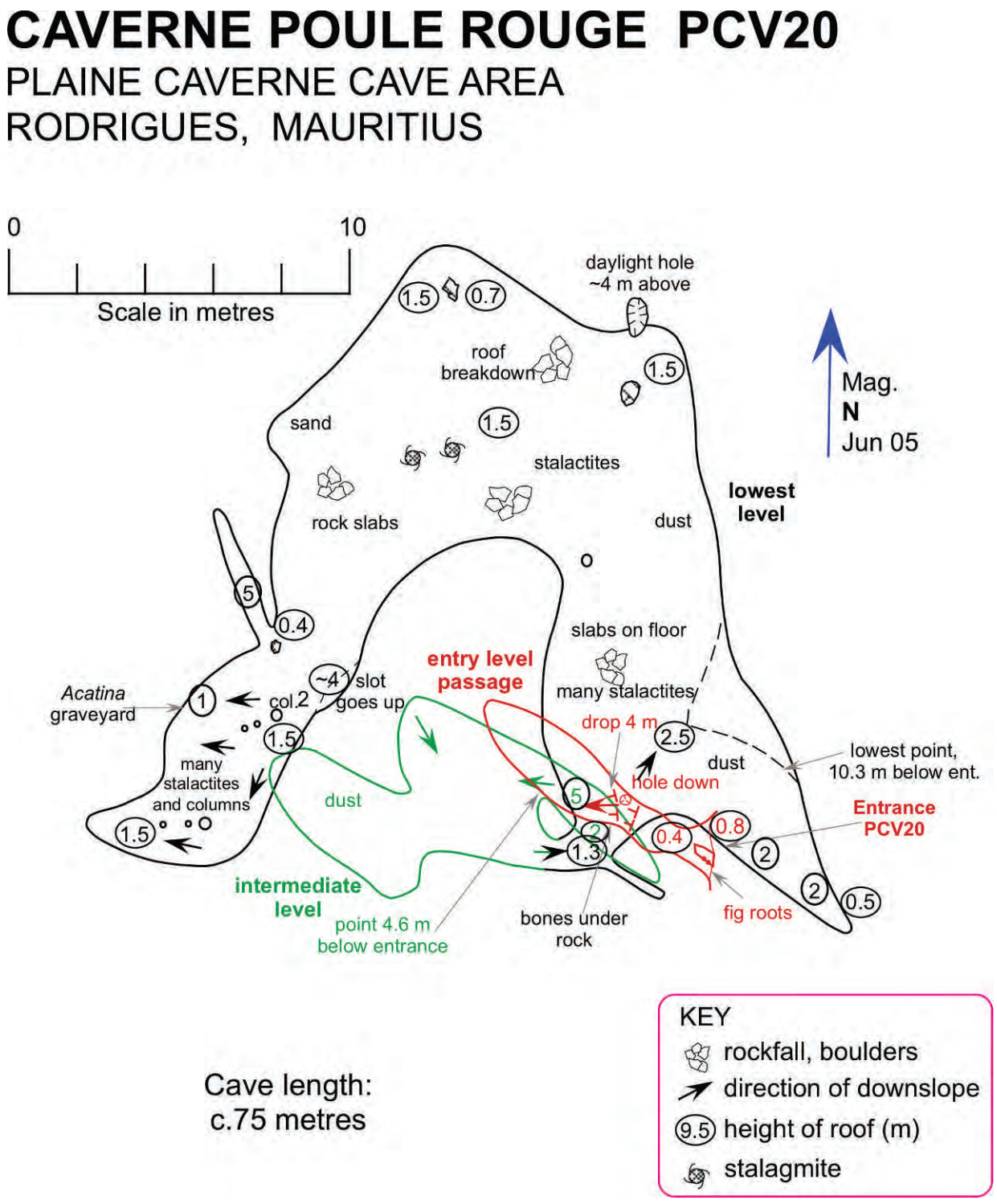

Figure 9. Map of Caverne Poule Rouge on the upland adjacent to Canyon Tiyel. It strives to show the vertical complexity of the passages, which spiral downward through three distinct levels.

found anywhere (Cheke and Hume, 2008). But the chemistry of these caves appears to be largely unsuitable for preservation of bone collagen, which limits their suitability for addressing chronological issues. Collagen preservation was poor in nearly all materials examined, both in our excavations and in museum specimens accumulated from previous investigations. Neither the calcareous breccias, with very high pH, nor the relatively

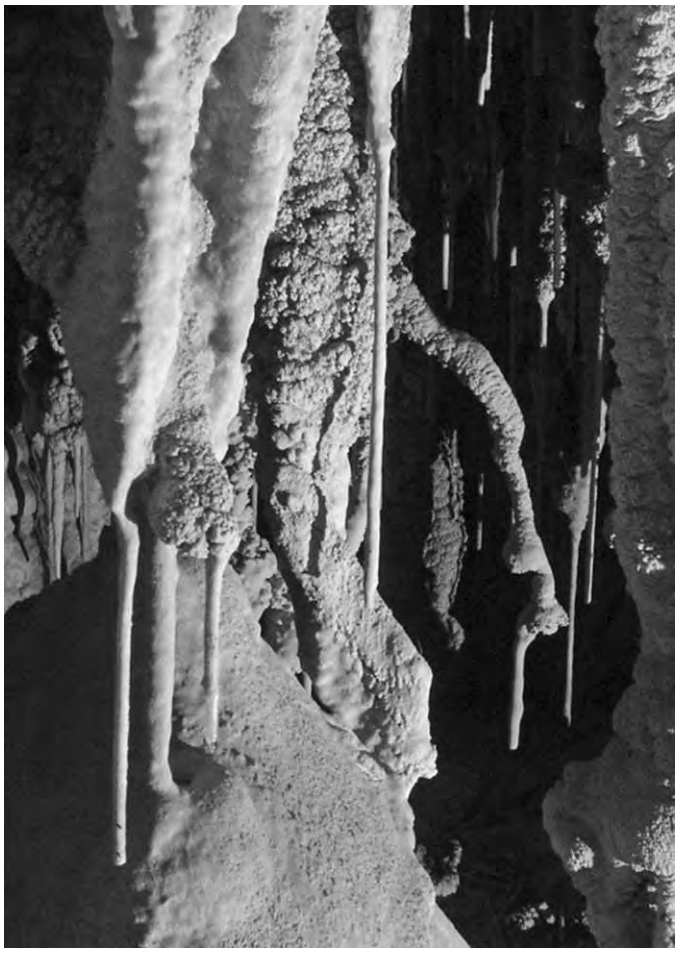

Figure 10. Delicate and grotesquely twisted helictites adorn the cave ceiling in some chambers in Caverne Poule Rouge on the upland adjacent to Canyon Tiyel.

acidic clays accumulated on the floors of some caves were conducive to protein preservation, although the former often preserved the bone morphology reasonably well, allowing positive identification. Likewise, the absence of natural lakes and extensive marshlands on the island poses a challenge for recovery of microfossil evidence.

We now know many things about the island's past environment, however, that we didn't know before embarking on this project. The caves of the Plaine Caverne and Plaine Corail are in a body of eolianite not previously surveyed in detail. Now that we realize the considerable height above sea level of some of the largest and probably oldest caves and the thickness of the calcarenite deposit, which has only weak stratification other than cross-bedding and an absence of thick intercalated clay layers, the case is strong that they represent the product of a single, drawn-out depositional event. Since the relatively uniform deposits extend from the highest calcarenite quarry at 73 m to sea level and perhaps lower, possibly without major hiatus, this would imply the formation of large dunes at some time in the middle to late Pleistocene, possibly during a period that includes an extreme high-stand of the sea. Although no literature has been found that dates these deposits on Rodrigues or analyzes them in detail, similar deposits exist in the Hawaiian Islands, the Bahamas, and Bermuda (Blay and Siemers, 1998; Hearty and Kindler, 1995). Although these islands are in the both the Pacific and Atlantic Oceans, eustatic sea-level change is of course a worldwide phenomenon, and the effects of interglacial sea-level rise would be expected to be similar on any tropical island not subject to rapid isostatic rebound or tectonic subsidence.

For instance, this type of thick deposit on Kaua'i has been indirectly datable, owing to the convenient presence of a basaltic lava flow that caps the deposit. This basalt has been dated to about 350,000 yr BP with K-Ar radiometric methods, leading to the tentative conclusion that the highest-elevation eolian calcarenite deposits are from Oxygen Isotope Stage 11, about 400,000 years ago, when sea level reached its highest extent, perhaps 20 m or more above present sea level, in the late Pleistocene (Hearty *et al.*, 2000; Blay and Longman, 2001; but see Rohling et al., 2010). Of course, it is possible that, as in the Hawaiian Islands, some lower-elevation deposits are from subsequent high-stands of the sea during later interglacials. The apparent absence of extensive intercalated clay or lithified red soil layers within the calcarenite beds on Rodrigues, unlike those documented for Kaua'i (Hearty et al. 2000) and Madagascar (Burney et al. 2008), for instance, would suggest that the eolianite bodies were deposited during one interglacial, since these contrasting glacial-age deposits appear to be absent. However, remarkably little is known about the Pleistocene geology of Rodrigues, and the case may not be exactly parallel.

In any case, our dating of Canyon Tiyel clastic sediments suggests that the present landforms of the Rodrigues karst were largely shaped prior to the Holocene, with subsequent subaerial formation and deposition of clays since that time. It appears that much of this deposition occurred early in the present interglacial, with the land surface inside the canyon reaching its present configuration in recent millennia. Dating of the owl bone from near the surface in adjacent Caverne Dora likewise confirms that relatively little sedimentation has occurred there in the last two millennia.

Although interesting, and useful to know, this finding also explains why our search for high-resolution deposits in the past millennium and recent centuries has proved nearly fruitless. This hampers our goal of finding paleoecological deposits coeval with the transition from the prehuman endemic biota to the current anthropogenic, biologically depauperate landscapes, which historical evidence suggests began in the late seventeenth century, later than perhaps any other habitable landscape on earth. Instead, we typically have found, on or very near the surface in cave deposits, a mixture of extinct forms, recently introduced species, and industrial materials such as glass and even plastic. If there has been human-caused erosion during the

Figure 11. An essentially complete skeleton of the giant extinct flightless pigeon of Rodrigues, the solitaire (*Pezophaps solitaria*) is mantled by flowstone on the floor of a distant passage in Caverne Poule Rouge.

last two centuries, this material has for the most part not been deposited in the investigated calcarenite caves of Rodrigues, or if it has, it has been hopelessly mixed with redeposited material from earlier times, perhaps by large introduced land snails and endemic land crabs. It is more likely that the long horizontal passages in caves near the level of the floor of Canyon Tiyel, such as Grand Caverne and Caverne Bambara, were formed during earlier

Table 4. Endemic and native vertebrate taxa identified from bones collected.

Reptiles		Birds		Mammals	
Scientific Name	Common Name	Scientific Name	Common Name	Scientific Name	Common Name
Cylindraspis vosmaeri	Tortoise	*Acrocephalus rodericana*	Rodrigues Warbler	*Pteropus rodricensis*	Rodrigues Fruit Bat
Cylindraspis peltastes	Tortoise	*Alectroenas payandeei*	Rodrigues Blue Pigeon		
Phelsuma gigas	Rodrigues Night Gecko	*Eurythromachus leguati*	Rodrigues Rail		
Phelsuma edwardnewtoni	Rodrigues Day Gecko	*Foudia flavicans*	Rodrigues Warbler		
Phelsuma/*Nactus*	small geckos ×4 sp.	*Hypsipetes sp.*	Bulbul		
		Necropsar rodericanus	Rodrigues Starling		
		Necropsittacus rodericanus	Rodrigues Parrot		
		Nycticorax megacephalus	Rodrigues Night Heron		
		Nesoenas rodericana	Rodrigues Turtle Dove		
		Mascarenotus murivorus	Rodrigues Owl		
		Passerines	Undescribed ×2		
		Pezophaps solitaria	Solitaire		
		Phaethon lepturus	White-tailed Tropicbird		
		Psittacula exsul	Rodrigues Parakeet		
		Pterodroma sp.	Petrel		

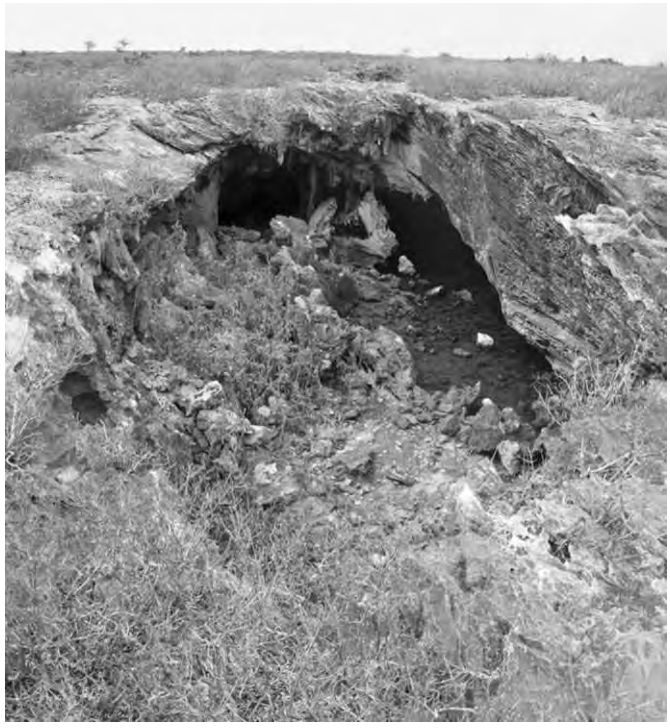

Figure 12. Grotte Fougère (Fern Grotto) near Pointe Corail is a collapse feature with an anchialine pond inside that is under some tidal influence.

interglacials, when sea level may have been higher; and therefore, the wedge of fresh water forming the phreatic zone near the coast was at the approximate level of these cave passages and actively cutting the calcarenite deposits. In the Holocene, sea level has risen only to a much lower level, so that surface drainage is out of the adjacent Anse Quitor River, which forms the present estuary. This reconstruction, while hypothetical, is consistent with the presence of very large speleothems in these caves. During the Holocene, including the present, water only accumulates in the caverns adjacent to Canyon Tiyel during severe rainstorms, depositing the Holocene clays studied and ensuring that bone preservation is poor on the cave floors. By contrast, the higher fissure caves on the walls of Canyon Tiyel, such as Dora and Poule Rouge, show no signs of water-born clay deposition, have only thin (<1 m) mantles of clastics derived from breakdown and infiltration from cracks in the ceiling, and contain some bones in a better state of preservation.

Of the many caves investigated, only Grotte Fougère near Pointe Corail shows any promise for future efforts at reconstructing late Holocene paleoenvironments from microfossils, seeds, and datable bones and land snail shells from an exceptional cave site, as was done at Makauwahi Cave, Kaua'i (Burney et al., 2001). Work underway on cores and excavated materials from Grotta Fougère on Rodrigues will be used in studies aimed at reconstructing paleoenvironments of the centuries just prior to the human transformation of the island. It is also conceivable that, by comparing stratigraphic records of human-caused change here to known historical events, Rodrigues could be realized as a potential Rosetta Stone for deciphering paleoecological records for other sites around the world, where the human transformation was an entirely prehistoric phenomenon known only from paleoecological inference. In this sense, Rodrigues may be highly relevant to interpreting late-prehistoric events in lands as disparate as Australia, the Americas, and large and small islands colonized by preliterate peoples, from Madagascar to Hawai'i (Burney and Flannery, 2005). Whatever the case, the many interesting caves and other karst features on this tiny remote island certainly merit further attention from the speleological community.

Figure 13. Panoramic view of the subterranean pond in Grotte Fougère. Coring sites were on the far left of the view.

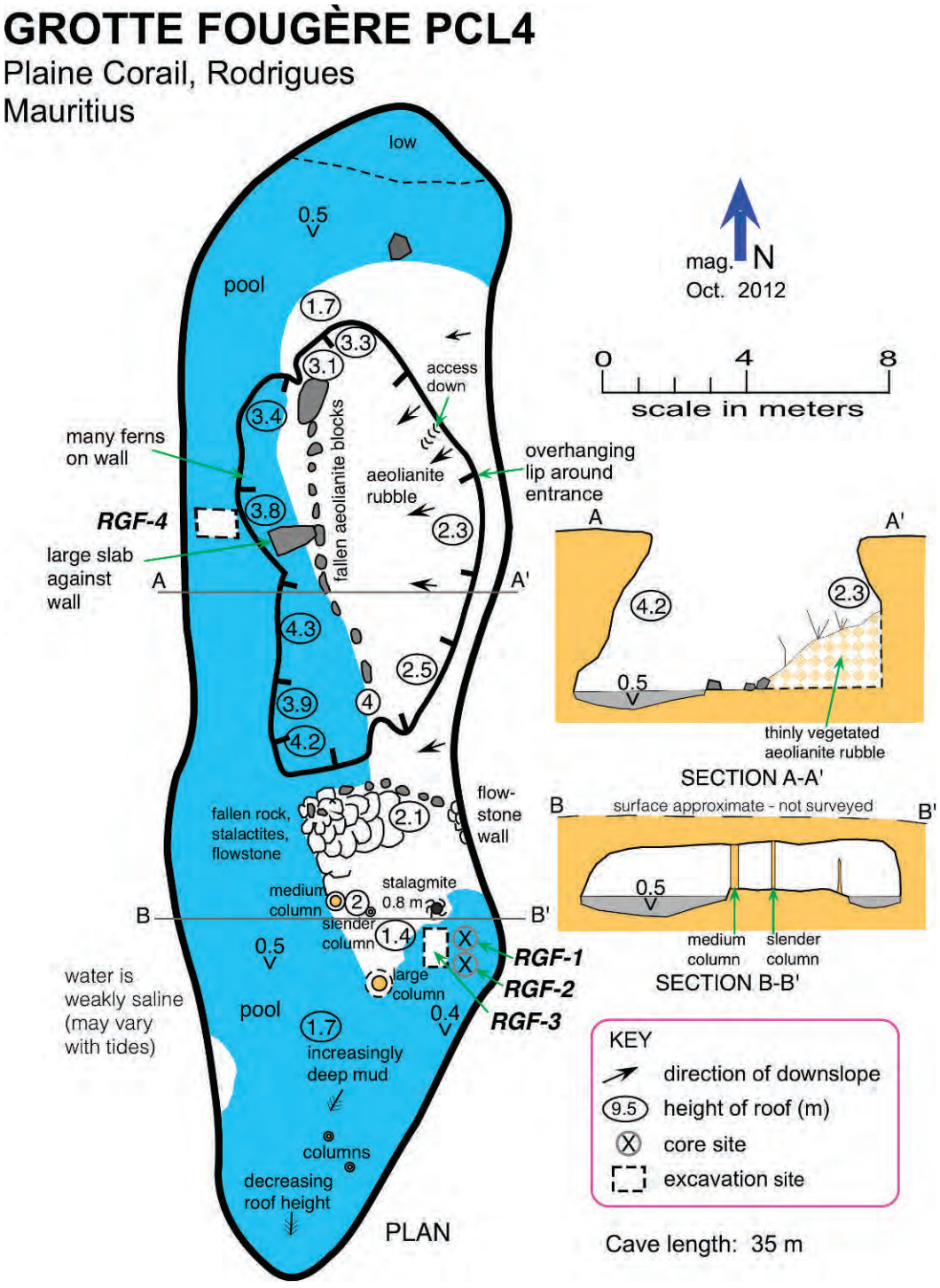

Figure 14. Map showing the location of piston coring sites RGF-1 and 2 and excavation sites RGF-3 and 4 in Grotte Fougère.

Conclusions

The thick calcarenite deposits of southwestern Rodrigues Island contain a rich variety of cave and karst features. Coring and excavations in sediments of a range of site types reveal that cave and canyon floors in the calcarenite contain thick clay-based deposits of Holocene age. The chemistry and hydrology of many of the lower caves is not conducive to fossil preservation, although higher, well-drained caves, and one small cave pool, show more promise. This body of brackish water inside Grotte Fougère contains sediments with well-preserved bones, shells, plant macrofossils, and microfossils. Although suitable sites for paleoecological research are now known to be scarce on Rodrigues, the potential exists for using recovered stratigraphy in comparisons with other islands. Rodrigues and the rest of the Mascarenes hold considerable potential as a Rosetta Stone for comparison to landmasses colonized prehistorically by humans. On Rodrigues, to a greater extent than almost any other place on the planet, virtually the entire history of human colonization and subsequent transformation was recorded contemporaneously by literate eyewitnesses.

Acknowledgements

We thank the National Geographic Society for grants #8819-10 and #W263-13 (Waitt Foundation) for funding of the Rodrigues research. Additional support was provided by the Natural History Museum (UK) Departmental Investment Fund to JPH and the museum's Department of Earth Sciences to LS. Staff of the François Leguat Giant Tortoise and Cave Reserve (Anse Quitor, Rodrigues Island, Mauritius) assisted with logistics. For guidance in all phases of local research, we thank Aurele André, Arnaud Meunier, and Owen Griffiths.

References

Blay, C.T., and Longman, M.W., 2001, Stratigraphy and sedimentology of Pleistocene and Holocene carbonate eolianites, Kaua'i, Hawai'i, U.S.A., *in* Abegg, F.E., Harris, P.M., and Loope, D.B., eds., Modern and Ancient Carbonate Eolianites: Sedimentology, Sequence, Stratigraphy and Diagenesis, Tulsa, Society for Sedimentary Geology, SEPM Special Publication, v. 71, p. 93–115. doi:10.2110/pec.01.71.0093.

Blay, C., and Siemers, R., 1998, Kauai's Geologic History: A Simplified Guide: TEOK Investigations, Kaua'i, 33 p.

Braithwaite, C.J.R., 1994, Quaternary oolites in the Indian Ocean, Washington, National Museum of Natural History, Atoll Research Bulletin, no. 420, 10 p. doi:10.5479/si.00775630.420.1.

Burney, D.A., and Flannery, T.F., 2005, Fifty millennia of catastrophic extinctions after human contact: Trends in Ecology and Evolution, v. 20, p. 395–401. doi:10.1016/j.tree.2005.04.022.

Burney, D.A., James, H.F., Burney, L.P., Olson, S.L., Kikuchi, W., Wagner, W.L., Burney, M., McCloskey, D., Kikuchi, D., Grady, F.V., Gage, R. II, and Nishek, R., 2001, Fossil evidence for a diverse biota from Kaua'i and its transformation since human arrival: Ecological Monographs, v. 71, no. 4, p. 615–641. doi:10.1890/0012-9615(2001)071[0615:FEFADB]2.0.CO;2.

Burney, D.A., Vasey, N., Godfrey, L.R., Ramilisonina, R., Jungers, W.L., Ramarolahy, M., and Raharivony, L., 2008, New findings from Andrahomana Cave, southeastern Madagascar; Journal of Cave and Karst Studies, v. 70, no. 1, p. 13–24.

Cheke, A., and Hume, J., 2008, Lost land of the dodo: An ecological history of Mauritius, Réunion and Rodrigues: T & AD Poyser, London, 464 p.

Hearty, P.J., and Kindler, P., 1995, Sea-level highstand chronology from stable carbonate platforms (Bermuda and the Bahamas): Journal of Coastal Research, v. 11, no. 3, p. 675–689.

Hearty, P.J., Kaufman, D.S., Olson, S.L., and James, H.F., 2000, Stratigraphy and whole-rock amino acid geochronology of key Holocene and last interglacial carbonate deposits in the Hawaiian Islands: Pacific Science, v. 54, p. 423–442.

Middleton, G.J., and Burney, D.A., 2013, Rodrigues—An Indian Ocean island calcarenite: Its history, study, and management, *in* Lace, M.J., and Mylroie, J.E., eds., Coastal Karst Landforms: Dordrecht, Springer, Coastal Research Library no. 5, p. 261–276. doi:10.1007/978-94-007-5016-6_12.

North-Coombes, A., 1971, The Island of Rodrigues: Port Lovis, Mauritius, Book Printing Services, (reprinted 2002). 337 p.

Rohling, E.J., Braun, K., Grant, K., Kucera, M., Roberts, A.P., Siddall, M., and Trommer, G., 2010, Comparison between Holocene and Marine Isotope Stage-11 sea-level histories: Earth and Planetary Science Letters, v. 291, p. 97–105. doi:10.1016/j.epsl.2009.12.054.

S. Negri, S. Margiotta, T.A.M. Quarta, G. Castiello, M. Fedi, G. Florio – Integrated analysis of geological and geophysical data for the detection of underground man-made caves in an area in southern Italy. *Journal of Cave and Karst Studies,* v. 77, no. 1, p. 52–62. DOI: 10.4311/2014ES0107

INTEGRATED ANALYSIS OF GEOLOGICAL AND GEOPHYSICAL DATA FOR THE DETECTION OF UNDERGROUND MAN-MADE CAVES IN AN AREA IN SOUTHERN ITALY

Sergio Negri[1,2*], Stefano Margiotta[1,2], Tatiana Anna Maria Quarta[1], Gabriella Castiello[3], Maurizio Fedi[3], and Giovanni Florio[3]

Abstract: In Cutrofiano, in the southern part of the Salento Peninsula, Apulia, Italy, a Pleistocene calcarenitic sequence was quarried by digging extensive networks of galleries along the geological succession most suitable for the quarrying activity. These caves represent a potential hazard for the built-up environment due to the occurrence of underground instability that may propagate upward and eventually reach the surface, causing sinkholes. In this work we propose integrated interdisciplinary methods for cavities detection. The methodology was applied at a test area located along a major road near Cutrofiano using geological and electrical-resistivity tomography and microgravity geophysical methods.

Introduction

Natural and anthropogenic caves represent potential hazards for the built-up environment because local instability may propagate upward and eventually cause the formation of sinkholes. The effects at the ground surface may be severe when the caves are at shallow depth. In the Apulia region of southern Italy there are many sites where underground quarrying was done in the past, due to the presence of good rocks for building purposes (Parise, 2010; Parise and Lollino, 2011). Cutrofiano is a site affected by a network of man-made cavities that underlie major roads and part of the urban center. Due to several soil collapses, sinkholes formed near roads and houses. In order to protect the potentially affected areas, the municipal and provincial authorities are very interested in evaluating the risk of collapses and tackling the problem of instability. Unfortunately, the technical information about the sinkholes is often poor and the maps of the man-made caves are incomplete, making any forecast inaccurate. In these cases, non-destructive geophysical methods can play an important role in identifying and mapping the unknown cavities.

In scientific literature, many papers report on the successful application of geophysical prospecting for the detection of natural cavities: Gibson et al. (2004), Leucci et al. (2004), Mochales et al. (2008), Kaufmann et al. (2011), Gambetta et al. (2011), Gómez-Ortiz and Martín-Crespo (2012) and Pueyo Anchuela et al. (2013). This is probably because natural cavities are often isolated, with a high contrast between their physical parameters and those of the host material. Applications of geophysical prospecting in areas of abandoned networks of manmade cavities are less frequent: Margiotta et al. (2012), Martinez-Lopez et al. (2013), Martinez-Pagan et al. (2013), Bianchi Fasani et al. (2013), and Kotyrba and Schmidt (2014). In these more complex cases, we propose the application of integrated interdisciplinary methods that consist of creating a conceptual hydrostratigraphical model using geological data like quarry plans and boreholes, selection of geophysical methods appropriate to the physical parameters of the setting to obtain detailed subsurface information, planning of boreholes based on the geological and geophysical results, and matching of the hydrostratigraphic and geophysical models, constrained by boreholes data, to obtain a detailed characterization of the subsoil and successful quarry location.

This methodology was applied to a test area near an important road that links Cutrofiano to Collepasso and Supersano that is probably at risk by the presence of quarries, whose floor plans are, however, unknown.

Morphological and Historical Setting

The study area in Cutrofiano (Fig. 1) is located in southern Apulia at an average altitude of about 100 m above sea level. Here, the Pleistocene calcarenite, a typical soft rock, was quarried by digging extensive networks of underground galleries that followed the levels within the local geological succession most suitable for the quarrying activity (Fig. 2). Extraction employed manual tools in the past and mechanical tools in more recent times. Some of the oldest quarries reveal areas excavated both by hand and mechanically. The blocks of stone were removed so as

[1] Department of Biological and Environmental Science and Technologies (DiSTeBA), University of Salento (Italy)
[2] GEOMOD S.r.l. Spin-off, University of Salento
[3] Dipartimento di Scienze della Terra, dell'Ambiente e delle Risorse, Università Federico II di Napoli (Italy)
* Corresponding author: sergio.negri@unisalento.it (Sergio Negri)

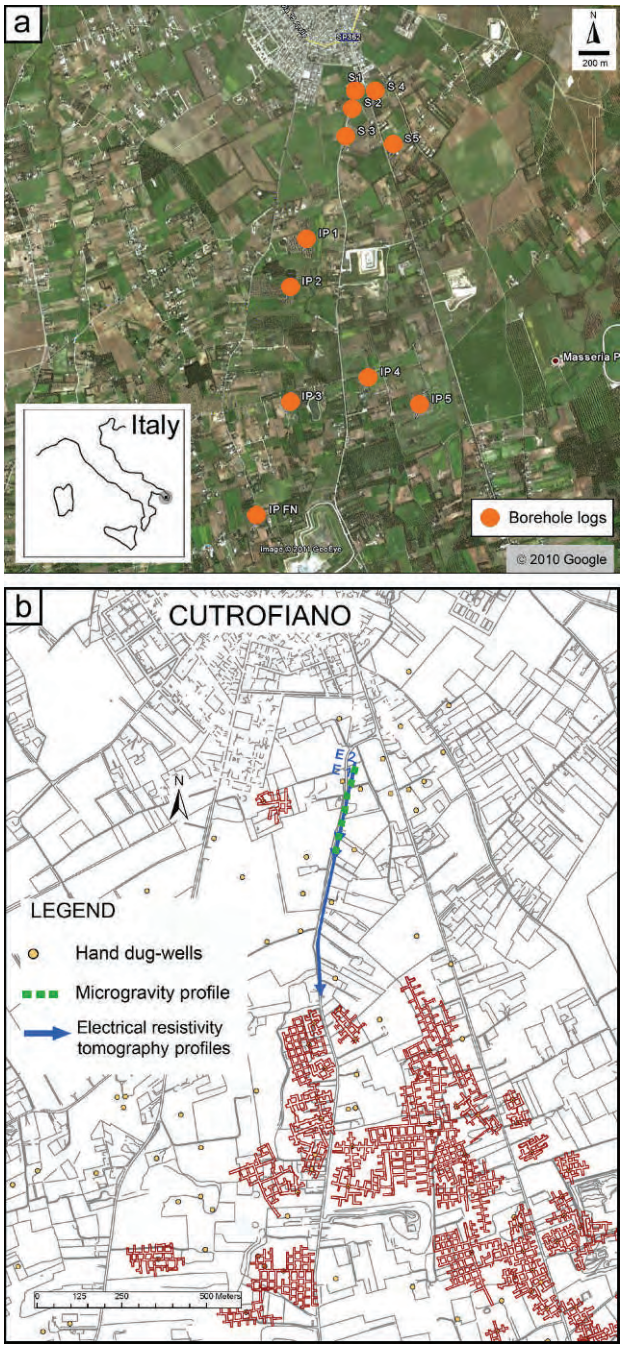

Figure 1. (a) Aerial view of the study area, with boreholes that provided stratigraphic information shown. The holes S1, S2, and S3 were drilled as part of this study and are described in the text. (b) Map of the area, with known, surveyed parts of the quarry networks shown. The hand-dug wells hint at the extent of unknown quarries. The paths of the electrical-resistivity surveys are shown in blue, E1 being the longer line and E2 being the top portion. The microgravity profile extended along the part of the traverses as indicated, but many more points were measured.

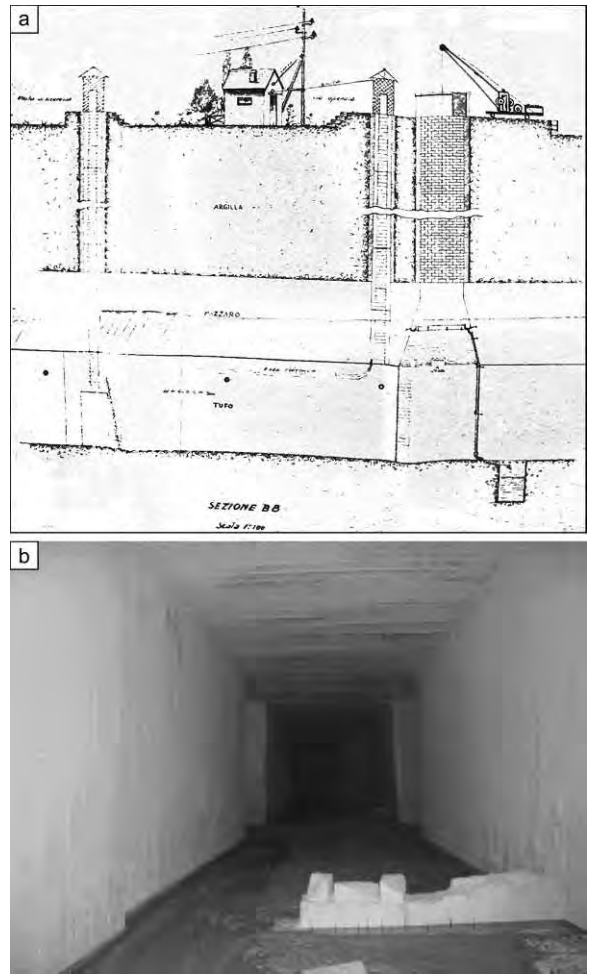

Figure 2. (a) Old drawing of quarry tunnel with hand-dug wells for access (filed at the Municipality of Cutrofiano) (b) Photo of quarry tunnels, with intersection in the distance.

to leave lines of pillars in a more or less regular way and aligned to support the roof of the excavated cavity. The initial geometry of the quarries was a chessboard with tunnels and lines of pillars arranged orthogonally to each other. Subsequently, after the first cases of subsidence, the mining office of Apulia advised a plan with staggered pillars. While this arrangement of the supporting structure makes the transport operations of quarry materials slower and more difficult, it gives greater stability to the roof of the tunnels. The tunnels are of variable size (Bruno and Cherubini, 2005; Parise and Lollino, 2011), 5 to 6 m wide, 6 to 8 m high, with a maximum observed of 10 m, and length greater than 20 m (Figure 1b). The presence of underground cavities is indicated on the surface by the hand-dug wells by which the quarrymen reached the calcarenitic sequence and removed quarried material.

If the network is accessible and well preserved, an underground geological and topographical survey may completely define the location within the local stratigraphy

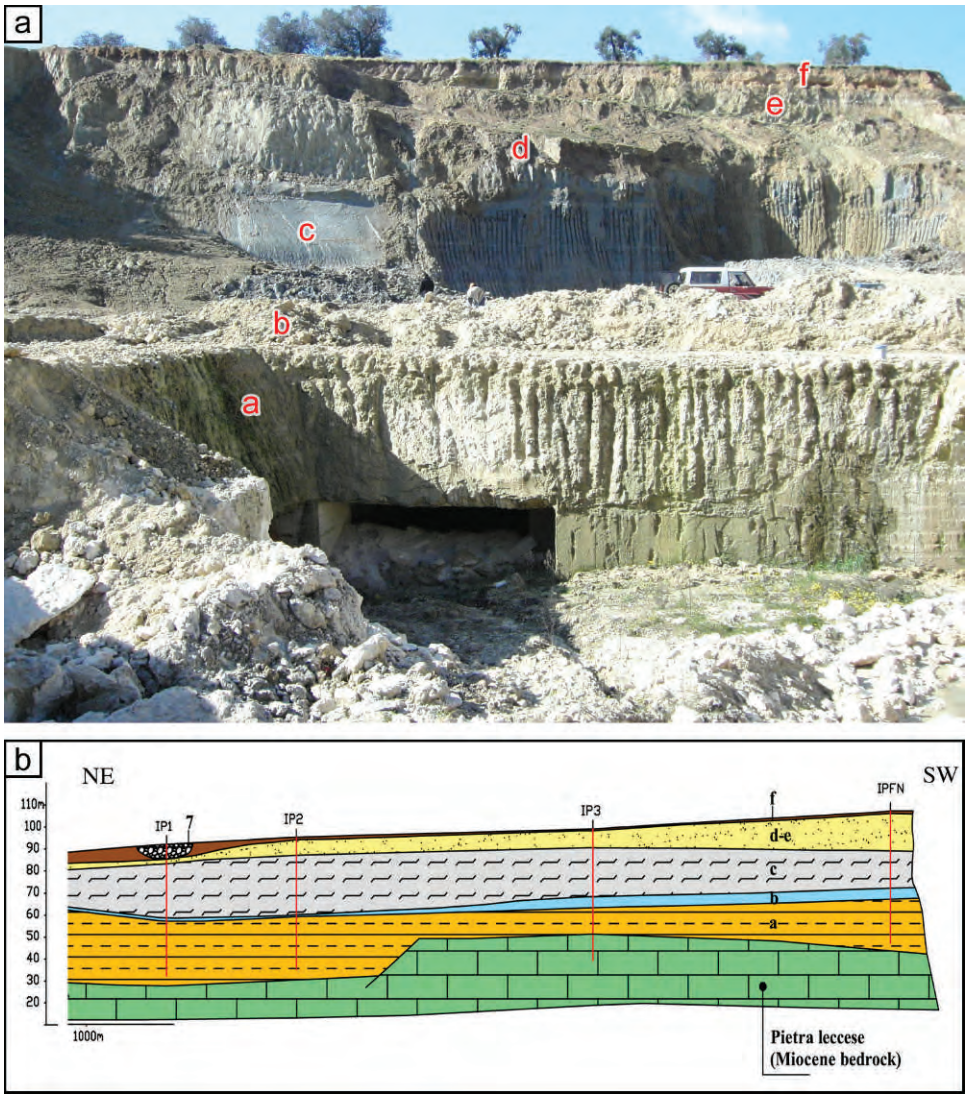

Figure 3. (a) Photograph of modern Signorella quarry some distance south of the geophysical traverses, showing the stratigraphy there. (b) Geological section, based on boreholes with locations shown in Figure 1a. In both parts, the units are a, the Gravina Calcarenite overlying the Miocene basement rock; b, the Brachiopods sands; c, the Subapennine clays; d, the Brindisi sands; e, Terraced deposits; and f, top soil.

and the position of the galleries (Parise and Lollino, 2011). In this case, the physical parameters that are needed for a complete soil characterization are estimated on the basis of high-quality samples collection and high-resolution boreholes. However, the underground activities in Cutrofiano have been progressively abandoned, and many quarries have been used for other purposes, including illegal discharge of solid and liquid wastes, making many of the galleries inaccessible. Geophysical surveys could be suitable for developing a model of the subsoil before drilling (Bianchi Fasani et al., 2013). To identify single cavities, it is necessary to drill with a spacing less than the tunnel size. As a consequence, a high number of boreholes and a considerable expense are required.

Instability of underground cavities, resulting from the progression of deformation in the quarried rocks, can involve the whole rock mass overlying the cave, thus giving rise to a true sinkhole or to a subsidence phenomenon (Parise, 2012). In other cases, only small portions of the rock mass around the cave are initially involved, with local failures that may induce a gradual and progressive enlargement or increase of the height of the cave, up to a critical configuration that later can develop into the complete collapse of the rock mass (Parise and Lollino, 2011). Currently in Cutrofiano, the shallow layers of clay are quarried at many sites (Fig. 3a); for this reason, the roads are intensely traveled by heavy vehicles carrying quarried material, likely contributing to increase in the risk of collapse (Fig. 4).

Figure 4. The development of a sinkhole near a road in the area.

Hydrostratigraphy

The conceptual hydrostratigraphic model was developed using a large set of data provided by our initial field surveys: geological data (Margiotta and Varola, 2007), plans of the quarries, borehole and water-well data, laboratory analyses, and critical revision of well-core stratigraphies supplied by local agencies and professionals. From the stratigraphic point of view, five separate units above the Cretaceous and Miocene bedrock are recognizable (Fig. 3). From the most ancient to the most recent, they are:

(a) The Gravina Calcarenite (Ricchetti et al., 1988) is the most ancient of the Early Pleistocene formations of the area. This unit, transgressive on the Pietra leccese Formation of Miocene age, consists of yellow or white coarse-grained calcarenite with abundant fossils (*Cardium*, *Glycymeris*, *Pecten*). The natural water content varies with an average value of 30%, with the porosity index varying between 0.5 and 0.7. This unit is the one quarried.

(b) Brachiopods sands (D'Alessandro et al., 1994, 2004), a greenish clayey-sandy interval a maximum of 4-m thick overlying the Gravina Calcarenite with an irregular erosive surface. A transgressive lag, up to 50-cm thick, characterized by an abundant concentration of randomly oriented casts of both articulated and unmatched bivalve shells (such as *Arctica islandica*, *Pecten jacobeus, Acanthocardia* sp., *Terebratula ampulla*, and *Terebratula scilla,*), gastropods, rhodolits, and *Ditrupa* tubes, overlies the erosional surface.

(c) Subapennine clays (Early Pleistocene) are characterized by blue-gray clayey silts, rich in fossils such as *Arctica islandica*, *Pecten jacobaeus*, *Aequipecten opercularis*, *Dentalium rectum,* and *Mya truncata*, both dispersed in the sediments and concentrated in continuous decimeter-thick intervals. The contact with brachiopods sands is sharp and indicated by a decimeter-thick hard ground covered by a reddish, sandy interval including a horizontally developed *Thalassinoides* system.

(d) Brindisi sands are composed of fine-grained sands whose color shifts from gray to yellow or light brown moving upward; these sands contain abundant diagenetic concretions that are aligned in the upper part and became scattered downwards. The granulometry of the sandy facies, in terms of gravel (<5%), and clay (<10%), varies depending on the stratigraphic level. The contact with subapennine clays is characterized by an undulating erosional surface. The lower part of this formation is made up of gray clayey sandy silts, with carbonaceous fragments with common presence of fossils of Arcticidae, Cardiidae, Pectinidae, and Nuculidae. The stratification is indistinct. The age, according to its stratigraphic position, is Early-Middle Pleistocene.

(e) Terraced deposits from the Middle-Upper Pleistocene are lithologically composed of yellowish coarse-grained biocalcarenites rich in ostreids, with sandy layers or layers of organogenic limestones varying in thickness from a few centimeters to 15 cm. The contact with Brindisi sands is characterized by an abrupt lithological variation from diagenetic calcarenite to sands.

The densities of these lithological units are listed in Table 1. The Pleistocene deposits are covered by soil (f) that lies over almost all the area examined. The thickness of the soil varies considerably, from a few decimeters to about 5 m, although the most frequent values are in the range of 1 to 2 m.

On the basis of the previously described stratigraphy, the Cutrofiano area shows two overlapping and hydraulically independent aquifers. A deep aquifer lies in the Mesozoic Altamura Limestone hydrogeologic unit, made up of fractured and karstic carbonatic rocks (Giudici et al., 2012). A deep fresh water aquifer overlies more dense seawater, and the thickness of this fresh water above the interface with saline water can be estimated based on the

Table 1. The specific weights of the stratigraphic units underlying the study area.

Lithostratigraphic Units	Specific Weight γ (kN/m^3)
Terraced deposits	19.50
Brindisi sands	18.93
Subapennine clays	19.40
Brachiopods sands	18.44
Gravina Calcarenite	15.49

relationship of Ghyben-Herzberg. Unlike the shallow groundwater, found only in places, the deep groundwater extends across the whole of the Apulia region. The deep aquifer, lying below the miocenic Leccese Pietra, contains water under pressure and is, therefore, artesian.

There is also a shallow, porous aquifer formed by the Middle–Upper Pleistocene marine calcarenitic and sandy deposits overlying the lower Pleistocene clays. This aquifer is phreatic, with semiconfined conditions where its upper part is overlain by recent sediments of low permeability. Based on lithostratigraphy, this aquifer can be subdivided into several hydrogeologic units. The Early Pleistocene subapennine clays constitute the impermeable base of the aquifer, with groundwater velocities of only 3×10^{-7} m s^{-1} (Margiotta et al., 2010). The Pleistocene aquifer system involves two hydrogeologic units. The greatest permeability is found in the terraced deposits from the Middle-Upper Pleistocene. As the fraction of silt increases, the permeability of the deposit decreases. The lower section of the aquifer, the silty-sandy sediments of the Early-Middle Pleistocene Brindisi sands hydrogeologic unit, has low permeability. The shallow aquifer flows towards Cutrofiano, but the lack of homogeneous distributed and contemporaneous data does not permit the development of a piezometric map.

Geophysical Methods

The main objective of the geophysical survey was to identify unknown cavities along the road shown in Figure 1b. In the case of Cutrofiano, there are difficulties linked to the presence of an aquifer and the required resolution for the detection of voids less than 10-m high and wide, though greater than 20-m long, located from 7-m to 40-m depth. These factors, and particularly the presence of conductive materials such as silty and clayey layers, have driven the choice of the methods. In this context, one of the most suitable method for our aim is the electrical-resistivity tomography (Loke, 2014; Reynolds, 1997). ERT is sensitive to resistivity changes in the subsoil and it allows a good investigation depth in the presence of conductive materials, unlike ground-penetrating radar (Jol, 2009). Furthermore, ERT has good resolution and it is expeditious. One other suitable method is microgravity, which is very sensitive to density changes between the cavities and the host material, and so is able to detect voids (Reynolds, 1997). We decided to use both methods in the test area, in order to perform an integrated interpretation to improve on the information from each individual method.

Resistivity Survey

Electrical-resistivity measurements were made by using an IRIS SYSCAL R1 (48 electrodes). These measurements, acquired along the survey line, produce an apparent resistivity cross-section (Reynolds, 1997) based on the subsoil electrical properties. Apparent resistivity data are then inverted to generate a resistivity model of the subsurface structures and stratigraphy. In general, the Wenner array allows high-resolution whenever horizontal structures are involved. The dipole-dipole array instead is preferred to map vertical structures, such as dykes and cavities (Dahlin and Zhou, 2004). The acquisition parameters were chosen according to the degree of resolution required, taking into account the depth of the calcarenite with the quarries in the investigated area (Fig. 3). For ERT investigations, the electrode spacing ranged 5 m to 10 m, depending on the depth target and the required resolution. We carried out two profiles labelled E1 and E2, placed along the roadside (Figure 1b). ERT E1 was performed to search for the cavity in ranges depth 8 m to 40 m, while the E2 line employed a shorter electrode spacing of 5 m for enhanced resolution of the near-surface to search for the cavities.

We first carried out the profile E1, 670-m long, joining one roll-along, starting at 200 m, multi-channel acquisition with an electrode spacing 10 m and reaching an investigation depth of about 50 m, because we expected the calacarenite at about 30 m depth (Figure 3b). The maximum depth reached, max, depends on the electrode arrays used. For Wenner and dipole-dipole arrays, this max depth is estimated as $0.2 \times$ L, L being the total length of the E1 (470 m). In our case, with the beginning of the roll-along at 200 m, we investigated to a depth of about 50 m because the maximum depth that ensures a continuity of the bottom part of the image is about one half the max (Bernard et al., 2014).

Later we carried out the profile E2 with a 5 m electrode spacing to improve the resolution. Both dipole-dipole and Wenner array (Reynolds, 1997) were performed to obtain information for both quarries and stratigraphy.

The tomographic inversion was performed using RES2DINV (Geotomo Software) with the L2-norm least-squares optimization method, the smoothness-constrained by deGroot-Hedlin and Constable (1990), and model cells with widths of half-unit spacing. The topographic effect was taken into account, because there is an elevation difference of about 5 m along the E1 profile.

The electrical model shows a range of resistivity values, from 10 to more than 4000 ohm m and a RMS errors of 3.6% (Wenner), 5.8% (dipole-dipole, spacing 10 m), and 8.6% (dipole-dipole, spacing 5 m) after five iterations (Fig. 5). The choice to stop the data inversion procedure at the result of the first iteration is due to the unchanged value of RMS error in additional iterations.

Microgravity Survey

To reduce the uncertainty in interpreting the electrical-resistivity tomography profile, we decided to carry out a microgravity survey along the first part of the E1 ERT profile (Figure 1b). The measurement stations were planned according to the expected dimensions and depth of the target and after considering the results of synthetic models of the caves designed on the basis of the available

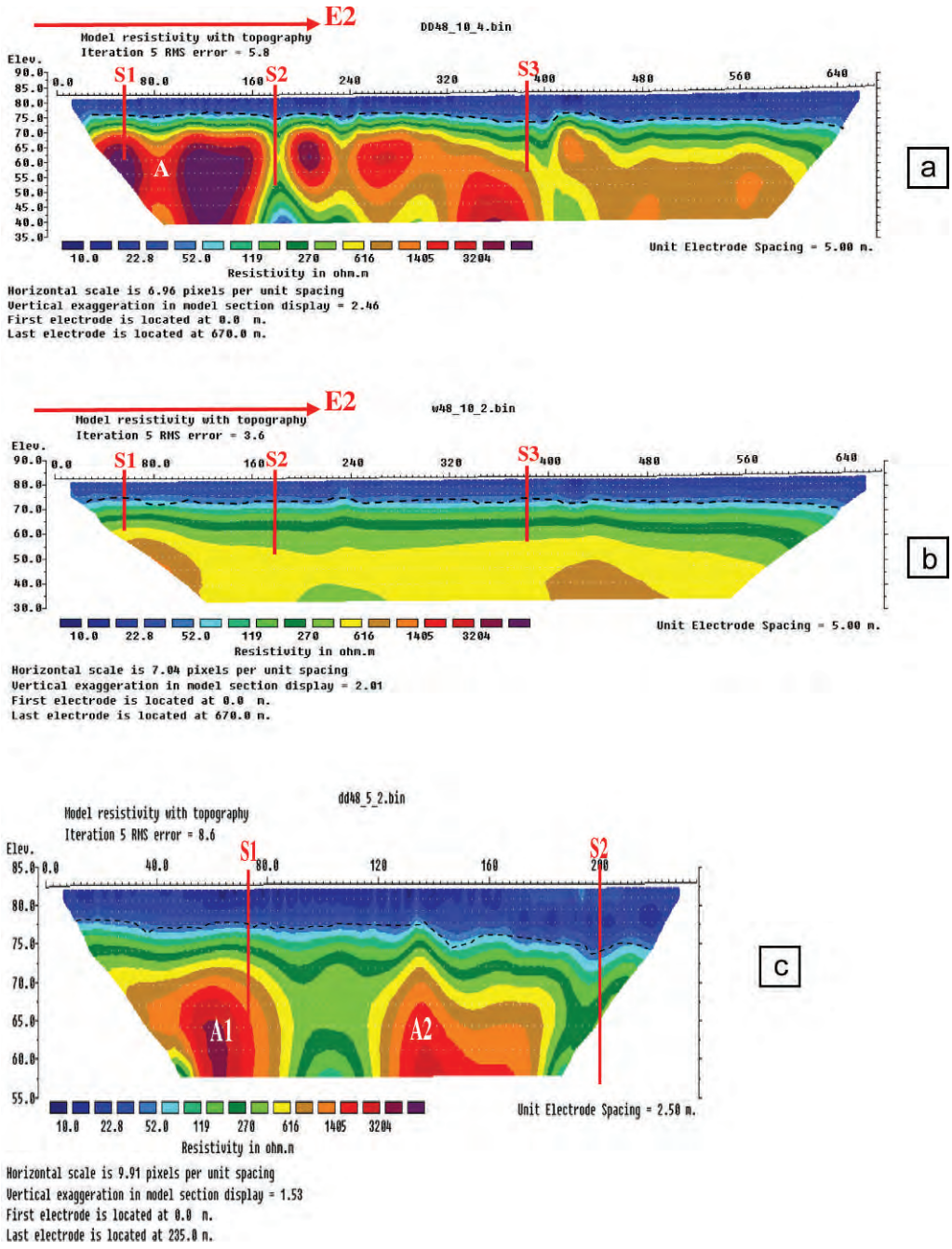

Figure 5. 2-D profile results of electrical-resistivity tomography. (a) Traverse E1 with dipole-dipole array, 10 m spacing. (b) Traverse E1 with Wenner array, 10-m spacing. (c) Shorter E2 traverse with 5 m spacing to obtain better detail on the high-resistivity areas shown as A in part (a) and A1 and A2 here.

geological and ERT information. The data were acquired along the profile P1, with a variable sampling step from 3 m to 6 m, yielding a total of 68 observations (Fig. 6a).

The gravity survey was conducted using an Auto-Grav Scintrex CG5. At least three values of gravity were stored at each station; each measurement lasted 60 seconds. For measurements performed on the roadway, due to the noise associated with vehicular traffic, the number of readings was increased to nine or twelve, until the repeatability was satisfactory. The repeatability was judged satisfactory when the difference between the readings at a station was not greater than 5 microGal. Measurements were repeated at a base station about every hour to sample the instrumental drift curve. The base station (green circle in Fig. 6a) was located along the profile P1 at station number 19. Simultaneously, a topographic survey was carried out, by measuring the elevation differences at each station using differential GPS. Station number 12 was

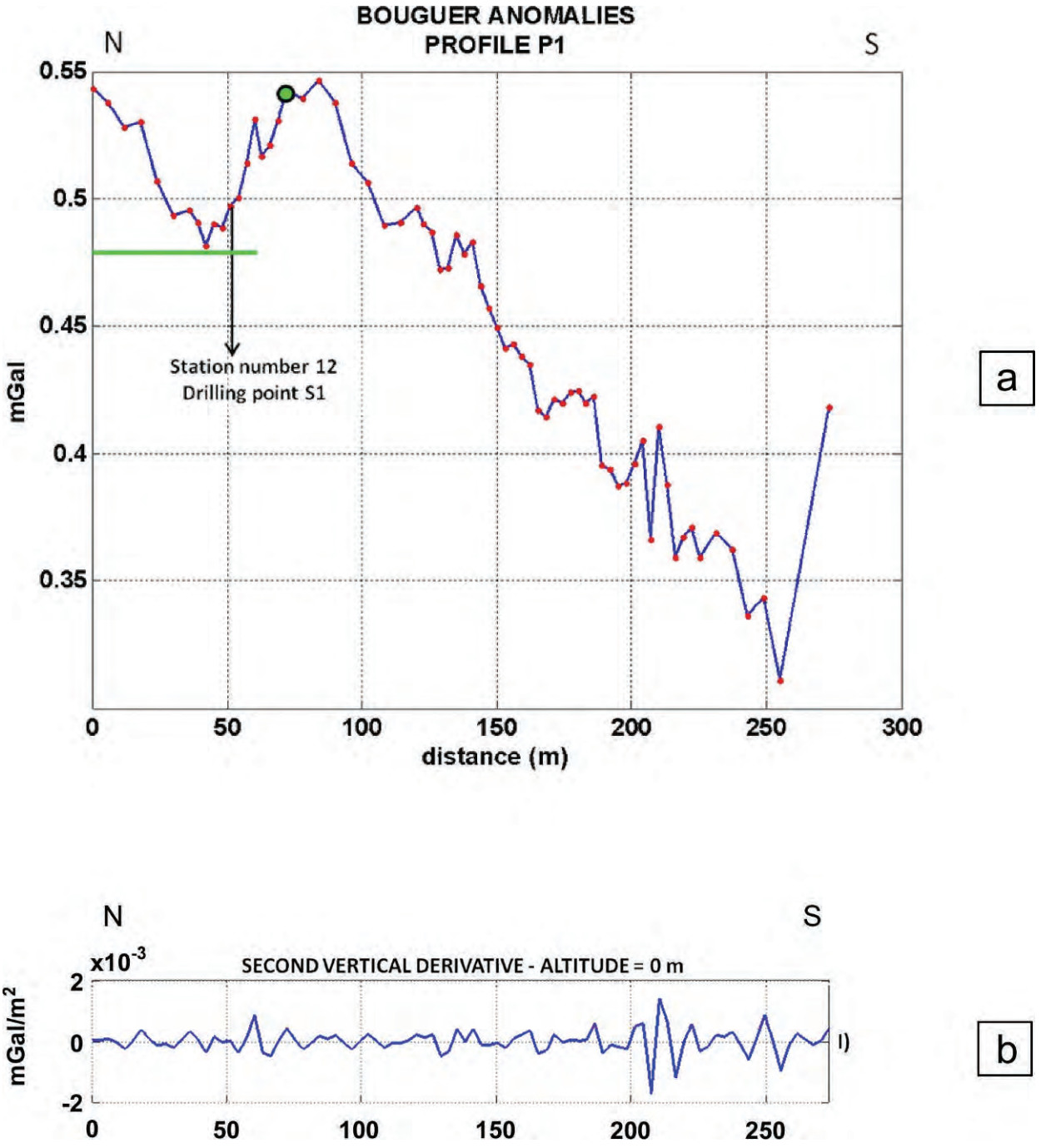

Figure 6. (a) The gravity profile along traverse P1. The location of the borehole S1 is shown. The green line indicates the position of one conspicuous low. The green dot is the station visited repeatedly to correct for instrument drift. (b) The second vertical derivative of the data at ground level; compare to Figure 7a.

located close to the borehole S1 (Figure 6a) in correspondence of the resistivity anomaly A1 (Fig. 5c). The data were corrected for tidal and instrumental drift effects, and free-air and complete Bouguer anomalies (Fig. 6a) were computed (Talwani et al., 1959), taking into account that the maximum elevation difference is 1.89 m and using a plate density of 1.9 g cm^{-3}, according to the stratigraphy data in Fig. 3b.

Actually, buildings near the profiles represent the main topographical disturbance in the area. The main walls of the buildings were modelled by thirty prisms and their gravity effect computed by using a density contrast of 2.5 g cm^{-3}, since walls are generally made of the same calcarenite present at depth in the area. A water-collecting channel was also modelled; the density contrast chosen for it was -1.9 g cm^{-3}.

To reduce the trend effect, we computed the second vertical derivative of the Bouguer anomalies at ground level (Figure 6b) and upward continued it up to 30 m (Fig. 7a) to reduce the high-frequency noise enhancement related to the field differentiation. The depth-from-extreme-points (DEXP) method (Fedi, 2007) was then used to yield an image of the source distribution (Fedi and Pilkington, 2012), in which the maxima or minima define the top or the mean position of the sources (Fig. 7b). It allows also the estimation of the structural index N, a source parameter related to the general shape of the source. For gravity anomalies, N is equal to 2 for a spherical source, 1 for a cylindrical source, and 0 for a thin dyke or sill, tending to -1 for a fault. In our case, it is appropriate to approximate the shape of underground caves with horizontal cylinders.

Results and Discussion

Electrical-resistivity data inversion allowed us to obtain a possible resistivity model, and the DEXP method applied to the microgravity data has located the possible sources of Bouguer anomalies. The resistivity models (Fig. 5) show two main layers. The first layer is conductive, with resistivity values in the range 10 to 50 ohm m and thickness of about 5 m (Fig. 5a). The model from the E1 Wenner profile in Figure 5b shows increasing thickness of this layer going southward. The second layer is resistive, with resistivity values in the range 600 to 5000 ohm m. In Figure 5a, the strongest resistivity anomaly along profile E1 is labelled A, at a distance of about 120 m. We carried out the dipole-dipole array profile E2 to better define anomaly A, using a 5 m electrode-spacing that allowed for improved resolution. The model from the E2 profile shows the anomaly A as two distinct anomalies A1 and A2 (Fig. 5c).

The Bouguer anomalies along the microgravity traverse are shown in Fig. 6a. A gravity anomaly of about 0.07 mGal is present between 0 m and 57 m, indicated by the green line. From 57 meters to 85 meters there is a gravity high, and from 85 meters to 273 meter, the end of the gravity data, we can see a regular decrease of the gravity-anomaly field. This trend may be interpreted as a regional trend and may mask anomalies characterized by small wavelengths.

The upward-extrapolated anomalies in Figure 7a are much clearer, and the main features are the four anomalies indicated as A, B, C, and D. The white dots in the DEXP-calculated section in Figure 7b show the estimated depths of the low-density sources, in blue, of the dips in the curve in 7a. The top of the source anomaly A in Fig.7a, in correspondence of the resistivity anomaly A1 in Fig.7c is at about 10-m depth. The source of the anomaly D in Fig.7a is at the same depth of A. The tops of sources of the gravity anomalies at A and D in Figure 7a are located at about 10-m depth; the anomaly A is at a location corresponding to electrical-resistivity high A1 in Figure 5b or 7c. The anomalies associated with areas B and C in Figure 7a are due to shallow sources located at about 4-m depth or laterally located. The resistivity models in Figure 5 show a strong resistivity break between the first and the second layers at a mean depth of 6 m below ground level.

On the basis of the geological section in Figure 3b we expected the Gravina Calcarenite, where the quarries are present, to be at a depth from 20 m to 30 m below ground level. Therefore, that geological section, compiled on the basis of other observations, is not able to describe the geology in the survey area.

By a theoretical point of view of voids, we are likely to expect a gravity low coupled to resistivity high; on the other hand, for unexcavated mine pillars, we expect an increase in the Bouguer anomaly and decreasing resistivity values. We located boreholes S1 and S2 along the traverse at locations demonstrating both these features. Hence, we located borehole S1 at about 72 m, corresponding to the first gravity low A in Figure 6a and the resistivity high A1 in Figure 7c. The borehole S2 was located at about 200 m at a resistivity low and a gravity high (Figs. 7b,c). This last choice also took into account the E1 resistivity profile in Figure 5a that shows a zone at about 180 m, between two resistivity highs, where probably there are no quarries.

The borehole S3 was located taking into account only the ERT model (lacking the gravity survey) relative to E1 (Figure 5a). We planned other boreholes at the resistivity highs between 200 m and 400 m. Unfortunately, due to the presence of obstacles on the roadside, it was not possible to reach this goal. However, we did locate borehole S3 along the E1 traverse on the basis of only the resistivity model, since the gravity data did not reach its location. On the basis of the geological data, geophysical models, and core data from the S1, S2, and S3 boreholes, we realized a detailed interpretative geological model (Fig. 7d).

Along our traverse, the terraced deposits are some meters thick, with an average of 2 m. The thickness of Brindisi sands varies from 2 to 3 m, compared to 7 to 8 m a few kilometers south (Fig. 3b). The thickness of the subapennine clays varies greatly. Specifically, it increases moving southward from Cutrofiano, where it is absent or only decimenters thick at the northern limit of the investigated area, to the Signorella locality to the south, where it averages 12-m thick (Figs. 3a,b). These three units constitute the first resistivity layer; the resistivity values are affected by the presence of the aquifer that does not allow discriminating the lithological changes. The E1 Wenner traverse profile in Figure 5b shows increasing thickness of this layer going southward, in agreement with the detailed model of the subsoil (Fig. 7d).

The thickness of the Gravina Calcarenite varies considerably and reaches maximum values of more than 30 m. Moving from our traverse at Cutrofiano to the south, the top of the Pleistocene calcarenite deepens from 5 m (Fig. 7d) to over 30 m (Fig. 3b). This unit, together

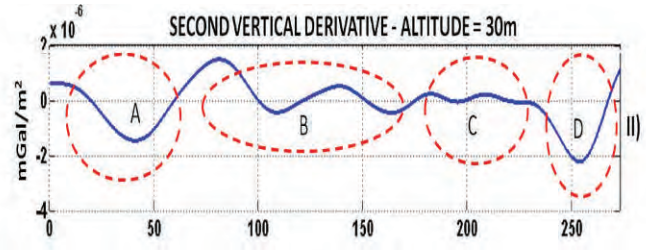

a

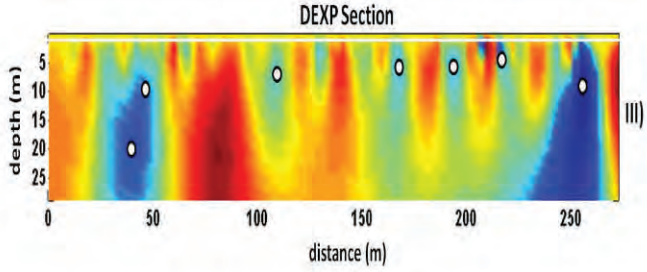

b

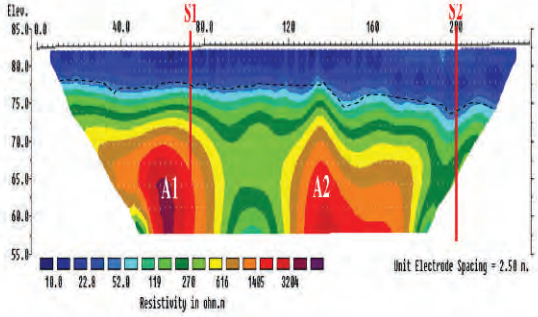

c

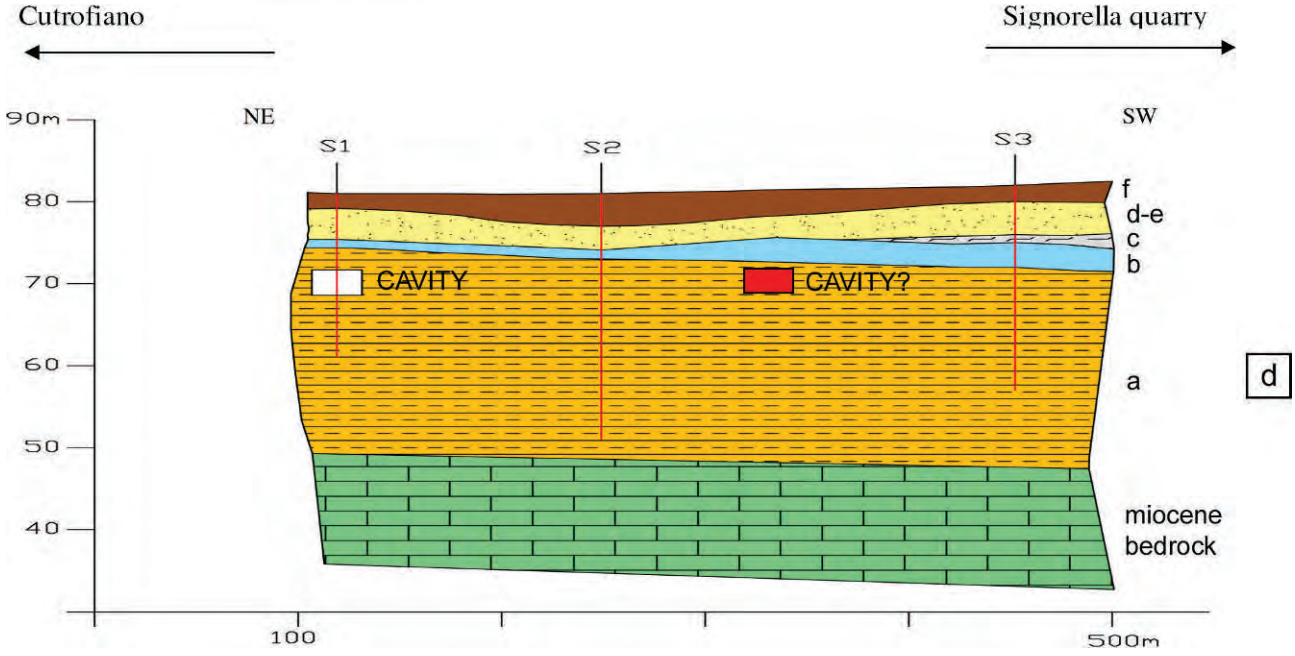

d

Figure 7. (a) The second vertical derivative of the gravity data extrapolated to a height of 30 m; compare to Figure 6b. Regions of anomolous lows are circled. (b) Subsurface model derived from the gravity data using the DEXP (depth-from-extreme-points) method, with white dots showing the depths. (c) Electrical-resistivity tomography result for traverse E2;

with the brachiopods sands, corresponds to the second resistivity layer.

The greatest relative minima in Fig. 7a are those in regions A and D. The S1 drilling (Figure 7d) confirmed the presence of a void at a depth between 9.5 m and 12.5 m, consistent with the resistivity high A1 (2000 to 4000 ohm m, Fig. 7c) and the gravity low A. The gravity low at D, near the location of a resistivity high at 265 m (Fig. 5a), could be due at a cavity located at about 10 m.

The conjectured cavity is shown at more like 340 m in Fig. 7d. The smaller gravity anomalies B and C located between 100 m and 240 m in Figure 7a correspond to resistivity highs in Figures 5a and 7c, but the sources are at a shallower depth of about 4 m, according to the gravimetry model in Figure 7b. If these sources were directly below the traverse, they would not be located in the Gravina Calcarenite, so we may suppose that these anomalies correspond to caves located off to the side of the road in a maze of tunnels like those shown in Figure 1b.

Conclusions

This study tried to ascertain the validity of an integrated approach, based on geophysical and geological methods, for the identification of the spatial distribution and extension of underground man-made cavities. Where the galleries are not accessible, non-destructive geophysical methods can have an important role in locating the unknown cavities and providing an interpretative model of the subsoil.

Detailed stratigraphic knowledge helps in the correct choice of the geophysical methods. Detailed stratigraphic analysis was carried out by means of soil and subsoil surveys, integrated by critical review of the data available in the literature. Results of our new geophysical studies supplement the stratigraphic model of the Cutrofiano area previously presented in literature (Parise and Lollino, 2011) with new data; the decametric thickness of subapennine clays observed in the subsoil immediately south of the area here studied are absent or have a decimetric thickness near the urban center of Cutrofiano. The detailed knowledge of the local stratigraphy was crucial for the interpretation of the geophysical surveys and is a mandatory step to properly focus subsequent studies to detect underground caves and mitigation or recovery projects.

Joint interpretation of electrical-resistivity and microgravity data was effective in reducing the uncertainty about the possible presence of cavities in the subsoil. The borehole data, used to validate and interpret the geophysical results, show that the presence of cavities in the subsoil is signaled by strong gravity lows and resistivity highs; on the other hand, with a resistivity low and gravity high we found an undisturbed zone, presumably a pillar in the cave network. The geophysical surveys and core data improved the previous geological knowledge. The resolutions of the methods worsen where there are caves located to the side of the road. In this last case, additional 2D surveys would be required to reduce the uncertainty and obtain a 3D model of the subsoil.

Acknowledgements

This research work has been funded by a grant from the Province of Lecce and performed by GEOMOD S.r.l Spin-off University of Salento. The authors would like to thank the Province of Lecce and the municipal authorities of Cutrofiano for their logistics support. The authors also acknowledge the assistance provided by Massimo Luggeri in the figures.

References

Bernard, J., Leite, O., and Vermeersch, F., 2014, Multi-electrode resistivity imaging for environmental and mining applications, technical note, IRIS Instruments, Orléans, France, www.iris-instruments.com/Pdf%20file/5-Resistivity_Imaging/Resistiivty_Imaging_text.pdf, [accessed in May 2014].

Bianchi Fasani, G., Bozzano, F., Cardarelli, E., and Cercato, M., 2013, Underground cavity investigation within the city of Rome (Italy): A multi-disciplinary approach combining geological and geophysical data: Engineering Geology, v. 152, p. 109–121. doi:10.1016/j.enggeo.2012.10.006.

Bruno, G., and Cherubini, C., 2005, Subsidence induced by the instability of weak rock underground quarries in Apulia: Giornale di Geologia Applicata, v. 1, p. 33–39. doi:10.1474/GGA.2005-01.0-04.0004.

Dahlin, T., and Zhou, Bing, 2004, A numerical comparison of 2D resistivity imaging with 10 electrode arrays: Geophysical Prospecting, v. 52, p. 379–398. doi:10.1111/j.1365-2478.2004.00423.x.

D'Alessandro, A., Massari, F., Davaud, E., and Ghibaudo, G., 2004, Pliocene-Pleistocene sequences bounded by subaerial unconformities within foramol ramp calcarenites and mixed deposits (Salento, SE Italy): Sedimentary Geology, v. 166, p. 89–144. doi:10.1016/j.sedgeo.2003.11.017.

D'Alessandro, A., Mastronuzzi, G., Palmentola, G., and Sansò, P., 1994, Pleistocene deposits of Salento leccese (southern Italy): Problematic relationships: Bollettino della Società Paleontologica Italiana, v. 33, p. 257–263.

←

this plot is identical to Figure 5c. The locations of boreholes S1 and S2 are shown. (d) Subsurface stratigraphy inferred from the geophysical data and drilling. The layers are labeled the same as in Figure 3: a, the Gravina Calcarenite overlying the Miocene basement rock; b, the Brachiopods sands; c, the Subapennine clays; d, the Brindisi sands; e, Terraced deposits; and f, top soil. The white box is a cavity intersected by borehole S1; the red box is symbolic of other cavities that may be the causes of other, less conspicuous features in the data.

deGroot-Hedlin, C., and Constable, S., 1990, Occam's inversion to generate smooth, two-dimensional models from magnetotelluric data: Geophysics, v. 55, p. 1613–1624. doi:10.1190/1.1442813.

Fedi, M., 2007, DEXP: A fast method to determine the depth and the structural index of potential fields sources: Geophysics, v. 72, p. I1–I11. doi:10.1190/1.2399452.

Fedi, M., and Pilkington, M., 2012, Understanding imaging methods for potential field data: Geophysics:, v. 77, p. G13–G24. doi:1.1190/geo2011-0078.1.

Gambetta, M., Armadillo, E., Carmisciano, C., Stefanelli, P., Cocchi, L., and Tontini, F.C., 2011, Determining geophysical properties of a near-surface cave through integrated microgravity vertical gradient and electrical resistivity tomography measurements: Journal of Cave and Karst Studies, v. 73, no. 1, p. 11–15. doi:10.4311/jcks2009ex0091.

Gibson, P.J., Lyle, P., and George, D.M., 2004, Application of resistivity and magnetometry geophysical techniques for near-surface investigations in karstic terranes in Ireland: Journal of Cave and Karst Studies, v. 66, no. 2, p. 35–38.

Giudici, M., Margiotta, S., Mazzone, F., Negri, S., and Vassena, C., 2012, Modelling hydrostratigraphy and groundwater flow of a fractured and karst aquifer in a Mediterranean basin (Salento peninsula, southeastern Italy): Environmental Earth Sciences, v. 67, no. 7, p. 1891–1907. doi:10.1007/s12665-012-1631-1.

Gómez-Ortiz, D., and Martín-Crespo, T., 2012, Assessing the risk of subsidence of a sinkhole collapse using ground penetrating radar and electrical resistivity tomography: Engineering Geology, v. 149–150, p. 1–12. doi:10.1016/j.enggeo.2012.07.022.

Jol, H.M., 2009, ed., Ground Penetrating Radar: Theory and Applications, Amsterdam, Elsevier, 544 p.

Kaufmann, G., Romanov, D., and Nielbock, R., 2011, Cave detection using multiple geophysical methods: Unicorn cave, Harz Mountains, Germany: Geophysics, v. 76, no. 3, p. B71–B77. doi:10.1190/1.3560245.

Kotyrba, B., and Schmidt, V., 2014, Combination of seismic and resistivity tomography for the detection of abandoned mine workings in Münster/Westfalen, Germany: Improved data interpretation by cluster analysis: Near Surface Geophysics, v. 12, p. 415–425. doi:10.3997/1873-0604.2013056.

Leucci, G., Margiotta, S., and Negri, S., 2004, Geological and geophysical investigations in karstic environment (Salice Salentino, Lecce, Italy): Journal of Environmental and Engineering Geophysics, v. 9, p. 25–34.

Loke, M.H., 2014, Tutorial: 2-D and 3-D Electrical Imaging Surveys, PDF file at http://www.geotomosoft.com/coursenotes.zip, [accessed Nov. 2014].

Margiotta, S., Mazzone, F., and Negri, S., 2010, Stratigraphic revision of Brindisi – Taranto plain: Hydrogeological implications: Memorie Descriptive della Carta Geologica d'Italia, v. 90, p. 165–180.

Margiotta, S., Negri, S., Parise, M., and Valloni, R., 2012, Mapping the susceptibility to sinkholes in coastal areas, based on stratigraphy, geomorphology and geophysics: Natural Hazards, v. 62, p. 657–676. doi:10.1007/s11069-012-0100-1.

Margiotta, S., and Varola, A., 2007, Il paleosito di Cutrofiano (Salento), proposta per l'istituzione di un parco – museo. Atti della Società Toscana Di Scienze naturali - Memorie. Serie A 112,1–8.

Martínez-López, J., Rey, J., Dueñas, J., Hidalgo, C., and Benavente, J., 2013, Electrical tomography applied to the detection of subsurface cavities: Journal of Cave and Karst Studies, v. 75, no. 1, p. 28–37. doi:10.4311/2011ES0242.

Martínez-Pagán, P., Gómez-Ortiz, D., Martín-Crespo, T., Manteca, J.I., and Rosique, M., 2013, The electrical resistivity tomography method in the detection of shallow mining cavities: A case study on the Victoria Cave, Cartagena (SE Spain): Engineering Geology, v. 156, p. 1–10. doi:10.1016/j.enggeo.2013.01.013.

Mochales, T., Casas, A.M., Pueyo, E.L., Pueyo, O., Román, M.T., Pocoví, A., Soriano, M.A., and Ansón, D., 2008, Detection of underground cavities by combining gravity, magnetic and ground penetrating radar surveys: A case study from the Zaragoza area, NE Spain: Environmental Geology, v. 53, p. 1067–1077. doi:10.1007/s00254-007-0733-7.

Parise, M., 2010, The impacts of quarrying in the Apulian karst, *in* Carrasco, F., LaMoreaux, J.W., Durán, J.J., and Andreo, B. eds., Advances in Research in Karst Media, Heidelberg, Springer Environmental Earth Sciences series, p. 441–447.

Parise, M., 2012, A present risk from past activities: Sinkhole occurrence above underground quarries: Carbonates and Evaporites, v. 27, no. 2, p. 109–118. doi:10.1007/s13146-012-0088-3.

Parise, M., and Lollino, P., 2011, A preliminary analysis of failure mechanisms in karst and man-made underground caves in Southern Italy: Geomorphology, v. 134, p. 132–143. doi:10.1016/j.geomorph.2011.06.008.

Pueyo Anchuela, Ó., Pocoví Juan, A., Casas-Sainz, A.M., Ansón-López, D., and Gil-Garbi, H., 2013, Actual extension of sinkholes: Considerations about geophysical, geomorphological, and field inspection techniques in urban planning projects in the Ebro basin (NE Spain): Geomorphology, v. 189, p. 135–149. doi:10.1016/j.geomorph.2013.01.024.

Reynolds, J.M., 1997, An Introduction to Applied and Environmental Geophysics, New York, Wiley, 796 p.

Ricchetti, G., Ciaranfi, N., Luperto Sinni, E., Mongelli, F., and Pieri, P., 1988, Geodinamica ed evoluzione sedimentaria e tettonica dell'Avampaese Apulo: Memorie della Società Geologica Italiana, v. 41, p. 57–82.

Talwani, M., Worzel, J.L., and Landisman, M., 1959, Rapid gravity computations for two-dimensional bodies with application to the Mendocine submarine fracture zone: Journal of Geophysical Research, v. 64, p. 49–61. doi:10.1029/JZ064i001p00049.

M. Akgöz and M. Eren – Traces of earthquakes in the caves: Sakarlak Ponor and Kepez Cave, Mersin, (southern Turkey). *Journal of Cave and Karst Studies,* v. 77, no. 1, p. 63–74. DOI: 10.4311/2013ES0120

TRACES OF EARTHQUAKES IN THE CAVES: SAKARLAK PONOR AND KEPEZ CAVE, MERSIN, (SOUTHERN TURKEY)

Murat Akgöz[1] and Muhsin Eren[2]

Abstract: The study area is located in the central part of the Taurus Mountains, where karstification is widespread and strongly influenced by tectonic rise of the region and sea-level changes in the Mediterranean Sea during the Pleistocene. Young karstification in the area was largely affected by NE-SW trending left-lateral strike-slip faults and NW-SE trending discontinuities. The general extension of discontinuities is perpendicular to the faulting direction indicated by evaluation of the caves with the digital elevation model and lineament analysis. Findings of this investigation suggest that differences in the periodic development of the stalagmites are mainly due to tectonic movements. Therefore, the times of the growth-axis angle deviations for representative stalagmite samples from the Sakarlak Ponor and Kepez Cave were determined by U/Th analyses. The results tend to significantly overlap with times of historical earthquakes.

Introduction

A stalagmite is a type of speleothem or cave deposit usually consisting of calcium carbonate that grows upward from the dripping water, and forms over a very long time. Therefore well-developed and protected stalagmites allow us to obtain a fairly long record of seismicity of a region. In recent years, this topic has increasingly gained interest of researchers and been the subject to many studies (e.g., Ford and Hill, 1999; Gilli, 1999; Forti, 2001; Angelova et al., 2003; Gilli, 2005; Becker et al., 2006; Gunn, 2006; Šebela, 2008; Garduño-Monroy et al., 2011). In longitudinal sections of stalagmites, a sudden change in growth orientation is taken as evidence of possible paleoseismic activity (Postpischl et al., 1991; Forti, 2001; Gilli, 2005; Šebela, 2008). In fact, deviations from vertical growth of stalagmites can be due to seismic activity, glacial intrusion, or anthropogenic impact. For this reason, as a priority, paleoseismology studies have attempted to determine the causes of the deviations.

Throughout the history of humanity, caves have been used for various purposes, such as shelter, protection, hunting bases, or faith centers. Therefore, deformations like breakage, tipping, drying, or fracturing in cave sediments have been largely human effects. In addition, vibrations caused by blasting and heavy duty vehicles caused by nearby mining can also lead to deformations in the cave sediments. Another source of deformations in speleothems is considered to be glacial intrusion. Spötl and Mangini (2007) reported that glacial intrusion caused the breakage of speleothems in Snežna Jama Cave. Glacial notches and remains of moraine deposits are generally sought on the cave wall and floor as evidence of glacial intrusion. However, the effects of glacial intrusion on caves, their hydrology, and internal atmospheric conditions are not known (Šebela, 2008). So paleoseismic studies require elimination of the other effects on stalagmite deformation. Deviations of the stalagmite growth axis provide fairly good data for paleoseismological work. Forti's investigation (2001) regarding different tectonic effects on stalagmites accepted them as a proof for paleoseismic activities. In addition, Bayarı and Özyurt (2005) point out that those stalagmite growth axis-changes depend on the changes of the primary stalagmite position with time caused by tectonic raise or subsidence of the region.

This study aims to determine deviations of the growth-axis angle in the stalagmite samples and their age by U/Th (uranium/thorium) analysis and to correlate them with the paleoseismological record.

Description of the Study Area

Turkey is a fairly rich country with respect to karstification, and about 40% of its surface area is covered by carbonate rocks. In southern Turkey, the Tauride Mountains (also called Torid) consist mostly of platform carbonates deposited during Palaeozoic to Cenozoic. The study area is located in the central part of Taurides between the Lamas Canyon/Erdemli and the Göksu Valley/Silifke in the Mersin province (Fig. 1), where karstification is widespread. In the area, karst has been developed in carbonates at the edges of the Taurus Mountains, where hundreds of caves can be found with different features and formation histories. Almost all of the caves in the study area are located within early to middle Miocene reefal limestone, the Karaisalı Formation consisting of gray- to beige-colored, medium- to thick-bedded limestone containing lots of reef-forming organisms such as coral and red alga, and also molluscs, bryozoans, and echinoderms (Eren et al., 2004; Eren 2008; Alan et al., 2011). In places, these limestones are highly fractured, and the fractures are generally filled with calcite.

[1] MTA- General Directorate Of Mineral Research And Exploration, TR-06800 Ankara, Turkey, murat_akgoz@yahoo.com
[2] Department of Geological Engineering, Mersin University, TR-33343 Mersin, Turkey

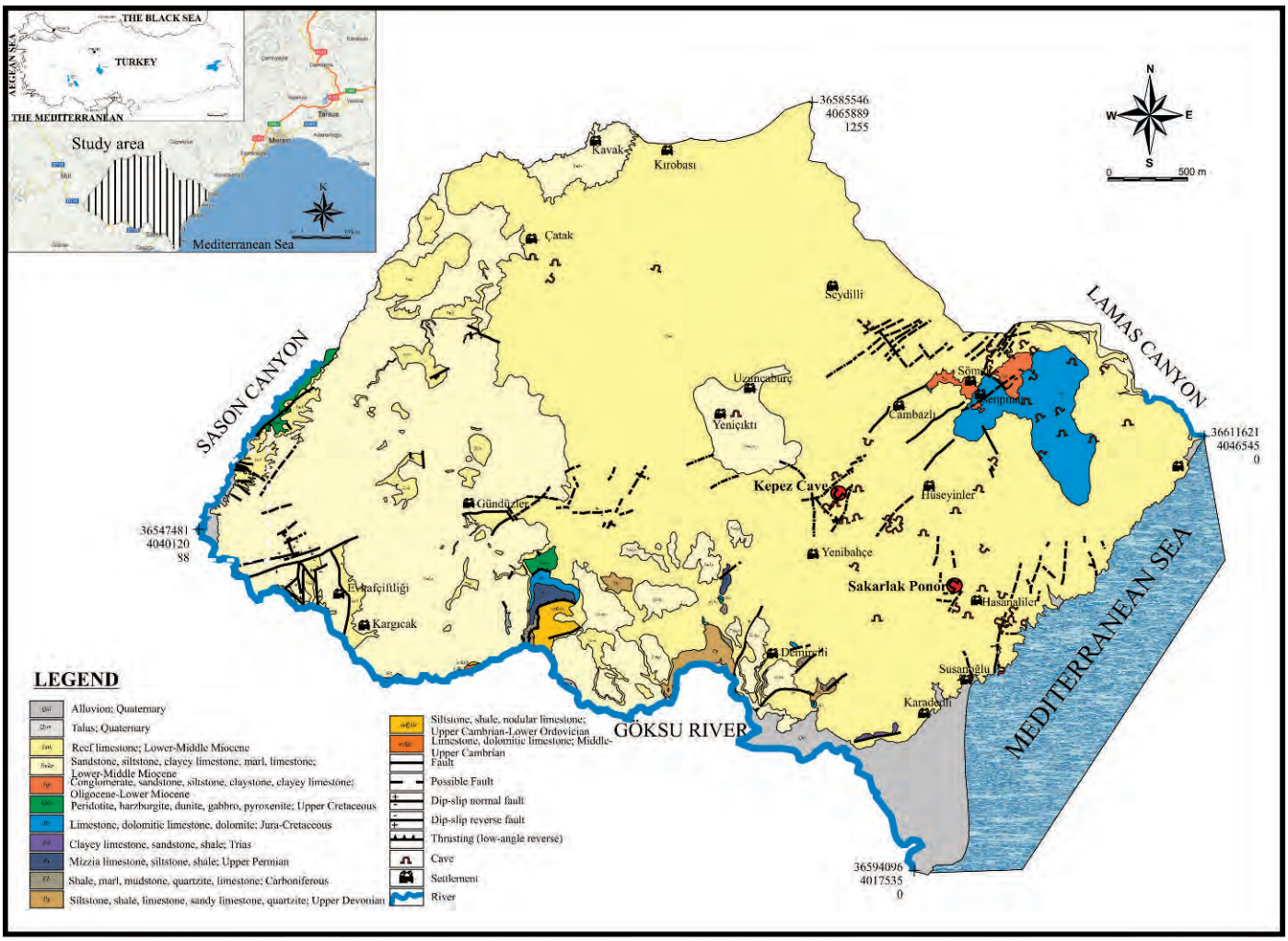

Figure 1. Geological map of the study area, with the locations of sample sites Sakarlak Ponor and Kepez Cave. The inset shows the location of the area within Turkey.

One of the most important things that have affected the karstification pattern is tectonic structure. In the area, karstification probably started after emergence of the central Taurus due to epeirogenetic raise at the end of Miocene. Following the middle Miocene, karstification in the region must have deepened due to dry and hot climate. This period is called the Messinian Salinity Crisis. Demirkol (1986) stated that the upper Miocene to Pliocene tectonic development of the region formed under a compressional regime. After these tectonic changes, NNW-SSE trending folds and reverse faults were formed. In addition, the region was affected by the ENE and WSW directed compression as the westward-moving Anatolian plate probably encountered great resistance in the Agean region. On the other hand, Akay and Uysal (1988) reported that the region was later subjected to only ineffective compression during the upper Pliocene. At the later stages, the region was affected by N-S compression. Today, the region continues to be under N-S directional compression and continues to rise as a block. With sea level changes in the Mediterranean Sea during the upper Pliocene, the elevation of karstification started to decrease, and rapid development was caused by the NW-SE trending discontinuities. As a result, caves of multiple periods and stages were developed with youthful features such as canyons that are parallel to the NW-SE trending discontinuities. At the same time, these caves are evidence for regional uplift due to tectonic movements and change of the morphological base level due to climatic changes.

Most of the studied caves are well-developed vertical caves in cross-section. The vertical caves occur in areas where the base level of cave development is ambiguous or deep, characteristic of a young uplifted region (Ozansoy and Mengi 2006). However six caves with a mixture of horizontal and vertical development shows that the region was tectonically active (Garašić, 1991; Akgöz, 2012). In the region, orientation of surface karst features and the distribution of caves show consistency with distinct tectonic lines, which indicates the effect of tectonics on karstification. The orientations of the main faults and lineaments were

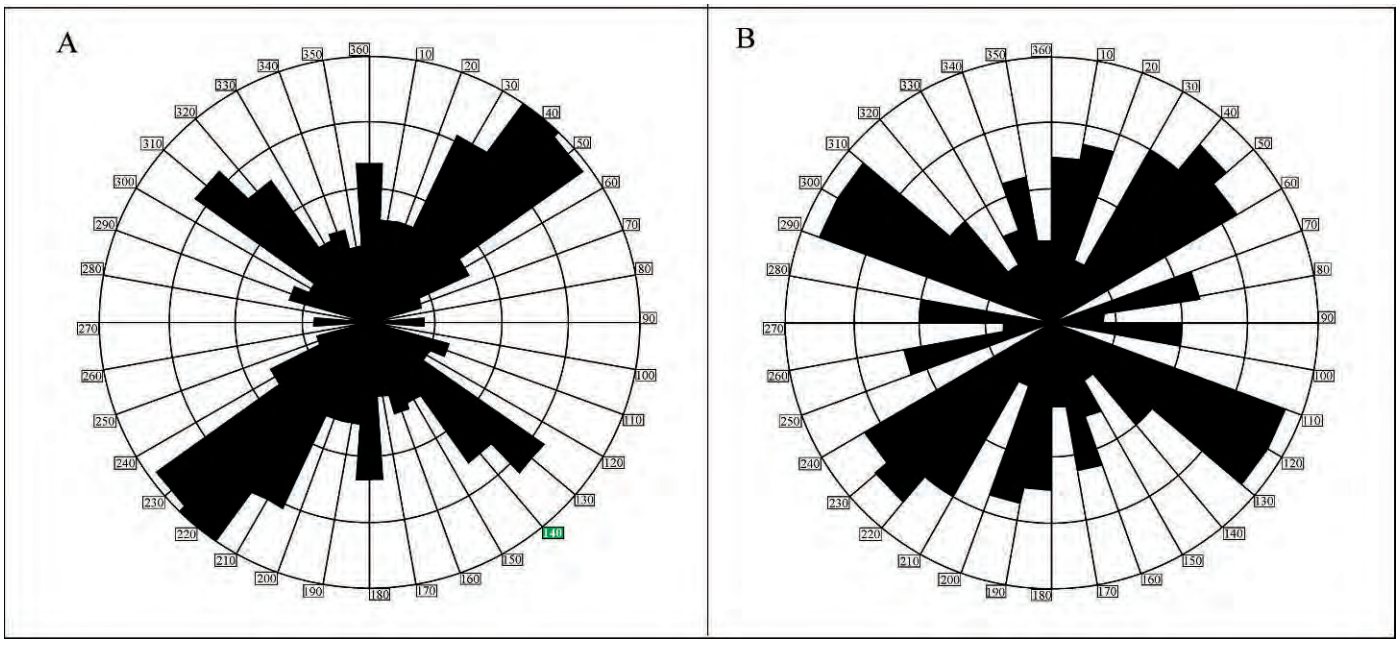

Figure 2. Rose diagrams showing (A) orientations of the main faults and lineaments obtained from digital elevation model of the study area and (B) the long axis-orientation of caves in the study area.

measured on a digital elevation model (Fig. 2A), and horizontal directions of cave passages were plotted (Fig. 2B). It is clearly seen that the directions of faults and discontinuities in the region are exactly compatible with the orientations of the caves. The majority of the caves were developed in the NW-SE direction. On the other hand, if their development started at NE-SW direction, then new branches were formed along NW-SE trending discontinuities that caused changes in direction of the cave development.

Sakarlak Ponor

The Sakarlak Ponor is a sinkhole formed by collapse of a cave roof. It is located in the bottom of a blind valley running N-S (Fig. 3). The original entrance to the ponor must have been at a lower elevation to serve as a drain for the valley. One of the characteristic features of blind valleys is that the valley ends downstream in either a sinkhole or a cave. Two sinkholes located to the south of the Sakarlak Ponor in the same valley may indicate former ponors at the end of the valley, with northward migration of the end point over a period of time (Fig. 3B). The cave developed within reef limestone and consists of a main gallery and a fossil branch indicating a multi-stage development (Fig. 4). The main gallery of the ponor occurred along NW-SE trending discontinuities, whereas the fossil branch extends parallel to the NE-SW trending main tectonic line.

At the junction point of the main gallery with the fossil branch, there are numerous fallen columns and stalagmites (Fig. 5). Here displacement must have been caused by possible collapse and tectonic depression during the ponor's development, because of its hard-to-access position with a depth of 51 meters. In the Sakarlak Ponor, episodic mud flows inhibited stalagmite development except in some protected areas showing well developed primary and secondary stalagmites (Fig. 6).

Kepez Cave

The Kepez Cave is in reef limestone and shows multiple stages of development. The cave, located on the edge of a doline (Fig. 3A), consists of the main gallery and lots of secondary branches. The Kepez Cave has a depth of 65 meters and a length of approximately 370 meters (Fig. 7). The cave branches extend parallel to NW-SE trending discontinuities, whereas the main gallery is parallel to the NE-SW trending tectonic line, with an average inclination of 45 degrees, and has a ceiling height up to 26 meters. The main gallery is fairly rich with speleothems. Some reach a height of up to 10 meters (Fig. 8). Initially, evolution of the main gallery parallel to main tectonic lines was interrupted by NW-SE trending discontinuities, where new branches emerged towards to the end of the gallery.

Methods

The most appropriate samples for paleoseismological studies are cylindrical stalagmites with uniform growth, because uniform stalagmites reflect formation under unchanged conditions, such as water amount and chemistry. Throughout the last three years, paleoseismological data were collected from the caves located in the southern Taurus Mountain. Three stalagmite samples used in this study were taken from two different caves, namely the

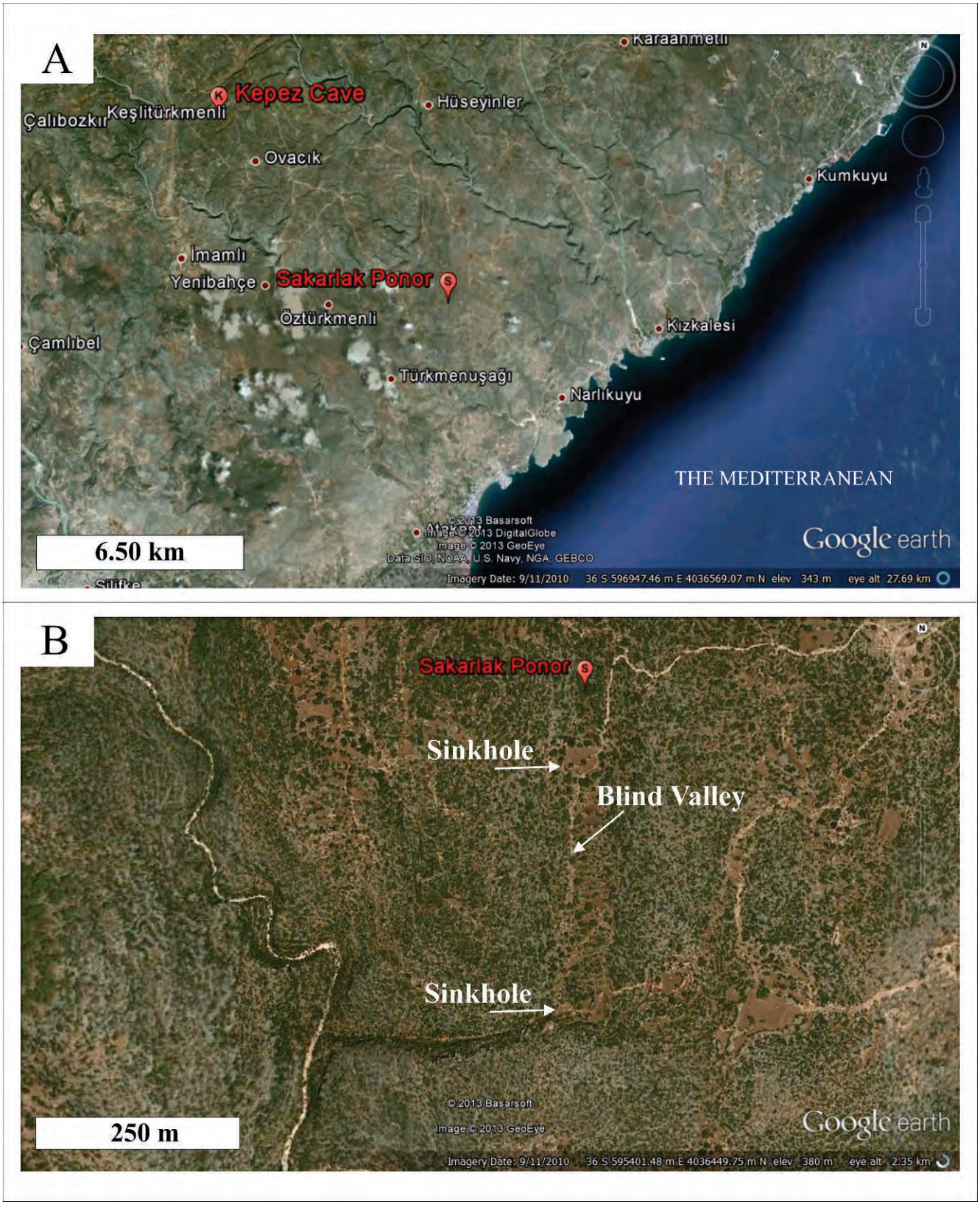

Figure 3. Satellite images from Google Earth showing locations of the Sakarlak Ponor and Kepez Cave (A) and an enlargement of the the Sakarlak Ponor area showing its relationship to the blind valley and two sinkholes (B).

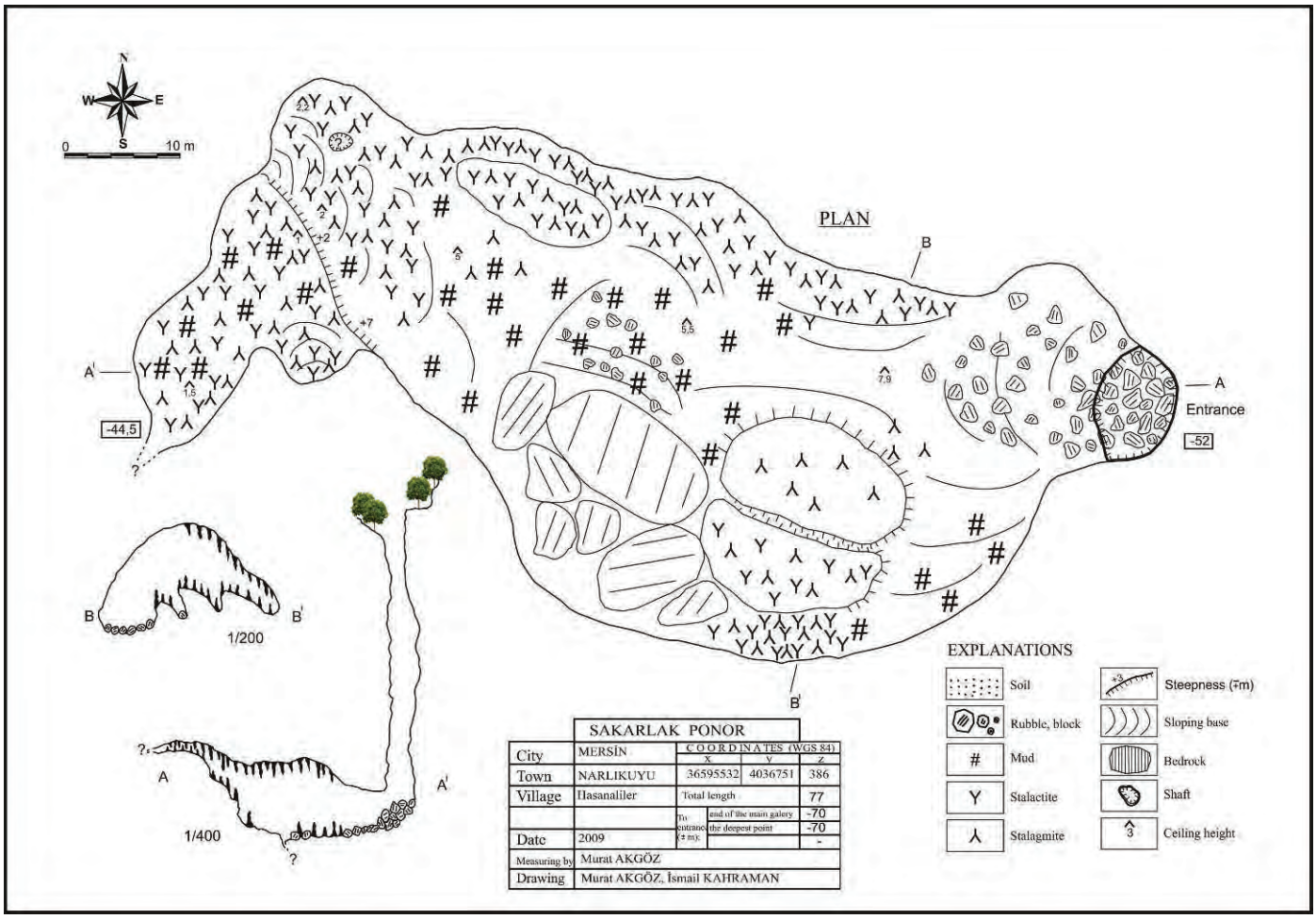

Figure 4. A plan map and cross-sections of the Sakarlak Ponor.

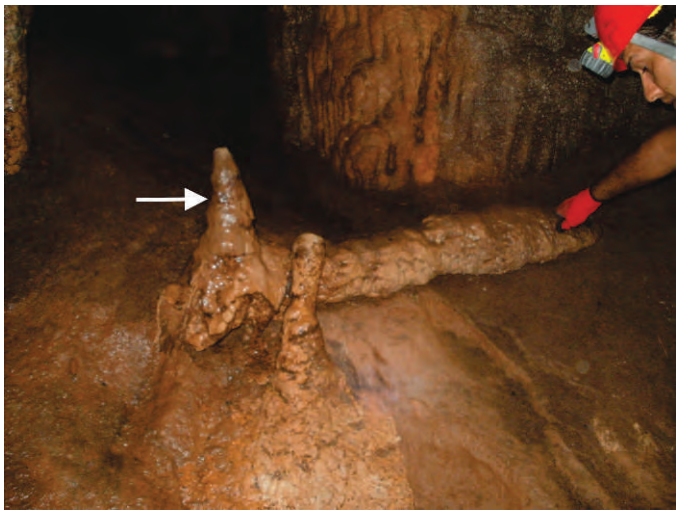

Figure 5. A fallen stalagmite with more recent stalagmites at the junction of the fossil passage and the main gallery in Sakarlak Ponor.

Sakarlak Ponor and Kepez Cave by using SRT (single rope technique) for access. The reason for selecting these locations is their protection from anthropogenic and glacial effects. The stalagmites were cut along the growth axes, then polished, examined under a binocular microscope for corrosive hiatuses, and dated using U/Th dating.

From each stalagmite, two distinctive samples from the top and bottom portions of the stalagmite were taken by dental drilling to determine U/Th age for deviations in the growth axis angle. After the Hendy Test determining dateable ^{230}Th mineral in the samples, the U/Th analyses were performed using the high-precision mass spectrometry at the Environment Change Laboratory (HISPEC) of the National Taiwan University. In general, U samples are low levels and a large part of the samples in the range of 90 to 182 ppb (Table 1). Ages in Table 1 were calculated in the standard way.

Results

Sakarlak 4

The sample S4 was taken from the southern side of the main gallery, where numerous large blocks have collapsed

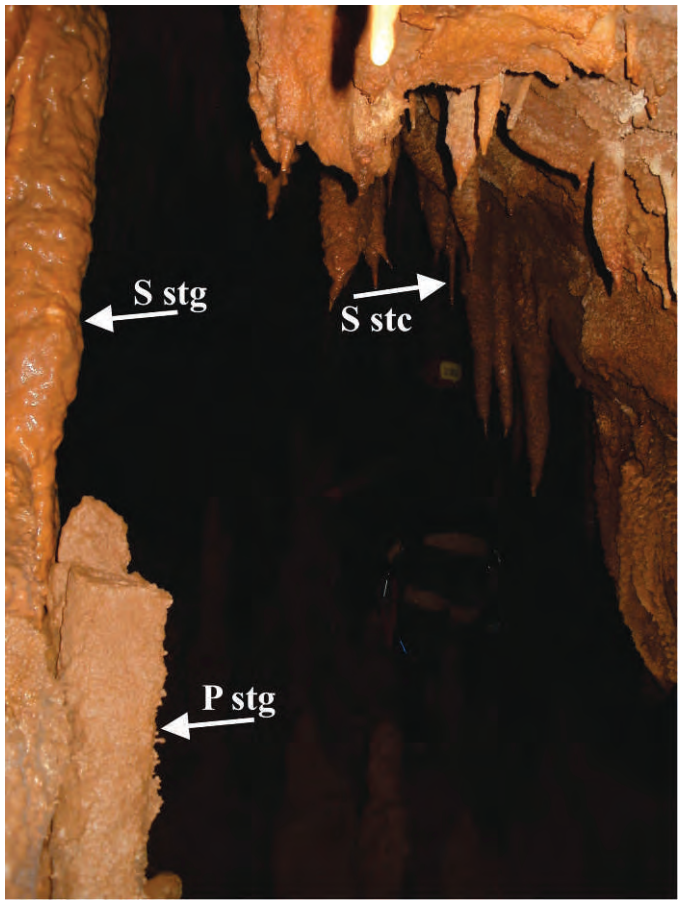

Figure 6. Primary (P) and Secondary (S) stalactites (stc) and stalagmites (stg) in the Sakarlak Ponor.

from the cave ceiling. The sample S4 has a length of 32.3 cm, with base and tip diameters of 11.1 and 3.8 cm (Fig. 9) respectively. The deposition rate changes with amount of water, water flow type, and content of carbon dioxide. Therefore, diameter changes in a stalagmite indicate fluctuation in water supply. Stalagmite S4 consists of dark and light colored laminae, and in some cases, gaps are present between these laminae. In general, such gaps occur through evaporation due to temperature rise, loss of moisture, and air circulation (Boch, 2008; Meyer et al., 2008).

For the formation time of S4, U/Th age determination was performed on two different parts of sample using MC-ICPMS technique. Based on age determinations, sample age of the base and the tip portions were determined 780 ± 919 and 775 ± 2732 years, respectively. For S4, the average growth rate was estimated from ratio of time difference to the distance between the sampling points. This rate for uniformly developed stalagmite is 1.25 mm for each year. This value is not within the range of 0.015 mm and 0.37 mm for each year reported in the literature (Fairchild et al., 2010; Fleitmann et al., 2004; Frisia et al., 2003; Genty et al., 2001; Polyak and Asmeron, 2001; Treble et al., 2003; White, 2007). This may be explained by differences in the growth rate of stalagmites, as well as variety in their structure, texture, and chemical composition. The stalagmite sample was formed over approximately 258 years between AD 55 and AD 313. This time interval remains within the specified period in a general upward trend the global air temperature between AD 0 and 1000, as is known from various climate indicators such as tree rings, lake sediments, and cave deposits (Şenoğlu, 2006).

Deviations of growth axis angle are in keeping to a very large extent with the historical earthquake times. A comparison of the occurrence time of historical earthquakes in the literature with predicted ages for growth axis angle deviations provides a possible evidence for earthquakes. The margin of error between historical earthquakes and predicted years about deviation of the growth axis angles is maximum 5 years. Stalagmite growth axis angle deviation of approximately 16 degrees corresponds to year AD 115 (Fig. 9). This date coincides with the AD 110 and AD 115 Antioch Earthquakes in literature (Altınok et al., 2011; Erel and Adatepe, 2007; Sbeinati et al., 2005). In the same literature, it is specified that the intensities of AD 110 and AD 115 Antioch Earthquakes were respectively 8 and 9, and 260,000 people died as a result of these earthquakes. In a modeling of the historical tsunami with a tectonic origin in the Mediterranean, tsunami waves reached to south coast of Turkey in one hour after a magnitude 8 earthquake in Helenic Arc, and the south coast of Turkey was strongly affected by tsunami waves (Tinti et al., 2005). Similarly, relatively small deviations of the growth axis angle and the differences in the lamina thickness and color seen in the stalagmite tip are largely consistent with historical earthquakes. These earthquakes, AD 334 Antioch, AD 341 Antioch, AD 344 Rhodes, and AD 365 Cyprus, had intensities of 9, 8, 9, and 9, respectively (Antonopoulos, 1980; Pararas-Carayannis, 2011; Erel and Adatepe, 2007; Papadopoulos et al., 2007; Sbeinati et al., 2005; Soloviev et al., 2000; Tinti et al., 2005). In literature, Rhodes was largely collapsed as a result of Rhodes Earthquake in AD 344. In addition, there were approximately 9 m high tsunami waves in the Mediterranean after the Cyprus and Crete Earthquake in AD 365 (Erel and Adatepe, 2007). Data for the Sakarlak 4 sample are a very good example of the effects of seismic activity on aspects of stalagmite development such as growth-axis angle and thickness and color differences of laminae. These changes are records of past earthquakes, and hence, they are very useful data for the study of cave sediments for paleoseismology.

SAKARLAK 1

The sample Sakarlak 1 was taken at the junction of the main gallery and fossil branch in the nothwestern part of the main gallery. The stalagmite S1 developed uniformly and has a length of 29.8 cm. During its development, the average diameter of approximately 5 cm remained

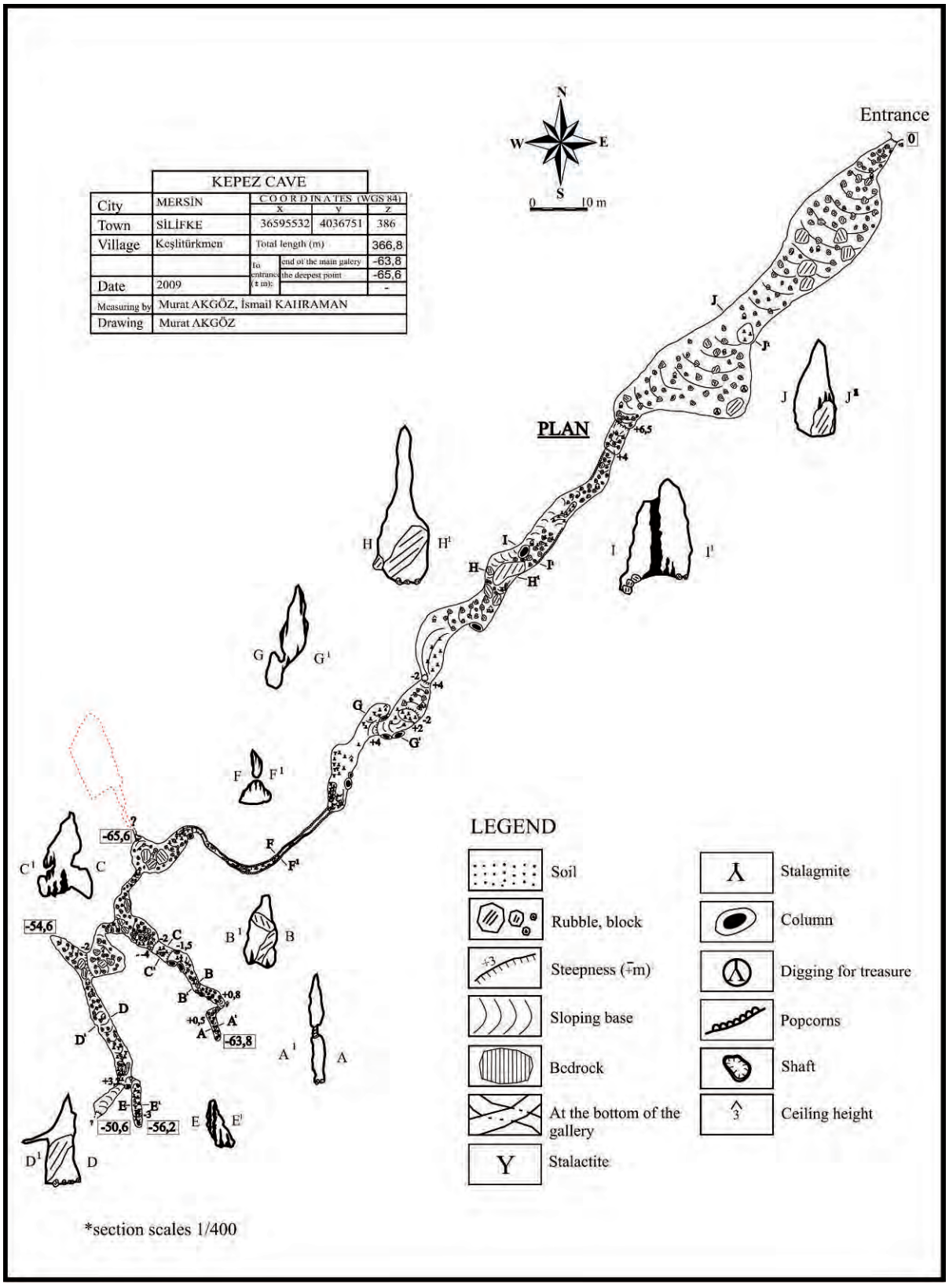

Figure 7. A plan map and cross-sections of Kepez Cave.

Figure 8. Mud-covered speleothems in the Kepez Cave.

unchanged. The unchanged diameter shows that there is no significant change in the amount of dripping water that fed this stalagmite.

The longitudinal cross-section of S1 revealed, especially at the end portion the stalagmite, laminae with different thicknesses and color. This part of the stalagmite also shows a different growth axis (Fig. 10). Stalagmite growth-axis angle changes and differences between laminae in sediment were caused by tectonic effects and settlement and collapse of the cave during precipitation.

For the formation time of S1, U/Th age was determined from two different parts of sample using MC-ICPMS technique. Based on these determinations, sample ages of the base and tip portions are 65,929 ± 337 and 56,439 ± 517 years, respectively. For S1, the average growth rate was calculated from time difference and distance between the sampling points. The stalagmite shows a uniform development with a growth rate of 0.03 mm for each year. This value is within the range of 0.015 mm and 0.37 mm for each year given in literature (Genty et al., 2001; Polyak and Asmeron, 2001; Frisia et al, 2003; Treble et al., 2003; Fleitmann et al., 2004; White, 2007; Fairchild et al., 2010). Considering the average growth rate, we concluded that the sample was formed over 9310 years during the Pleistocene.

Figure 10 shows the deviations of the stalagmite growth-axis angle labeled with times determined by taking into account the color and sedimentary changes between laminae, the average growth rate, and the sample length. The most significant deviation of the growth axis angle of stalagmite occurred approximately 61 ± 0.5 ka years ago, when there was a sudden deviation of 26 degrees in the growth caused by seismic activities (Fig. 10). Values of subsequent deviations in the growth axis range from 12 to 15 degrees. However, it is difficult to determine the causes of the deviations. Their occurrence is probably due to seismic activity or settling and subsidence of the floor of the cave. The view of the stalagmite was taken out of a collapsed block. About 56 ± 0.5 ka years before present, a stalagmite growth-axis deviation of about 21 degrees was due to tectonic activities rather than settling or subsidence in the cave. The conclusion is based on the difference in the color of the deposit during approximately 156 years, based on the length of the lamina and the average growth rate. During the formation of this stalagmite, climatic oscillation is characterized by changes in carbonate sediment color. Dark-colored laminae rich in organic matter (Fig. 10) indicate deposition during period of relatively abundant vegetation (Bradley, 1999 p. 326–335; Van Beynen et al., 2004; Bayarı and Özyurt, 2005; Webster et al., 2007; White, 2007; Meyer et al., 2008; Fairchild et al., 2010). Feed-water from which the stalagmite formed had more organic substance after passing through the soil zone due to more intense organic activities. Therefore, these dark-colored laminae indicate stalagmite development under a temperate or warm climate, whereas the light-colored laminae are poor in organic material and indicate relatively cold climatic conditions.

According to U/Th age determination, the Sakarlak 1 stalagmite was formed during the Pleistocene. According to the literature, during the period of about 9,000 to 90,000 years before the Holocene, a large part of the European continent was covered with ice having a thickness up to 3 km. During this time period, there was a climatic fluctuation characterized with long-term cooling and short-term warming periods that would cause color variations in stalagmites (Altın, 2007).

SAMPLE OF KEPEZ CAVE

The sample from Kepez Cave was taken from the first point of intersection of a side branch with the main gallery (Fig. 7). The sample has a length of 16 cm, and its base and tip diameters are 7.2 and 3.5 cm, respectively (Fig. 11). In general, the stalagmite shows regular vertical diameter changes along the growth axis. However, narrowing in diameter is observed at four different points. Possible causes of these diameter narrowing's in the stalagmite are changes in the amount of water feeding it, interruption of the dripping water due to tectonic movements, and seasonal cold and dry climatic conditions.

U/Th ages from two different parts of the sample from Kepez Cave were determined using MC-ICPMS technique.

Table 1. U and Th isotope composition of the stalagmite samples and their ^{230}Th ages.

	I.D.		
Isotope	Sakarlak 1	Sakarlak 4	Kepez
^{238}U, ppb			
Sample 1	97.99 ± 0.11	57.399 ± 0.045	182.01 ± 0.17
Sample 2	94.499 ± 0.069	58.414 ± 0.053	48.940 ± 0.051
^{232}Th, ppt			
Sample 1	2963 ± 16	5237 ± 15	755 ± 18
Sample 2	544 ± 10	15285 ± 75	485 ± 9.1
δ^{234}U, measured			
Sample 1	335.7 ± 2.4	340.9 ± 1.7	97.4 ± 1.5
Sample 2	330.2 ± 1.8	337.7 ± 2.0	112.1 ± 1.9
Age, uncorrected			
Sample 1	57015 ± 432	2593 ± 88	31787 ± 188
Sample 2	66038 ± 333	4520 ± 281	58784 ± 426
Age, corrected			
Sample 1	56439 ± 517	780 ± 919	31688 ± 194
Sample 2	65929 ± 337	775 ± 2732	58552 ± 441
$^{234}U_{initial}$, corrected			
Sample 1	393.7 ± 2.8	341.6 ± 1.9	106.6 ± 1.7
Sample 2	397.8 ± 2.2	336.9 ± 3.3	132.3 ± 2.3

Note: Analytical errors are 2σ of the mean. $^{234}U_{initial}$ corrected was calculated based on ^{230}Th age (T) (i.e., $d^{234}U_{initial} = d^{234}U_{measured} X e^{l234*T}$, and T is corrected age); ppb = parts per billion; ppt = parts per trillion.

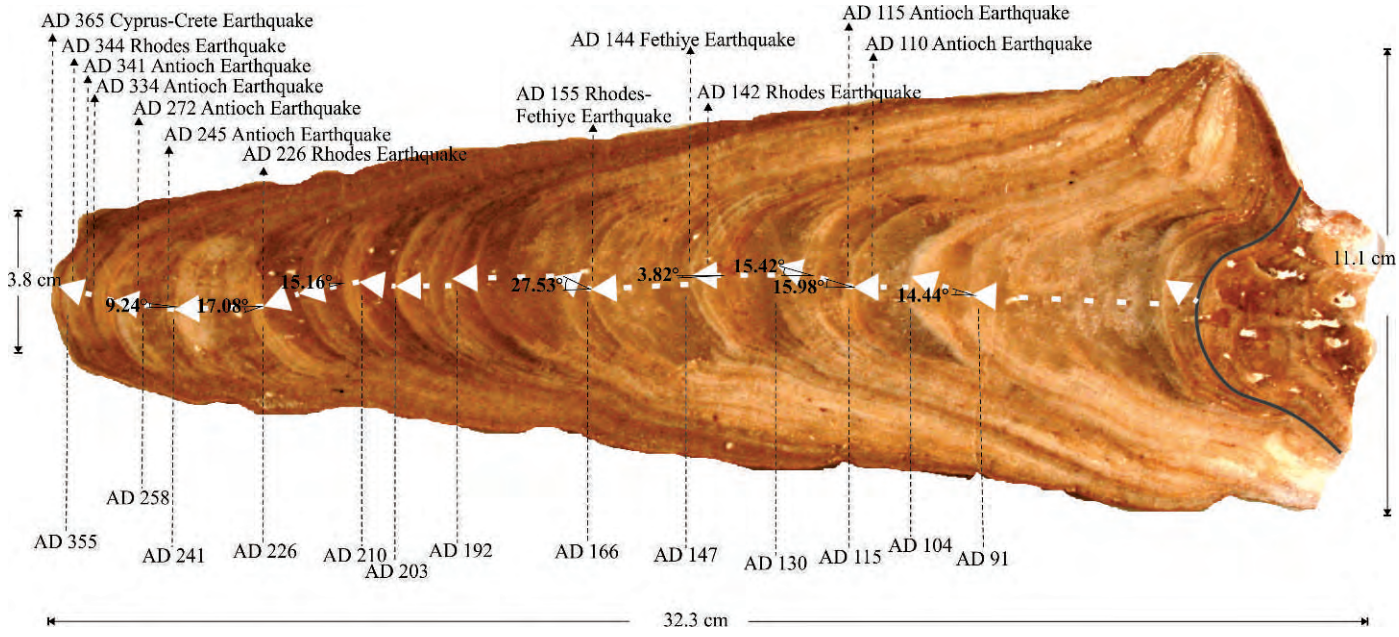

Figure 9. Longitudinal section of the Sakarlak 4 sample showing deviations in the growth-axis angle. Dates of the deviations are derived by interpolating between the dates locations. Historic earthquakes known to have occurred in the area are also indicated.

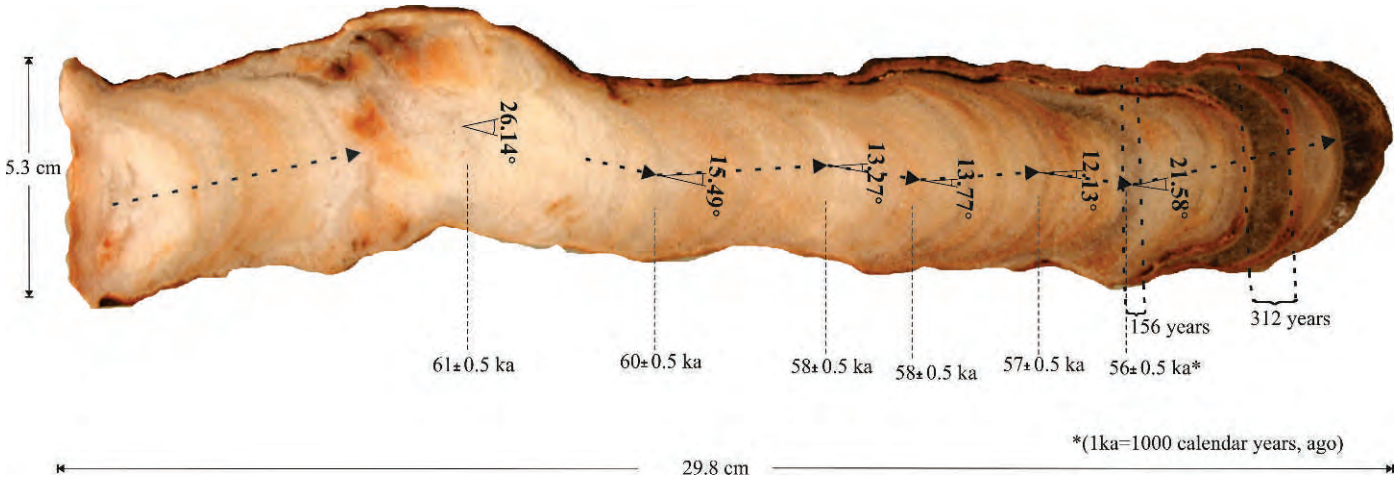

Figure 10. Longitudinal section of the Sakarlak 1 sample showing deviations in the growth axis angle, with corresponding ages.

The ages of the base and tip portions of the stalagmite are 31,688 ± 194 and 58,552 ± 441 years, respectively. The average growth rate calculated from the time difference and the distance between the sampling points is 0.006 mm for each year for the stalagmite. This value is not within the range of 0.015 mm and 0.37 mm for each year (Genty et al., 2001; Polyak and Asmeron, 2001; Frisia et al., 2003; Treble et al., 2003; Fleitmann et al., 2004; White, 2007; Fairchild et al., 2010). The growth rates of stalagmites, as well as their structures, textures, and chemical compositions, may differ. The stalagmite was slowly formed during a time of about 27 ka years toward the end of the Pleistocene based on average growth rate, the distance between the dated points, and the total length of the stalagmite. As mentioned before, the majority of the European continent was under a thick layer of glacial ice at this time. Warm periods were shorter than the periods of cooling. In the longitudinal cross-section of the Kepez sample, light-colored laminae are poor in organic matter, whereas dark-colored laminae are enriched in organic matter due to rapid change in climate during warm periods (Bradley, 1999 p. 326–335; Van Beynen et al., 2004; Bayarı and Özyurt, 2005; Webster et al., 2007; White, 2007; Meyer et al., 2008; Fairchild et al., 2010). As a result of these data, it could be said that the light-colored deposition showing the cooling period in climatic fluctuation repeated approximately 49,410 years ago, and also in climate fluctuation warming was repeated during a period of about 43,493 years before present (Fig. 11).

In the longitudinal cross-section of the Kepez Cave stalagmite, there are three different deviations of the stalagmite growth axis. The clearest deviation of the

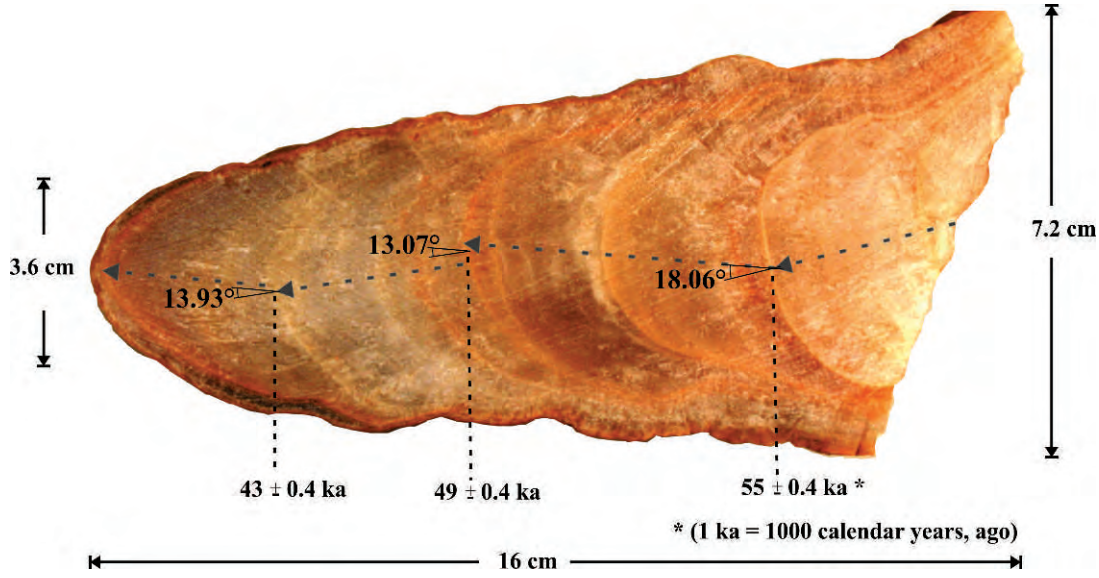

Figure 11. Longitudinal section of the Kepez Cave sample showing deviations in the growth axis angle and approximate ages.

growth axis angle is about 18 degrees and occurred 55 ± 0.5 ka ago. This value could be correlated with the Sakarlak Ponor sample 1, located approximately 9 km from the southwest of the Kepez Cave. Considering the S1 age data and the margins of error, this deviation could be caused by the same seismic activities that led to its growth-axis change of 21 degrees. Except for the clearest deviation of the growth axis in the Kepez sample, the other two deviations of 13 and 14 degrees occurred at different times (Fig. 11). These data, in addition to the thickness and color differences among laminae in the sample from Kepez Cave, indicate that the Kepez Cave was affected by seismic activity at three different times.

Conclusions

Caves in the study area are clearly developed on the fault, fracture, and crack systems. According to the lineament map generated from the digital elevation model, the main tectonic line is a NE-SW–trending left-lateral strike-slip fault. On the other hand, parts of the caves are parallel to NW-SE–trending discontinuities that are perpendicular to the main tectonic line. Karstification in the central Taurus Mountains and also in the study area began to develop at the transition from Pliocene to Pleistocene. The NW-SE trending discontinuities and the warm climatic intervals within the Pleistocene glacial periods have affected karstification and cave development in the region.

The U/Th analyses indicate low levels of U in the samples. Lamina thickness and color changes of the selected samples were examined together to determine changes of the stalagmite growth-axis angles, these changes are possibly due to seismic activity.

According to U/Th age data, the selected stalagmites were formed in the Pleistocene to Holocene. The S1 sample from the Sakarlak Ponor was developed over 9310 years during Pleistocene. During this time, the growth axis of the stalagmite has changed six times. The Kepez Cave sample was developed slowly over a time of about 27 ka in the Pleistocene during which the stalagmite's growth-axis position changed at three distinct times. The largest deviation times of growth axis angle for the Kepez Cave and Sakarlak 1 samples are 18 and 21 degrees, respectively. These deviation angles are very close to each other indicating that two samples were affected by the same seismic activities. On the other hand, periods of the dark-colored laminae in the sample reflect interglacial periods in Pleistocene. Based on the U/Th analytical results of the selected samples, the youngest dates belong to the Sakarlak 4 sample. When average growth rate, the distance between sampling points, and the U/Th age data of the sample S4 were evaluated together, the sample shows a rapid growth in a range of about 258 years between the years AD 55 and AD 313. In this time interval there was a tendency to an overall increase in global air temperature.

The deviation times of the stalagmite growth-axis angles are largely compatible with the times of historical earthquakes. The determined time of AD 115 yr for the S4 16 degree growth axis deviation corresponds to the magnitude 8 earthquake AD 110 or magnitude 9 earthquake AD 115 Antioch Earthquakes that caused the death of thousands of people. The deviation of 4 degrees having a formation time of AD 147 coincides with AD 142 Rhodes or AD 144 Fethiye magnitude 8 earthquakes. Ages of deviations with 17 and 9 degrees were determined as AD 226 and AD 241, respectively. These ages are coincident with the magnitude 8 earthquakes AD 226 Rhodes and AD 245 Antioch. In addition, lamina thickness and color differences near the tip of the stalagmite sample coincident with deviations of the growth-axis angle are thought to be coincident with magnitude 8 AD 334 and magnitude 9 AD 341 Antioch earthquakes, the magnitude 9 AD 344 Rhodes earthquake, which was largely caused by the collapse of Rhodes, or the AD 364 Cyprus-Crete earthquake.

In conclusion, dating deviations of the growth-axis angle in stalagmites provides information on growth deformation and development. These ages can be correlated with occurrence time of historical earthquakes, suggesting possible effects of earthquakes on stalagmite development.

Acknowledgements

The authors are thankful to Prof. Dr. Chuan Chou Shen (the National Taiwan University) for his valuable suggestions about U/Th dating. This paper is based on a part of the first author's dissertation, which was supervised by second author. Mersin University Research Fund financially supported this research under the project of BAP-FBE JM (MA) 2011-5 DR. The authors are much indebted to the anonymous reviewers for their extremely careful and constructive reviews that significantly improved the quality of the paper. Thanks are also due to Miss Sibel Kocaoğlan for language editing of the final text.

References

Akay, E., and Uysal, Ş., 1988, Orta Toroslar'ın post-Eosen tektoniği: Maden Tetkik ve Arama Dergisi, v. 108, p. 57–68.

Akgöz, M., 2012, Göksu nehri ve Lamas kanyonu (Mersin) arasında kalan bölgenin karst evrimi [Ph.D. thesis]: Mersin, Mersin Üniversitesi Fen Bilimleri Enstitüsü, 290 p.

Alan, İ., Şahin, Ş., Elibol, H., Keskin, H., Altun, İ., Bakırhan, B., Balcı, V., Böke, N., Kop, A., Esirtgen, T., and Hanilçi, N., 2011, Orta Torosların jeodinamik evrimi Bozyazı-Aydıncık-Gülnar-Silifke (İçel) yöresi: Ankara, Maden Tetkik ve Arama Raporu No: 11462, 308 p.

Altın, V., 2007, İklim dinamikleri: Bilim ve Teknik Dergisi, Şubat sayısı p. 2–4 (in Turkish).

Altınok, Y., Alpar, B., Özer, N., and Aykurt, H., 2011, Revision of the tsunami catalogue affecting Turkish coasts and surrounding regions: Natural Hazards and Earth System Sciences, v. 11, p. 273–291. doi:10.5194/nhess-11-273-2011.

Angelova, D., Belfoul, M.A., Bouzid, S., Filahi, M., and Faik, F., 2003, Paleoseismic phenomena in karst terrains in Bulgaria and Morocco: Acta Carsologica, v. 32, no. 1, p. 101–120.

Antonopoulos, J., 1980, Data from investigation on seismic sea-waves events in the Eastern Mediterranean from the Birth of Christ to 500 A.D: Annali di Geofisica, v. 33, p. 141–161.

Bayarı, S., and ve Özyurt, N., 2005, Mağara çökellerinden geçmiş ortam koşullarının belirlenmesi: Konya, Ulusal Mağara Günleri Sempozyumu, p. 19–29.

Becker, A., Davenport, C.A., Eichenberger, U., Gilli, E., Jeannin, P.-Y., and Lacave, C., 2006, Speleoseismology: A critical perspective: Journal of Seismology, v. 10, p. 371–388. doi:10.1007/s10950-006-9017-z.

Boch, R., 2008, Stalagmites from Katerloch Cave, Austria: Growth dynamics and high-resolution records of climate change [Ph.D. thesis]: Innsbruck, University of Innsbruck, 223 p.

Bradley, R.S., 1999, Paleoclimatology: Reconstructing Climates of the Quaternary, second edition, San Diego: Academic Press, International Geophysics Series no. 68, 613 p.

Cheng, H., Edwards, R.L., Hoff, J., Gallup, C.D., Richards, D.A., and Asmerom, Y., 2000, The half-lives of uranium-234 and thorium-230: Chemical Geology, v. 169, p. 17–33. doi:10.1016/S0009-2541(99)00157-6.

Demirkol, C., 1986, Sultandağ ve dolayının tektoniği: Maden Tetkik ve Arama Dergisi, v. 107, p. 111–118.

Erel, T.L., and Adatepe, F., 2007, Traces of historical earthquakes in the ancient city life at the Mediterranean region: Journal of the Black Sea/Mediterranean Environment, v. 13, p. 241–252.

Eren, M., 2008, Olba (Ura-Uğuralanı) jeoarkeolojisi (Silifke, Marsin), *in* Dönmez, H., and Özme, A., eds., Arkeometri Sonuçları Toplantısı: Ankara, Kültür ve Turizm Bakanlığı, no. 24, p. 181–192.

Eren, M., Kadir, S., Hatipoğlu, Z., and Gül, M., 2004, Mersin (İçel) Yöresinde Kaliş Gelişimi: TÜBİTAK Project, No. 102Y036, 136 p. (in Turkish with English abstract).

Fairchild, I.J., Spötl, C., Frisia, S., Borsato, A., Susini, J., Wynn, P.M., Cauzid, J., Edinburgh Ion Microprobe Facility, 2010, Petrology and geochemistry of annually laminated stalagmites from an Alpine Cave (Obir, Austria): Seasonal cave physiology: Geological Society, London, Special Publications, v. 336, no. 1, p. 295–321. doi:10.1144/SP336.16.

Fleitmann, D., Burns, S.J., Neff, U., Mudelsee, M., Mangini, A., and Matter, A., 2004, Palaeoclimatic interpretation of high-resolution oxygen isotope profiles derived from annually laminated speleothems from Southern Oman: Quaternary Science Reviews, v. 23, p. 935–945. doi:10.1016/j.quascirev.2003.06.019.

Ford, D.C., and Hill, C.A., 1999, Dating of speleothems in Kartchner Caverns, Arizona: Journal of Cave and Karst Studies, v. 61, no. 2, p. 84–88.

Frisia, S., Borsato, A., Preto, N., and McDermott, F., 2003, Late Holocene annual growth in three Alpine stalagmites records the influence of solar activity and the North Atlantic Oscillation on winter climate: Earth and Planetary Science Letters, v. 216, no. 3, p. 411–424. doi:10.1016/S0012-821X(03)00515-6.

Garašić, M., 1991, Morphological and hydrogeological classification of speleological structures (caves and pits) in the Croatian karst area: Geološki vjesnik, v. 44, p. 289–300.

Garduño-Monroy, V.H., Pérez-López, R., Rodríguez-Pascua, M.A., García-Mayordomo, J., Isarde-Alcántara, I., and Bischoff, J., 2011, Could large palaeoearthquakes break giant stalactites in Cacahuamilpa Cave? (Taxco, Central México): Corinth, Greece, 2nd INQUA-IGCP-567 International Workshop on Active Tectonics, Earthquake Geology, Archaeology and Engineering, p. 46–49.

Genty, D., Baker, A., and Vokal, B., 2001, Intra-and inter-annual growth rate of modern stalagmites: Chemical Geology, v. 176, p. 191–212. doi:10.1016/S0009-2541(00)00399-5.

Gilli, E., 1999, Breaking of speleothems by creeping of a karstic filling. The example of the Ribiere Cave (Bouches-du-Rhone): Comptes Rendus de l'Academie des Sciences, Series IIA: Earth and Planetary Science, v. 329, no. 11, p. 807–813. doi:10.1016/S1251-8050(00)88636-X.

Gilli, É., 2005, Review on the use of natural cave speleothems as palaeseismic or neotectonics indicators: Comptes Rendus Geoscience, v. 337, p. 1208–1215. doi:10.1016/j.crte.2005.05.008.

Jaffey, A.H., Flynn, K.F., Glendenin, L.E., Bentley, W.C., and Essling, A.M., 1971, Precision measurement of half-lives and specific of ^{235}U and ^{238}U: Physical Review C, v. 4, p. 1889–1906. doi:10.1103/PhysRevC.4.1889.

Meyer, M.C., Spötl, C., and Mangini, A., 2008, The demise of the Last Interglacial recorded in isotopically dated speleothems from the Alps: Quaternary Science Reviews, v. 27, p. 476–496. doi:10.1016/j.quascirev.2007.11.005.

Ozansoy, C., and Mengi, H., 2006, Mağarabilimi ve Mağaracılık: Ankara, Turkey, TÜBİTAK populer bilim kitapları, 235, 337 p.

Papadopoulos, G.A., Daskalaki, E., Fokaefs, A., and Giraleas, N., 2007, Tsunami hazards in the eastern Mediterranean Sea: Strong earthquakes and tsunamis in the East Hellenic Arc and Trench system: Natural Hazards and Earth System Sciences, v. 7, p. 57–64. doi:10.5194/nhess-7-57-2007.

Pararas-Carayannis, G., 2011, The earthquake and tsunami of July 21, 365 AD in the Eastern Mediterranean Sea - Review of impact on the ancient world - Assessment of recurrence and future impact: Science of Tsunami Hazards, v. 30, p. 253–292.

Polyak, V.J., and Asmerom, Y., 2001, Late Holocene climate and cultural changes in the southwestern United States: Science, v. 294, p. 148–151. doi:10.1126/science.1062771.

Postpischl, D., Agostini, S., Forti, P., and Quinif, Y., 1991, Palaeoseismicity from karst sediments: The "Grotta del Cervo" cave case study (Central Italy): Tectonophysics, v. 193, p. 33–44. doi:10.1016/0040-1951(91)90186-V.

Sbeinati, M.R., Darawcheh, R., and Mouty, M., 2005, The historical earthquakes of Syria: An analysis of large and moderate earthquakes from 1365 B.C. to 1900 A.D.: Annals of Geophysics, v. 48, p. 347–435. doi:10.4401/ag-3206.

Šebela, S., 2008, Broken speleothems as indicators of tectonic movements: Acta Carsologica, v. 37, no. 1, p. 51–62.

Şenoğlu, G., 2006, Mağara çökellerinin iz element içeriğinden paleoiklim koşullarının belirlenmesi [MSc thesis]: Ankara, Hacettepe Üniversitesi Fen Bilimleri Enstitüsü, 118 p.

Soloviev, S.L., Solovieva, O.N., Go, C.N., Kim, K.S., and Shchemikov, N.A., 2000, Tsunamis in the Mediterranean Sea 2000 BC - 2000 AD: Dordrecht, Netherlands, Kluwer Academic Publishers, Advances in Natural and Technological Hazards Research 13, 237 p.

Spötl, C., and Mangini, A., 2007, Speleothems and paleoglaciers: Earth and Planetary Science Letters, v. 254, p. 323–331. doi:10.1016/j.epsl.2006.11.041.

Tinti, S., Armigliato, A., Pagnoni, G., and Zaniboni, F., 2005, Scenarios of giant tsunamis of tectonic origin in the Mediterranean: ISET Journal of Earthquake Technology, v. 42, no. 4, p. 171–188.

Treble, P., Shelley, J.M.G., and Chappell, J., 2003, Comparison of high resolution sub-annual records of trace elements in a modern (1911–1992) speleothem with instrumental climate data from southwest Australia: Earth and Planetary Science Letters, v. 216, no. 1, p. 141–153. doi:10.1016/S0012-821X(03)00504-1.

Van Beynen, P.E., Schwarcz, H.P., and Ford, D.C., 2004, Holocene climatic variation recorded in a speleothem from McFail's Cave: Journal of Cave and Karst Studies, v. 66, p. 20–27.

Webster, J.W., Brook, G.A., Railsback, L.B., Cheng, H., Edwards, R.L., Alexander, C., and Reeder, P.P., 2007, Stalagmite evidence from Belize indicating significant droughts at the time of preclassic abandonment, the Maya hiatus, and the classic Maya collapse: Palaeogeogrphy, Palaeoclimatology, Palaeoecology, v. 250, p. 1–17.

White, W.B., 2007, Cave sediments and paleoclimate: Journal of Cave and Karst Studies, v. 69, p. 76–93.

V. Vanghi, E. Iriarte, A. Aranburu – High resolution X-ray computed tomography for petrological characterization of speleothems. *Journal of Cave and Karst Studies,* v. 77, no. 1, p. 75–82. DOI: 10.4311/2014ES0102

HIGH RESOLUTION X-RAY COMPUTED TOMOGRAPHY FOR PETROLOGICAL CHARACTERIZATION OF SPELEOTHEMS

VALENTINA VANGHI[1,2], ENEKO IRIARTE[1], AND ARANTZA ARANBURU[3]

Abstract: High resolution X-ray computed tomography (HRXCT) has been barely used in speleothem science. This technique has been used to study a Holocene stalagmite from Praileaitz Cave (Northern Spain) to evaluate its potential for petrologic studies. Results were compared with those derived from the routine procedures and a very good correlation was found. Our work indicates that HRXCT can be considered as a useful tool for a rapid and non-destructive characterization of the speleothem, providing important information about petrological textures, spatial distribution of porosity, and diagenetic alteration, as well as stratigraphic architecture. These encouraging results indicate that HRXCT can offer interesting perspectives in speleothem science that are worth future exploration.

INTRODUCTION

Speleothem records are widely considered as reliable archives for multi-proxy based paleoclimatic reconstruction of continental regions. Geochemical and physical changes that may occur during the formation of speleothems are controlled by environmental conditions (Fairchild and Baker, 2012). This is why the study of the petrology of a speleothem is important, because crystals' morphology and their mechanisms of growth may provide useful information related to the physical and chemical characteristic of the drips (Sunagawa, 1987; Frisia et al., 2000). Speleothems are also affected by diagenetic processes such as dissolution, corrosion, micritization, and recrystallization. (Frisia and Borsato, 2010; Railsback et al., 2011). These processes may lead to the modification of their original geochemical signals, thus compromising the validity of the chronological results and the environmental interpretations that may be extracted. For example, percolating water may infiltrate the crystalline fabrics through dissolution paths or a network of interconnected pores, thus inducing diagenetic transformations (Frisia et al., 2000; Borsato et al., 2003). Consequently, it is crucial to study the spatial distribution of the primary porosity in order to identify the existence of internal heterogeneities that may lead to the formation of secondary porosity. These petrophysical properties are directly related to speleothem fabrics, microfabrics, and internal microstratigraphy (Muñoz-García et al., 2012). These features are studied through the petrological analysis of speleothems, which is commonly based on a combination of techniques like optical microscopy and scanning and transmission electron microscopy (Frisia and Borsato, 2010; Fairchild and Baker, 2012; Railsback, 2000).

High-resolution X-ray computed tomography (HRXCT) is a technique that allows non-destructive imaging and quantification of internal features of objects. Originally developed as a medical-imaging tool, over the last decades it has been increasingly used for the study of geomaterials in engineering and geosciences such as petrology, sedimentology, and paleontology (e.g., Mees et al., 2003). However, this technique has only rarely been applied to speleothems (Mickler et al., 2004), although it has great potential, being non-destructive, allowing rapid acquisition, and producing high-resolution data. In 2004, Mickler and colleagues published a research paper concerning the application of HRXCT in speleothem science. In this paper, the authors use X-ray computed tomography to identify the position of the growth axes of two stalagmites to ensure a correct longitudinal cut without causing damage that would compromise their applicability as geochemical climate proxies. Following these encouraging results, we use this technique to evaluate the potential of HRXCT for petrophysical characterization of a speleothem. This study presents an evaluation of the spatial distribution and variation of the porosity and density values obtained by HRXCT on a stalagmite sample. Results were then compared with those derived from the standard procedure of optical and scanning electron microscopy.

MATERIALS AND METHODS

SAMPLING

The stalagmite, named Novella, was sampled at Praileaitz Cave in the Basque Country of northern Spain. Further information about this cave and its geological context may be found in Vanghi (2013a and b) and references therein. In the laboratory, the stalagmite was longitudinally cut in two halves with an electric saw

[1] Universidad de Burgos, Departamento Ciencias Históricas y Geografía Plaza de Misael Bañuelos s/n, 09001, Burgos, Spain, eiriarte@ubu.es
[2] Current: University of Newcastle, School of Environmental and Life Sciences, Faculty of Science and Information Technology, University drive, Callaghan 2308 NSW, Australia, valentina.vanghi@uon.edu.au
[3] Universidad del País Vasco, Dpto. de Mineralogía y Petrología, Facultad de Ciencia y Tecnología, Ap. 644-48080, Bilbao, Spain, arantza.aranburu@ehu.es

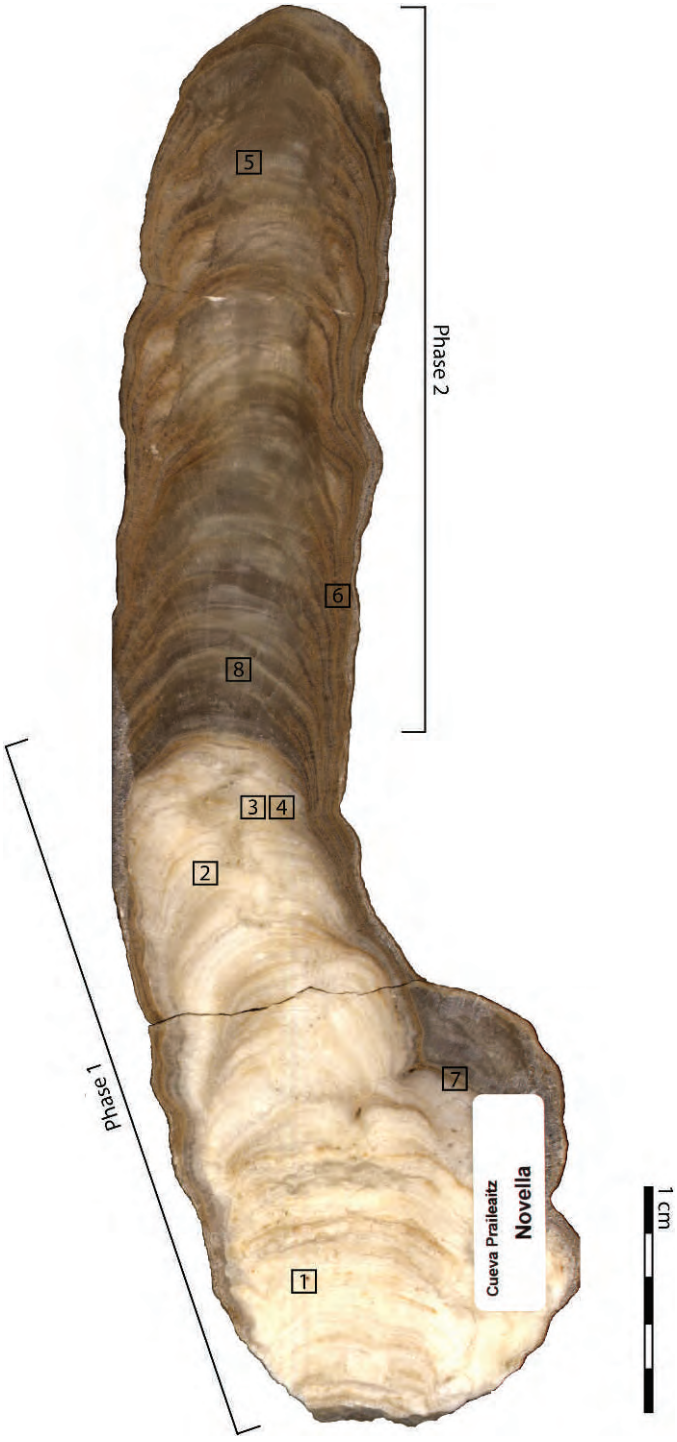

Figure 1. Longitudinal section of the stalagmite Novella. The two stratigraphic phases are also indicated. The numbered boxes correspond to the locations of the photographs showed in Figure 2.

(Fig. 1). The stalagmite is approximately 35-cm long and varies in width from 9.5 cm at the base to 6 cm at the top. Additionally to HRXCT and petrology studies, Novella's stable isotopes and trace elements were also studied (Vanghi, 2013a and b). This speleothem record is chronologically constrained by U-Th ages from two samples collected at the bottom of Phase 1 in its growth (10.7 ± 0.09 ka BP) and at the transition between Phases 1 and 2 (6.77 ± 0.07 ka BP) obtained by multi-collector inductively-coupled plasma mass-spectroscopy.

PETROLOGY

A petrologic study was carried out for the characterization and description of the different fabrics, as well as for the identification of all the diagenetic features present in the stalagmite. To do so, we made fourteen thin sections along the vertical growth axis of one entire fourth portion of the stalagmite. The areas chosen for each thin section were correlated between each other and overlapped in order to not lose information.

All the optical analyses were completed in the Laboratory of Human Evolution of the University of Burgos, Spain, using a Nikon Eclipse LV100POL optical microscope and the Nikon AZ100 binocular microscope coupled with the Nikon DS-FI1 digital camera. We got scanning electron microscope images using a GEOL JSM-6460LV microscope.

HIGH-RESOLUTION X-RAY COMPUTED TOMOGRAPHY

The basic components of X-ray computed-tomography scanners are an X-ray source, a detector, and a sample-rotation system. CT images are created by directing a planar fan beam towards an object from multiple angles around a central axis, producing a sinogram. This step is followed by the reconstruction of a succession of two-dimensional radiographs that correspond to what would be observed if the object was cut open along the image planes y-x, x-z, and y-z. The gray-scales in these images correspond to relative X-ray attenuation, which is a function of elemental composition and density; and therefore, they reflect the physical properties of the object (Mickler et al., 2004). In other words, gray-values in the images correspond to the density values, expressed in Hounsfield units (HU), measured by the scan.

The analyses were performed at the University of Burgos, using an industrial scanner Xylon CT Compact. X-ray energy and current were set to 225 kV and 2.8 mA, with a small focal spot. Only one half of the stalagmite was scanned by CT as the sample was previously sliced to perform the petrographic study. A total of 1780 slices were obtained, one slice every 0.2 mm, generating images with a pixel size of 0.69 mm. The data were processed using Materialise's Interactive Medical Image Control System (MIMICS) v.10 for reconstructing virtual images of scanned objects in two or three dimensions.

RESULTS AND DISCUSSION

An initial visual observation of the longitudinal section of the stalagmite led to the identification of two different phases of growth characterized by two different colorations

(Fig. 1). Phase 1 is about 17 cm long from the base of the stalagmite, and has a whitish color and a porous aspect, whereas Phase 2 is about 18-cm long and has a darker color, with compact and glassy aspect. The transition from Phase 1 to Phase 2 suggests some changes in the drip point, with a modification of the orientation of the growth axis of the stalagmite. X-ray diffraction analyses showed that the speleothem is entirely composed of calcite (Vanghi, 2013a).

Petrology

Petrological analyses allowed us to identify three different types of crystalline fabrics along the speleothem. Different crystalline fabrics dominate the two visible phases that show distinct colorations.

Phase 1 is dominated by the dendritic crystalline fabric, formed by interweaving thin and elongated crystals whose spatial distribution forms a net (Frisia, 2003; Fairchild et al., 2007) (Figs. 2.1 to 2.4). This texture is characterized by high intercrystalline porosity and thus by low density. The dimensions of the crystals vary, with widths between 25 and 50 μm and lengths between 200 and 550 μm. These dimensions are significantly larger than those from the dendritic texture defined by Frisia and Borsato (2010). Those authors describe this fabric as formed by crystals a few mm long and between 4 and 10 μm width; but nevertheless, we interpret ours as analogous and with the same genetic implications. Thin, closed dendritic fabric layers are present intercalated between dendritic fabric layers (Figs. 2.1 to 2.4). Closed dendritic crystals have more equal dimensions of 50 to 200 μm and form less porous laminae. Phase 1 shows an alternation of millimeter-scale white and dark layers that reflect the intercalation between the above mentioned closed dendritic (white) and properly dendritic (black) fabrics (Fig. 2.1). This variation in the crystalline fabric forms an alternating distribution of the porosity values that is also recognizable in the CT-scan data.

Phase 2 is entirely formed of big columnar crystals. Columnar fabric is characterized by large crystals more than 100-μm long and 50 to 100 μm in width, growing parallel to the central axis (Fig. 2.5 to Fig. 2.8). Their crystal boundaries are serrated, even if sometimes separated by voids filled by fluid inclusions (Frisia and Borsato, 2010). In general, the columnar fabric is less porous than the dendritic fabric. Along the central axis of the stalagmite, these crystals grow perpendicular to the surface. Close to the flank of the stalagmite, columnar crystals become smaller, and their growth orientation becomes oblique to the surface. Some micritic layers are observed in Phase 2, mainly on the edges of the speleothem, but they do not reach the central axis of the stalagmite.

Computed Tomography Scans

MIMICS v.10 software was used to create different colored masks (Fig. 3), each one corresponding to distinct intervals of density values and reflecting the internal variability of the porosity in the stalagmite. These data may be then compared to the results derived from the petrologic analysis.

Density Values vs. Fabrics

The results derived from the X-ray CT scans combined with the petrologic study highlight the strong correlation between density values and crystalline fabrics. Different density value intervals, represented by different colors, reflect different observed crystalline textures, allowing for the recognition and reconstruction of the internal petrological architecture of the speleothem (see Figs. 3 and 4).

In addition, with the MIMICs v.10 program it is also possible to create 3D models of each density interval. Different tools in the software allow manipulation of the 3D model of the object, such as rotations, cuts, measurements, and opacity readings (Fig. 5). These could be important to better study the distribution and quantification of the different crystalline fabrics and porosity.

Density Values vs. Stratigraphical Boundaries

Differences in density values correspond to changes of crystalline fabrics, reflecting different environmental conditions of formation. In the studied speleothem, the CT scan helped to identify several stratigraphic subunits, especially within Phase 2, where macroscopic laminations can hardly be identified (Fig. 6). Therefore, CT scanning can also be a valid alternative or complement to ultraviolet light to discriminate the stratigraphic architecture of speleothems.

Density Values vs. Distribution of the Porosity

Studying the spatial distribution and characteristics of the porosity makes it possible to detect stratigraphic discontinuities, such as phases of no deposition, leading to alteration, micritization, or dissolution in the speleothem. This is especially important in speleothem science, because an accurate age model has to consider any existing hiatuses and because the presence of porosity may have allowed alteration of the primary isotopic and elemental composition of a speleothem, thus making it unsuitable for palaeoclimate studies (e.g., Mickler et al., 2004; Muñoz-García et al., 2012). In Novella most of the porosity, shown in Part E of Figure 5, occurs along the dendritic texture, although sometimes it is also distributed along stratigraphic boundaries.

Other Interests

Computed tomography is also a useful non-destructive tool for rapid determination of the stalagmite growth axis position, as well as its spatial variation, without any sample manipulation or preparation. Growth bands' thicknesses in stalagmites tend to decrease away from the growth axis, so off-axis samples are more subject to non-equilibrium fractionation effects. This is why it is important to cut a stalagmite into longitudinal sections intersecting the central axis (Mickler et al., 2004). In addition, CT scanning could potentially be useful to identify the presence of other

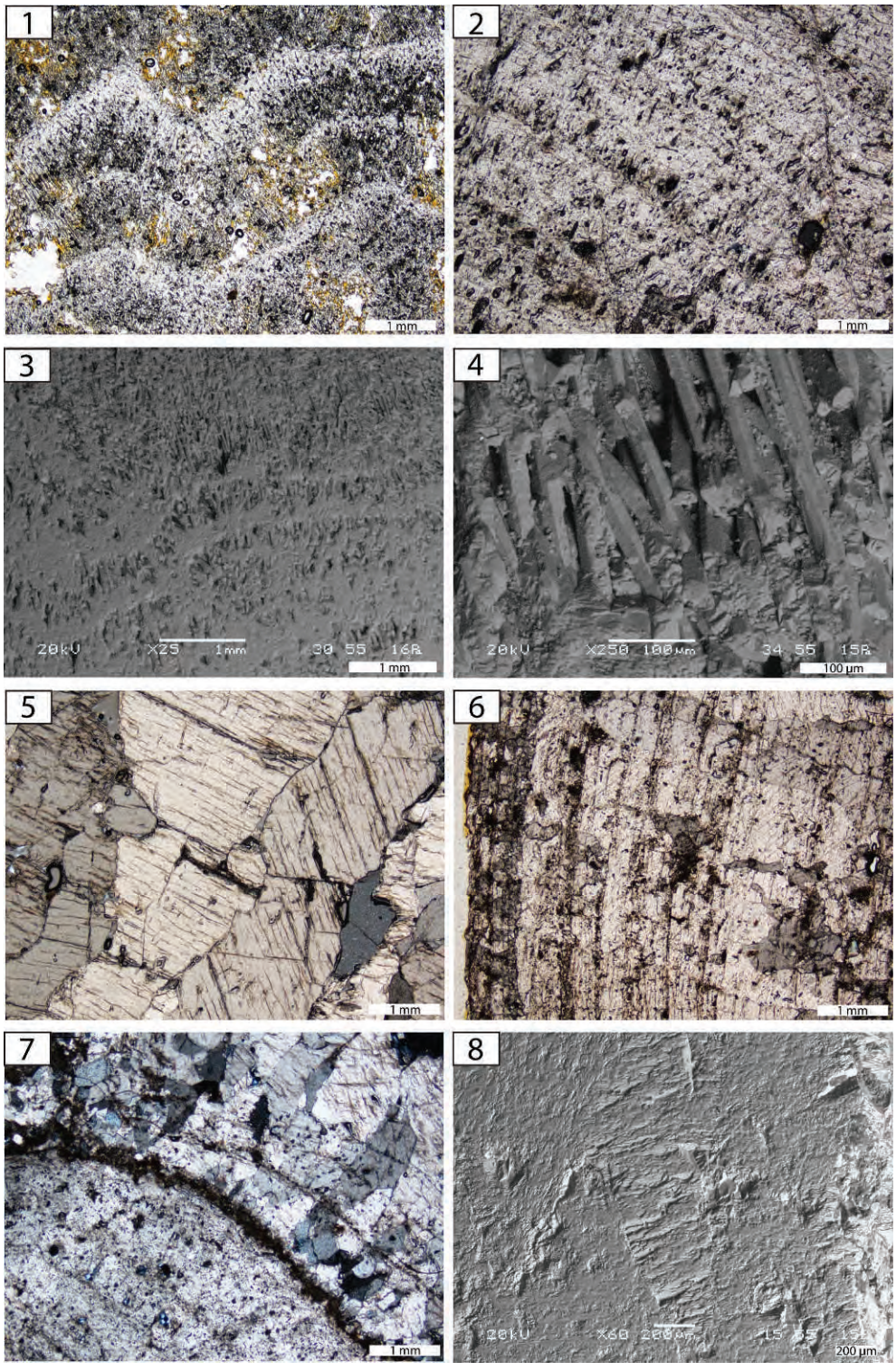

Figure 2. Thin-section photomicrographs under the petrographic microscope and the scanning electron microscope. Locations of the photographs are shown in Figure 1. (1) and (2) Alternation between dendritic and closed dendritic fabric in Phase 1. The white bands are formed by closed dendritic fabric, and the dark bands correspond to dendritic fabric. (3) Alternation of dendritic and mosaic fabrics under SEM. Notice the different porosity pattern in both fabrics. (4) Close up view of dendritic and mosaic crystals. (5) Columnar fabric in Phase 2. (6) Micritic layers interbedded in the columnar fabric close to the edge of the stalagmite. (7) Large dendritic crystals and small columnar crystals separated by a micritic layer, near the edge of the stalagmite. (8) SEM photograph of the columnar fabric in Phase 2.

Figure 3. 2D image of section of the stalagmite Novella. On the left is the unprocessed radiograph of the stalagmite. On the right is the radiograph of the stalagmite with the different calculated density-ranges. Each color has been found to correspond to different crystalline textures recognized in the petrographic study. Black is −1024–226 Hounsfield units, lowest density values, air-filled porosity; yellow is 227–776 HU, low density values, dendritic crystalline texture; fuchsia is 777–1176 HU, medium density values, closed dendritic crystalline texture; green is 1177–1576 HU, high-density values, columnar crystalline texture; and blue is 1577–3071 HU, highest density values, micritic crystalline texture. The colors are superimposed here, with those representing the lowest densities on top.

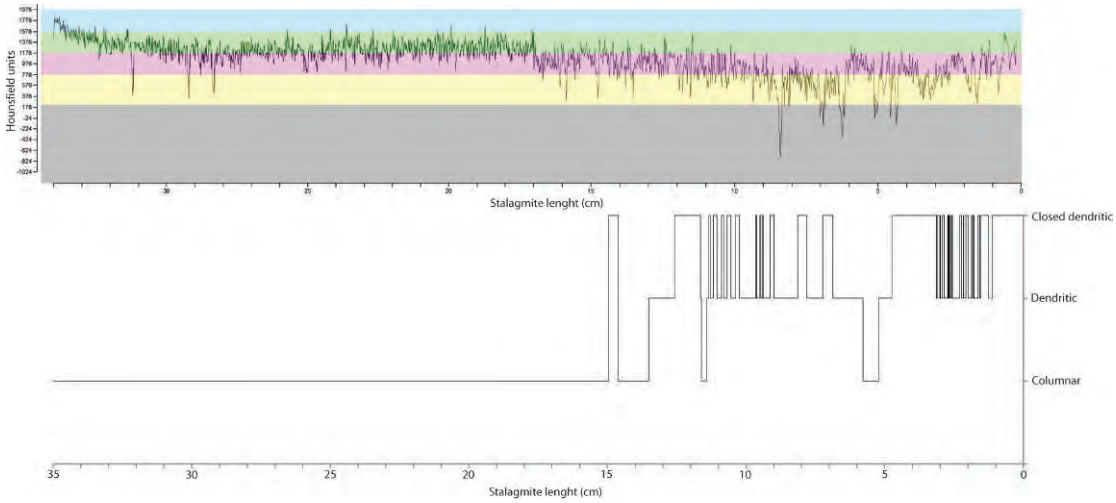

Figure 4. Petrographic log showing the different fabrics along the axis of the stalagmite compared with the graph of the density values in Hounsfield units, obtained with MIMICS v.10 software, that reflect the internal variability of the porosity in the speleothem. The color bands in the density graph correspond to the colors in Figures 3 and 5.

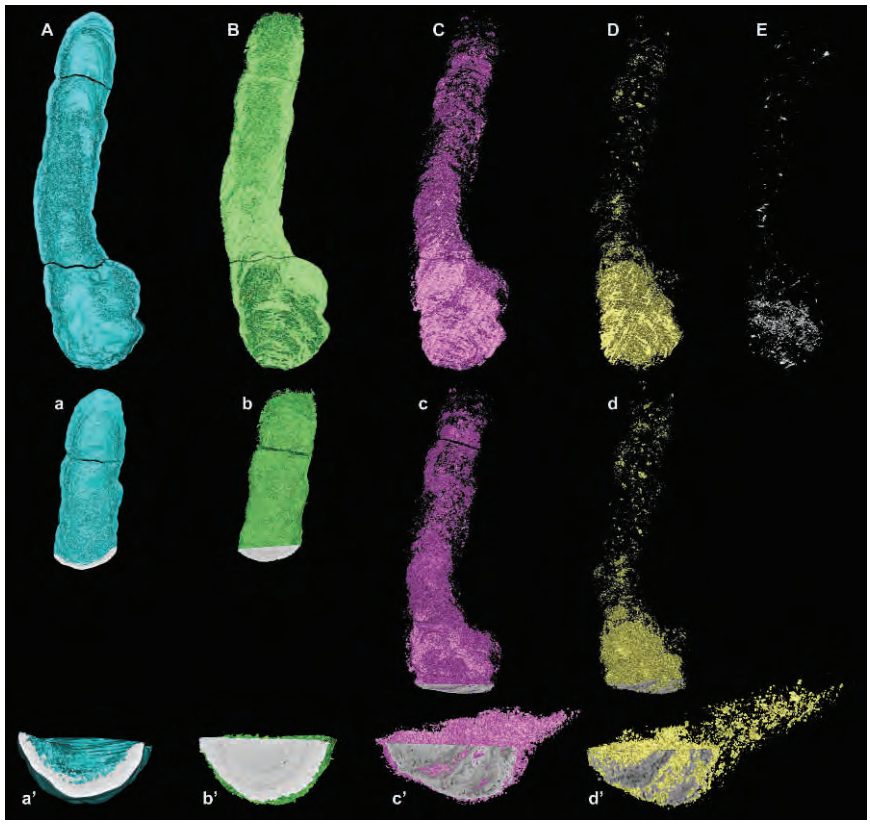

Figure 5. The top row is 3D models of the exterior of the stalagmite for different density value ranges according to MIMICS v.10. Density ranges corresponding to the inferred fabrics are listed in the caption for Figure 3. (A) Blue represents the lateral micrite-rich fabric; (B) green the columnar fabric; (C) fuchsia corresponds to closed dendritic fabric; (D) yellow correspond to the dendritic fabric; (E) stalagmite porosity distribution (density −1024 to 226 HU). The lower figures are the sections of each 3D image color that help to ascertain the fabric distributions.

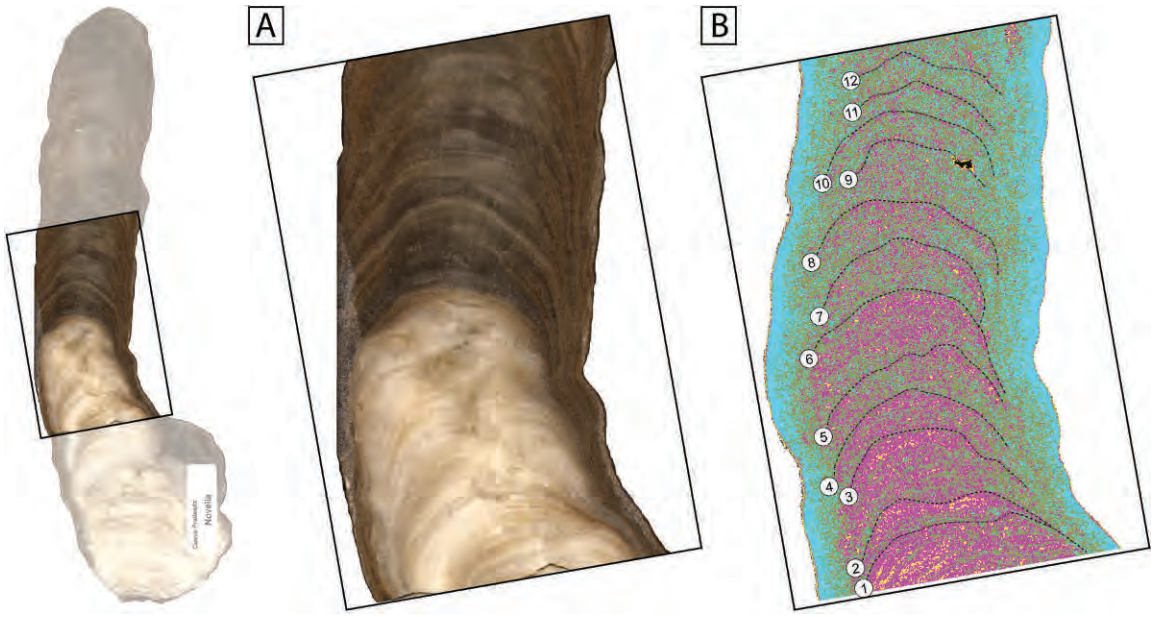

Figure 6. Enlargement of the images in Figures 1 and 3 of the phase-transition area in stalagmite Novella where stratigraphic architecture consisting of cyclic alternation of closed dendritic and columnar fabrics is visible. (A) is a photograph. (B) is the result of the computed-tomography scan, where fuscia color indicates closed dendritic fabric and green indicates columnar fabric. Compare the apparently sharp boundary between phases of the photograph and the gradual and cyclic pattern observed in the tomography. The annotations in (B) are explained in Vanghi (2013a).

interesting features, such as terrigenous, soot, charcoal, or guano laminae or masses inside the stalagmite.

Conclusions

In the present work, we evaluate the potential of computed-tomography scanning by comparing it with the results derived from a standard petrologic study. In that regard, our data indicate that CT scan has many interests for speleothem research. By definition, high-resolution X-ray computed tomography may detect subtle variations of density. As density values in a speleothem are controlled by primary crystalline texture and the presence of secondary porosity due to dissolution or fractures, CT scans can be used as a tool for a rapid and non-destructive characterization of the speleothem petrological textures, porosity distribution, and stratigraphical architecture prior to any further analysis.

Porosity is related to fluid behavior in the different fabrics, and consequently, with the spatial distribution of the diagenetic processes such as dissolution or recrystallization and neomorphism. In that regard, CT scanning may help to determine whether the speleothem has remained as a geochemically closed system.

As in previous work (Mickler et al., 2004), our work indicates that high-resolution tomography shows an interesting potential for the study of speleothem record. This technique offers many interests, being non-destructive and producing high resolution data in a few hours. It is a reliable complement to the standard petrological analysis, as it may help identify the domains within a speleothem that are the most suitable for bulk geochemical analysis and dating. In that regard, it could be especially interesting to develop a more rapid CT scanning procedure in the future to evaluate the suitability of a speleothem before any further sample manipulation, preparation and analysis.

Acknowledgements

We are grateful to Roberto Porres and Laura Rodríguez for their help and useful comments concerning the computed-tomography scan data-acquisition and processing. We would also like to thank Dr. Mathieu Duval for his helpful comments.

References

Borsato, A., Quinif, Y., Bini, A., and Dublyansky, Y., 2003, Open-system alpine speleothems: Implications for U-series dating and paleoclimate reconstructions: Studi Trentini di Scienze Naturali, Acta Geologica, v. 80, p. 71–83.

Fairchild, I.J., Frisia, S., Borsato, A., Tooth, A.F., 2007, Speleothems, *in* Nasch, D.J., and Oxford, S.J., Geochemical Sediments and Landscapes: Oxford, Blackwells, p. 201–245.

Fairchild, I.J., and Baker, A., 2012, Speleothem Science: From Process to Past Environment: Chichester, UK, Wiley-Blackwell, Quarternary Geoscience Series, 432 p.

Frisia, S., Borsato, A., Fairchild, I.J., and McDermott, F., 2000, Calcite fabrics, growth mechanisms, and environments of formation in speleothems from the Italian Alps and southwestern Ireland: Journal

of Sedimentary Research, v. 70, no. 5, p. 1183–1196. doi:10.1306/022900701183.

Frisia, S., 2003, Le tessiture negli speleotemi: Studi Trentini di Scienze Naturali, Acta Geologica, v. 80, p. 85–94.

Frisia, S., and Borsato, A., 2010, Karst, *in* Alonso-Zarza, A.M., and Tanner, L.H., eds., Carbonates in Continental Settings: Facies, Environments and Processes: Amsterdam, Elsevier, Developments in Sedimentology, no. 61, p. 269–318.

Mees, F., Swennen, R., Van Geet, M., and Jacobs, P., 2003, Applications of X-ray computed tomography in geosciences, *in* Mees, F., Swennen, R., Van Geet, M., and Jacobs, P., eds., Applications of X-ray Computed Tomography in Geosciences: The Geological Society of London Special Publications, v. 215, p. 1–6. doi:10.1144/GSL.SP.2003.215.01.01.

Mickler, P.J., Ketcham, R.A., Colbert, M.W., and Banner, J.L., 2004, Application of high-resolution X-ray computed tomography in determining the suitability of speleothems for use in paleoclimatic, paleohydrologic reconstructions: Journal of Cave and Karst Studies, v. 66, p. 4–8.

Muñoz-García, M.B., López-Arce, P., Fernández-Valle, M.E., Martín-Chivelet, J., and Fort, R., 2012, Porosity and hydric behavior of typical calcite microfabrics in stalagmites: Sedimentary Geology, v. 265–266, p. 72–86. doi:10.1016/j.sedgeo.2012.03.016.

Railsback, L.B., 2000, An Atlas of Speleothem Microfabrics, prepared by the University of Georgia Laboratory for Speleothem Studies, http://www.gly.uga.edu/railsback/speleoatlas/SAindex1.html [accessed November 2013].

Railsback, L.B., Liang, Fuyuan, Vidal Romaní, J.R., Grandal-d'Anglade, A., Vaqueiro Rodríguez, M., Santos Fidalgo, L., Fernández Mosquera, D., Cheng, Hai, and Edwards, R.L., 2011, Petrographic and isotopic evidence for Holocene long-term climate change and shorter-term environmental shifts from a stalagmite from the Serra do Courel of northwestern Spain, and implications for climatic history across Europe and the Mediterranean: Palaeogeography, Palaeoclimatology, Palaeoecology, v. 305, p. 172–184. doi:10.1016/j.palaeo.2011.02.030.

Sunagawa, I., 1987, Morphology of minerals, *in* Sunagawa, I., ed., Morphology of Crystals, Part B: Tokyo, Terra Scientific Publishing Company, p. 509–587.

Vanghi, V., 2013a, Estudio multianalítico de una estalagmita, *Novella* (Cueva de Praileaitz, Gipuzkoa): detección y caracterización de indicadores de cambios ambientales: CKQ Quaternary Studies, v. 3, p. 135–159.

Vanghi, V., 2013b, Trace element and isotopic study of a Holocene speleothem from Praileaitz Cave (Cantabrian Margin, Northern Spain): identifying proxies for paleoclimatological reconstruction [M.Sc. thesis]: University of Burgos, unedited.

GUIDE TO AUTHORS

The *Journal of Cave and Karst Studies* is a multidisciplinary journal devoted to cave and karst research. The *Journal* is seeking original, unpublished manuscripts concerning the scientific study of caves or other karst features. Authors do not need to be members of the National Speleological Society, but preference is given to manuscripts of importance to North American speleology.

LANGUAGES: The *Journal of Cave and Karst Studies* uses American-style English as its standard language and spelling style, with the exception of allowing a second abstract in another language when room allows. In the case of proper names, the *Journal* tries to accommodate other spellings and punctuation styles. In cases where the Editor-in-Chief finds it appropriate to use non-English words outside of proper names (generally where no equivalent English word exists), the *Journal* italicizes them. However, the common abbreviations i.e., e.g., et al., and etc. should appear in roman text. Authors are encouraged to write for our combined professional and amateur readerships.

CONTENT: Each paper will contain a title with the authors' names and addresses, an abstract, and the text of the paper, including a summary or conclusions section. Acknowledgments and references follow the text.

ABSTRACTS: An abstract stating the essential points and results must accompany all articles. An abstract is a summary, not a promise of what topics are covered in the paper.

STYLE: The *Journal* consults The Chicago Manual of Style on most general style issues.

REFERENCES: In the text, references to previously published work should be followed by the relevant author's name and date (and page number, when appropriate) in parentheses. All cited references are alphabetical at the end of the manuscript with senior author's last name first, followed by date of publication, title, publisher, volume, and page numbers. Geological Society of America format should be used (see http://www.geosociety.org/pubs/geoguid5.htm). Please do not abbreviate periodical titles. Web references are acceptable when deemed appropriate. The references should follow the style of: Author (or publisher), year, Webpage title: Publisher (if a specific author is available), full URL (e.g., http://www.usgs.gov/citguide.html) and date when the web site was accessed in brackets; for example [accessed July 16, 2002]. If there are specific authors given, use their name and list the responsible organization as publisher. Because of the ephemeral nature of websites, please provide the specific date. Citations within the text should read: (Author, Year).

SUBMISSION: Effective February 2011, all manuscripts are to be submitted via Peertrack, a web-based system for online submission. The web address is http://www.edmgr.com/jcks. Instructions are provided at that address. At your first visit, you will be prompted to establish a login and password, after which you will enter information about your manuscript (e.g., authors and addresses, manuscript title, abstract, etc.). You will then enter your manuscript, tables, and figure files separately or all together as part of the manuscript. Manuscript files can be uploaded as DOC, WPD, RTF, TXT, or LaTeX. A DOC template with additional manuscript specifications may be downloaded. (Note: LaTeX files should not use any unusual style files; a LaTeX template and BiBTeX file for the *Journal* may be downloaded or obtained from the Editor-in-Chief.) Table files can be uploaded as DOC, WPD, RTF, TXT, or LaTeX files, and figure files can be uploaded as TIFF, EPS, AI, or CDR files. Alternatively, authors may submit manuscripts as PDF or HTML files, but if the manuscript is accepted for publication, the manuscript will need to be submitted as one of the accepted file types listed above. Manuscripts must be typed, double spaced, and single-sided. Manuscripts should be no longer than 6,000 words plus tables and figures, but exceptions are permitted on a case-by-case basis. Authors of accepted papers exceeding this limit may have to pay a current page charge for the extra pages unless decided otherwise by the Editor-in-Chief. Extensive supporting data will be placed on the *Journal*'s website with a paper copy placed in the NSS archives and library. The data that are used within a paper must be made available. Authors may be required to provide supporting data in a fundamental format, such as ASCII for text data or comma-delimited ASCII for tabular data.

DISCUSSIONS: Critical discussions of papers previously published in the *Journal* are welcome. Authors will be given an opportunity to reply. Discussions and replies must be limited to a maximum of 1000 words and discussions will be subject to review before publication. Discussions must be within 6 months after the original article appears.

MEASUREMENTS: All measurements will be in Systeme Internationale (metric) except when quoting historical references. Other units will be allowed where necessary if placed in parentheses and following the SI units.

FIGURES: Figures and lettering must be neat and legible. Figure captions should be on a separate sheet of paper and not within the figure. Figures should be numbered in sequence and referred to in the text by inserting (Fig. x). Most figures will be reduced, hence the lettering should be large. Photographs must be sharp and high contrast. Color will generally only be printed at author's expense.

TABLES: See http://www.caves.org/pub/journal/PDF/Tables.pdf to get guidelines for table layout.

COPYRIGHT AND AUTHOR'S RESPONSIBILITIES: It is the author's responsibility to clear any copyright or acknowledgement matters concerning text, tables, or figures used. Authors should also ensure adequate attention to sensitive or legal issues such as land owner and land manager concerns or policies.

PROCESS: All submitted manuscripts are sent out to at least two experts in the field. Reviewed manuscripts are then returned to the author for consideration of the referees' remarks and revision, where appropriate. Revised manuscripts are returned to the appropriate Associate Editor who then recommends acceptance or rejection. The Editor-in-Chief makes final decisions regarding publication. Upon acceptance, the senior author will be sent one set of PDF proofs for review. Examine the current issue for more information about the format used.

ELECTRONIC FILES: The *Journal* is printed at high resolution. Illustrations must be a minimum of 300 dpi for acceptance.

Journal of Cave and Karst Studies

Volume 77 Number 1 April 2015

***Journal of Cave and Karst Studies* Distribution Changes**

During the November 9, 2013, Board of Governors meeting, the BOG voted to change the *Journal* to electronic distribution for all levels of membership beginning with the April 2014 issue. Upon publication, electronic files (as PDFs) for each issue will be available for immediate viewing and download through the Member Portal on www.caves.org. For those individuals that wish to continue to receive the *Journal* in a printed format, it will be available by subscription for an additional fee. Online subscription and payment options will be made available through the website in the near future. Until then, you can arrange to receive a print subscription of the *Journal* by contacting the NSS office at (256) 852-1300.